

UCSF

UC San Francisco Electronic Theses and Dissertations

Title

Mechanisms of Normal and Maladaptive Learning: Implications for Alcohol Use Disorder

Permalink

<https://escholarship.org/uc/item/6wp0317b>

Author

Hoisington, Zachary William

Publication Date

2024

Peer reviewed|Thesis/dissertation

Mechanisms of Normal and Maladaptive Learning: Implications for Alcohol Use Disorder

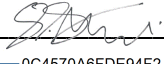
by
Zachary William Hoisington

DISSERTATION
Submitted in partial satisfaction of the requirements for degree of
DOCTOR OF PHILOSOPHY

in
Pharmaceutical Sciences and Pharmacogenomics

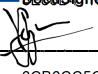
in the
GRADUATE DIVISION
of the
UNIVERSITY OF CALIFORNIA, SAN FRANCISCO

Approved:

DocuSigned by:

0C4570A6FDE94F2...
DEVANAND MANOLI
Chair

DocuSigned by:

Dorit Ron

DocuSigned by:

6CB6CC5CF18C4FD...
Vijay Mohan K Namboodiri

Committee Members

Dedicated to my parents.

Acknowledgements

It is impossible to comprehensively acknowledge those that have encouraged, supported, inspired, and motivated me throughout my journey. This work is a culmination of those influences.

To my dissertation advisor and mentor Dr. Dorit Ron: you have been there as a stalwart supporter of mine since my interview at UCSF. I fondly remember receiving the email where you congratulated me on my acceptance. I had known I wanted to work with you since my initial application, and that was solidified after my winter rotation, when I never left! You are a pillar of the addiction research community, and it is apparent when we attend conferences together that you are loved by many internationally. I have grown immensely because of your mentorship. It is enjoyable for me to look back on my early presentations and writing samples and see how far I have evolved with your guidance. You have given me so many opportunities to showcase the Ron Lab excellence and appropriately prepared me to perform at the highest level. You have pushed me and lifted me up, and I could not have done this without you!

To the Ron Lab members: you showed up for me every day. It was such a great opportunity to work with you. Thank you for making the lab such a fun environment even during my most difficult times. Ky: you are the most gifted biochemist there is. You have been the experimental backbone of the lab my entire time here, and longer, and I have learned so much from you, both experimentally and personally. Yann: some of my fondest memories are when we are having conversations that are half science, half laughing. The WhatsApp messages you sent me after my first journal club have been printed in my drawer for four years and have given me the drive to succeed. Alex: we have been through

so many tumultuous periods together. You are incredibly supportive and sitting next to you was continually a joy and a comfort for my time here. Jeff: you taught me nearly everything I know about behavior. Although you moved on before the completion of my schooling, you instilled foundations of experimental practices and people skills that have grown into skyscrapers. Chhavi: you have been incredibly dependable and made my experience so much easier. Whenever I needed help, you were there immediately and diligently. We had great fun together, and you were instrumental in my experimental success.

To my thesis committee members, Dev and Vijay: I have continually valued your scientific expertise. More than that, your support of my growth as a scientist has been revolutionary. Our meetings were always productive and collaborative, and I appreciate you treating me as an independent scientist rather than simply a trainee. This manner of instruction buffed my confidence and allowed me to become the scientist I am today.

To the 2019 PSPG cohort: we did it! My people. I am so lucky to have experienced some of the most formative years of my career with such a great group of people. I loved how we would spend all day together in our classes, and pizza talks, and study groups after. When I see you at our weekly seminar, it gave me a burst of enthusiasm to get through each week. I am appreciative of the bond we have formed and excited to see the continued success of you all.

To my great friends, Whitney and Aidan: our friendship throughout graduate school embodies the “if you want to go far, go together” quote. From our early days where Aidan would tutor us on Python, to Pop’s, to our weekend getaways to decompress, to our shared experience celebrating in Italy, you are integral to my life, and I could not ask for

a better duo. You are two of the realest people I have met. I feel comfortable pouring my heart's thoughts out to you and coming to you for scientific advice. We went through so many formative experiences together and have been inseparably molded by it.

To Hannah: I am grateful for your unwavering support and positivity. During my toughest days you were there to lift me up. Now, in our times of celebration, you are the first to start cheering. Your patience and encouragement have been invaluable to me. Thank you for being an essential part of my life and journey, and I am ecstatic to discover what the future holds.

To my parents: you have been my unconditional supporters since day one. You have continuously made sacrifices to allow me every opportunity to succeed. Whether it was attending every parent-teacher conference, or your involvement in extracurricular activities, or driving me to the SHHS parking lot at 5:30AM so I could take the bus to MMSTC, or pushing and supporting me throughout my time at the University of Michigan, your backing was continually felt throughout my two decades of schooling. There were times throughout my years where I was uncertain of myself, but your encouragement was always firmly planted in the back of my mind, no matter the distance between us. Your guidance instilled such valuable habits in me, and it allowed me to continue my academic development and succeed at the highest level. This dissertation is a testament to the values of hard work, determination, and teamwork you have instilled in me. Thank you for always being my greatest supporters, and I am endlessly grateful.

Contributions

Chapters in this dissertation contain previously published material or material that is currently under review for publication. In some cases, this material has been adapted to fit within the goals of this dissertation and does not necessarily reflect its published form.

Chapter 1 is reproduced with permission from the publication under revision: Zachary W. Hoisington, Alexandra Salvi, Sophie Laguesse, Yann Ehinger, Chhavi Shukla, Khanhky Phamluong, Dorit Ron. The small G-protein Rac1 in the dorsomedial striatum promotes alcohol-dependent structural plasticity and goal-directed learning in mice. *J Neuroscience*. 2024. Additionally, new, unpublished sections have been added.

Chapter 2 contains unpublished results from a manuscript that is in progress and will be submitted to a peer-reviewed journal: Zachary W. Hoisington, Himanshu Gangal, Khanhky Phamluong, Gregg E. Homanics, Jun Wang, and Dorit Ron. Prosapip1 in the dorsal hippocampus mediates long-term potentiation and spatial memory.

“The genius thing that we did was, we didn't give up.”

-Shawn Carter

Mechanisms of Normal and Maladaptive Learning: Implications for Alcohol Use Disorder

Zachary William Hoisington

Abstract

Addiction, including alcohol use disorder, is a maladaptive form of learning and memory. Initially, the effects of an addictive substance are rewarding, reinforcing the drug-seeking behavior. Over time, repeated exposure leads to changes in neuroanatomy, altering the brain's circuitry and resulting in cycles of drug binge, withdrawal, and craving, undermining the individual's health and functioning. This dissertation aims to examine the role of Rac1 in maladaptive learning and Prosapip1 in normal learning and memory.

The first chapter examines a protein that has not previously been studied in mammals in the context of AUD, Rac1. In this chapter, we present evidence that Rac1 is activated in the DMS in response to repeated cycles of alcohol binge and withdrawal. This subregion-specific activation leads to phosphorylation of downstream proteins and promotes F-actin assembly, which then causes increased dendritic arborization and dendritic spine maturation. We also show that Rac1 in the DMS is involved in alcohol-associated goal-directed behavior, and therefore likely contributing to the progression of AUD.

The second chapter investigates the physiological role of a protein previously associated with AUD, Prosapip1. We developed a Prosapip1 neuronal knockout mouse line to examine its mechanism of action *in vivo*. We present data to suggest that Prosapip1 is vital in regulating the PSD scaffold. Disruption of the PSD leads to a loss of

LTP. Finally, these biomolecular changes result in a spatial learning and memory deficit, which is localized to the dorsal hippocampus.

In summary, this dissertation contributes to the knowledge of molecular mechanisms controlling normal and maladaptive learning, and identifies potential targets for the treatment of AUD.

Table of Contents

Introduction to Chapter 1	1
Chapter 1: Rac1 and the Progression of Alcohol Use Disorder	3
1.1 Abstract	4
1.2 Significance Statement	5
1.3 Introduction	6
1.4 Results	9
1.4.1 <i>Alcohol activates Rac1 in the DMS of male mice</i>	9
1.4.2 <i>Rac1 activation by alcohol in the DMS is specific</i>	10
1.4.3 <i>Alcohol promotes LIM kinase activation and cofilin phosphorylation</i>	11
1.4.4 <i>Alcohol activation of the LIMK/cofilin signaling pathway in the DMS depends on Rac1</i>	14
1.4.5 <i>Alcohol promotes F-actin formation in the DMS via Rac1</i>	16
1.4.6 <i>Rac1 signaling is activated after voluntary and involuntary alcohol exposure in the central amygdala</i>	20
1.4.7 <i>Rac1 promotes the remodeling of dendritic arbors in the DMS</i>	25
1.4.8 <i>Rac1 in the DMS is required for the alcohol-mediated alteration in dendritic spine morphology</i>	30
1.4.9 <i>Rac1 does not play a role in the development and maintenance of voluntary alcohol intake</i>	36

1.4.10 <i>Rac1 in the DMS is required for alcohol-associated goal-directed learning</i>	40
1.4.11 <i>Rac1 in the DMS is not required for sucrose goal-directed learning</i>	47
1.4.12 <i>Systemic Rac1 inhibition reduces binge alcohol drinking in male and female mice</i>	49
1.5 Discussion	53
1.5.1 <i>Rac1 is activated in the DMS after alcohol consumption</i>	53
1.5.2 <i>Rac1 in the DMS promotes alcohol-dependent morphological adaptations</i>	56
1.5.3 <i>Rac1 and alcohol-associated behaviors</i>	57
1.6 Future Directions	61
1.7 Materials and Methods	64
Introduction to Chapter 2	76
Chapter 2: Prosapip1 in the dorsal hippocampus mediates long-term potentiation and spatial memory	77
2.1 Abstract	78
2.2 Introduction	79
2.3 Results	82
2.3.1 <i>Generation and characterization of Prosapip1(flx/flx) mice</i>	82
2.3.2 <i>Prosapip1 is required for synaptic localization of PSD proteins</i>	85

2.3.3 <i>Prosapip1 in the dorsal hippocampus plays a role in NMDA receptor-mediated transmission and long-term potentiation</i>	89
2.3.4 <i>Prosapip1 knockout does not affect locomotion or anxiety</i>	93
2.3.5 <i>Prosapip1 contributes to spatial memory</i>	95
2.3.6 <i>Prosapip1 in the dorsal hippocampus contributes to spatial memory</i>	102
2.4 Discussion	107
2.4.1 <i>Prosapip1 is a key protein in the PSD</i>	107
2.4.2 <i>Prosapip1 and LTP</i>	109
2.4.3 <i>Behavioral consequences of loss of Prosapip1</i>	110
2.5 Future Directions	114
2.6 Material and Methods	117
References	130

List of Figures

Model 1. Rac1 pathway	6
1.1. Alcohol activates Rac1 specifically in the DMS of male mice	12
Extended 1.1-1. Rac1 is activated after 4 weeks of IA20%2BC in male mice	13
1.2. Alcohol activation of the LIMK/cofilin signaling pathway and subsequent F-actin formation in the DMS depends on Rac1	18
1.3. Rac1 signaling is activated after voluntary and involuntary alcohol exposure in the central amygdala	23
1.4. Rac1 promotes remodeling of dendritic arbors in the DMS	28
1.5. Rac1 in the DMS is required for the alcohol-mediated morphological changes in dendritic spines	34
1.6. Rac1 does not play a role in the development and maintenance of voluntary alcohol intake	38
1.7. Rac1 in the DMS is required for alcohol-associated goal-directed learning	43
1.8. Rac1 in the DMS is required for alcohol action-outcome associations	46
1.9. Rac1 in the DMS is not required for sucrose goal-directed learning	48
1.10. Systemic Rac1 inhibition reduces binge alcohol drinking in male and female mice	51
Model 2. Upstream activation of Rac1 by NMDAR signaling	54
Model 3. Prosapip1 domains	79

Model 4. Prosapip1 is a key protein in the PSD	80
2.1. Generation and characterization of Prosapip1(flx/flx) mice	83
2.2. Prosapip1 is required for synaptic localization of PSD proteins	87
2.3. Prosapip1 in the dorsal hippocampus plays a role in NMDA receptor-mediated transmission and long-term potentiation	91
2.4. Prosapip1 knockout does not affect locomotion or anxiety	94
2.5. Prosapip1 contributes to spatial memory	100
Extended 2.5. Prosapip1 knockout did not affect Barnes maze habituation	101
2.6 Prosapip1 in the dorsal hippocampus contributes to spatial memory	105

List of Tables

Table 1.1. Average alcohol consumption for biochemical experiments	63
--	----

List of Abbreviations

10%CA, 10% alcohol continuous access

3CSI, 3-chamber social interaction

AAV, adeno-associated virus

aCSF, artificial cerebrospinal fluid

AMPA, α -amino-3-hydroxy-5-methyl-4-isoxazolepropionic acid receptor

ANOVA, analysis of variance statistical test

AP, anteroposterior

ASD, autism spectrum disorder

AUC, area under the curve

AUD, alcohol use disorder

B, binge

BL, baseline

C57BL/6J, "C57 black 6" mouse from Jackson laboratory

CNS, central nervous system

D, degraded

D1R, dopamine D1 receptor

D2R, dopamine D2 receptor

DG, dentate gyrus

dHipp, dorsal hippocampus

DLS, dorsolateral striatum

DMS, dorsomedial striatum

DNA, deoxyribonucleic acid

DV, dorsoventral

EGTA, ethylenediaminetetraacetic acid

EPM, elevated plus maze

EPSP, excitatory postsynaptic potential

F-actin, filamentous actin

FBS, fetal bovine serum

FR, fixed ratio

GABA, γ -aminobutyric acid

G-actin, globular actin

GAP, GTPase-activating protein

GDP, guanosine diphosphate

GEF, guanine exchange factor

GFP, green fluorescent protein

GTP, guanosine triphosphate

GWAS, genome wide association study

HFS, high-frequency stimulation

IA20%2BC, intermittent access to 20% alcohol two-bottle choice

IACUC, Institutional Animal Care and Use Committee

IPSP, inhibitory postsynaptic potential

ITI, inter-trial interval

L/D Box, light/dark box

LTP, long-term potentiation

MAGUK, membrane associated guanylate kinases

ML, mediolateral

MSN, medium spiny neuron

NAc, nucleus accumbens

ND, non-degraded

NIAAA, National Institute of Alcohol Abuse and Alcoholism

NMDAR, N-methyl-D-aspartate receptor

OSA, operant self-administration

PDZ, PSD-95/Dlg1/ZO-1

PSD, post-synaptic density

PPR, paired-pulse ratio

Rac1-DN, Rac1 dominant negative form (T17N)

RI, random interval

RNA, ribonucleic acid

RR, random ratio

SEM, standard error of the mean

Shank, Src homology 3 domain and ankyrin repeat protein

SPAR, spine-associated Rap GTPase-activating protein

UCSF, University of California, San Francisco

UTR, untranslated region

WD, withdrawal

Introduction to Chapter 1

Chapter 1 of this dissertation focuses on the role of the small G-protein Rac1 in promoting the progression of alcohol use disorder (AUD) in the central nervous system.

AUD is a devastating disease that affects nearly 30 million people in the United States (SAMHSA, 2022). Unfortunately, there are few medications (Wackernah et al., 2014). AUD is characterized by the inability to stop or control alcohol use despite negative consequences, ranging from damaging personal relationships to severe health effects. The cycle of addiction can be characterized by three major stages: binge/intoxication, withdrawal/negative affect, and preoccupation/anticipation (Koob and Volkow, 2010). While early drug studies focused on the immediate effect of drug use, the focus has now progressed to chronic use and the long-term neuroadaptive changes that lead to the continuation of this cycle (Koob and Kreek, 2007; Koob and Volkow, 2010). The transition from social intake of alcohol to AUD requires synaptic and structural plasticity changes in brain regions such as the striatum, prefrontal cortex, and the amygdala (Lovinger and Abrahao, 2018). Research has identified both protective mechanisms that confer resilience to AUD and molecular mechanisms that promote the transition to AUD (Ron and Berger, 2018). As AUD has few effective medications (Mark et al., 2009; Wackernah et al., 2014), understanding these neuromolecular mechanisms may unlock additional targets for the treatment of AUD.

Previous work from our laboratory focused on the alcohol-induced formation of F-actin and subsequent long-term structural plasticity, which has been hypothesized to reinforce alcohol-associated behaviors mice (Wang et al., 2015; Laguesse et al., 2018). To further examine the causal mechanisms of these dynamic changes in actin and

subsequent long-term structural plasticity, we surveyed upstream proteins that control the formation of F-actin.

Chapter 1

The small G-protein Rac1 in the dorsomedial striatum promotes alcohol-dependent structural plasticity and goal-directed learning in mice

Contributing Authors: Zachary W. Hoisington, Alexandra Salvi, Sophie Laguesse, Yann Ehinger, Chhavi Shukla, Khanhky Phamluong, and Dorit Ron

1.1 Abstract

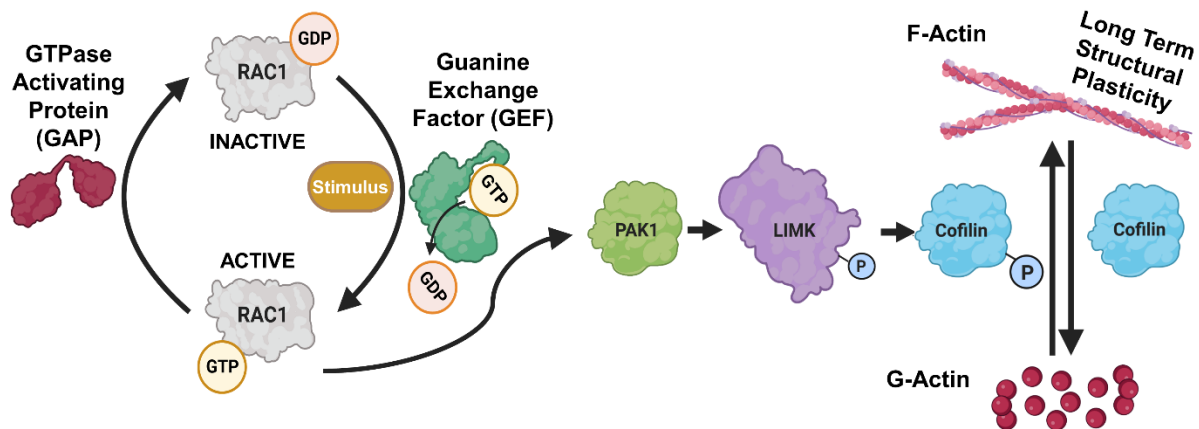
The small G-protein Rac1 promotes the formation of filamentous actin (F-Actin). Actin is a major component of dendritic spines, and we previously found that alcohol alters actin composition and dendritic spine structure in the nucleus accumbens (NAc) and the dorsomedial striatum (DMS). To examine if Rac1 contributes to these alcohol-mediated adaptations, we measured the level of GTP-bound active Rac1 in the striatum of mice following 7 weeks of intermittent access to 20% alcohol. We found that chronic alcohol intake activates Rac1 in the DMS of male mice. In contrast, Rac1 is not activated by alcohol in the NAc and DLS of male mice, or in the DMS of female mice. Similarly, closely related small G-proteins are not activated by alcohol in the DMS, and Rac1 activity is not increased in the DMS by moderate alcohol or natural reward. To determine the consequences of alcohol-dependent Rac1 activation in the DMS of male mice, we inhibited endogenous Rac1 by infecting the DMS of mice with an AAV expressing a dominant negative form of the small G-protein (Rac1-DN). We found that overexpression of AAV-Rac1-DN in the DMS inhibits alcohol-mediated Rac1 signaling and attenuates alcohol-mediated F-actin polymerization, which corresponded with a decrease in dendritic arborization and spine maturation. Finally, we provide evidence to suggest that Rac1 in the DMS plays a role in alcohol-associated goal-directed learning. Together, our data suggest that Rac1 in the DMS plays an important role in alcohol-dependent structural plasticity and aberrant learning.

1.2 Significance Statement

Addiction, including alcohol use disorder, is characterized by molecular and cellular adaptations that promote maladaptive behaviors. We found that Rac1 was activated by alcohol in the dorsomedial striatum (DMS) of male mice. We show that alcohol-mediated Rac1 signaling is responsible for alterations in actin dynamics and neuronal morphology. We also present data to suggest that Rac1 is important for alcohol-associated learning processes. These results suggest that Rac1 in the DMS is an important contributor to adaptations that promote alcohol use disorder.

1.3 Introduction

Rac1 (Ras-related C3 botulinum toxin substrate 1) is a small G-protein belonging to the Rho family of GTPases (Van Aelst and D'Souza-Schorey, 1997; Vetter and Wittinghofer, 2001; Bosco et al., 2009). Rac1 is expressed ubiquitously and plays a role in processes such as actin polymerization, endocytosis, transcription, and cell growth (Nakayama et al., 2000; Ridley, 2006; Bosco et al., 2009). Rac1 is highly expressed in the central nervous system (CNS) (Corbetta et al., 2009).



Model 1. Rac1 pathway

Rac1 cycles between a GDP-bound inactive state and a GTP-bound active state (**Model 1**) (Vetter and Wittinghofer, 2001). In the CNS, the transition between GDP-bound to GTP-bound Rac1 is catalyzed by the guanine nucleotide-exchange factors (GEFs) Tiam1 and Karilin-7 (Vetter and Wittinghofer, 2001; Tolias et al., 2005; Xie et al., 2007). The Rac1 GTPase activating proteins (GAPs), such as RacGAP1 or FilGAP (Toure et al., 1998; Nguyen et al., 2018), initiate the intrinsic GTPase activity of Rac1 resulting in the conversion of GTP to GDP (Vetter and Wittinghofer, 2001). Upon activation, Rac1 binds to p21-activated kinase (PAK1) leading to PAK1 autophosphorylation and activation

(Bokoch, 2003). PAK1 phosphorylates and activates LIM kinase (LIMK) (Edwards et al., 1999). LIMK then phosphorylates cofilin (Yang et al., 1998; Bernard, 2007; Scott and Olson, 2007). Cofilin's function is to sever actin filaments (F-actin) into globular actin (G-actin) (Yang et al., 1998; Bamburg, 1999; Maciver and Hussey, 2002; Andrianantoandro and Pollard, 2006; Chin et al., 2016; Kanellos and Frame, 2016). LIMK phosphorylation of cofilin prevents cofilin's ability to cleave actin, therefore enabling the formation and maintenance of F-actin (Yang et al., 1998; Pavlov et al., 2007; Scott and Olson, 2007). This mechanism promotes spine enlargement and stabilizes and strengthens synapses (Honkura et al., 2008; Chazeau and Giannone, 2016; Costa et al., 2020). As such, Rac1 is involved in long-term potentiation, the cellular mechanism of learning and memory (Haditsch et al., 2009; Haditsch et al., 2013; Lv et al., 2019).

Malfunction of Rac1 has been associated with multiple neurological and psychiatric disorders. For example, abnormal expression of Rac1 has been observed in humans with schizophrenia, autism spectrum disorders, and fragile X syndrome (Tejada-Simon, 2015; Reijnders et al., 2017; Wang et al., 2020). A reduction of Rac1 expression is also associated with stress, depression, and anhedonia in mice (Golden et al., 2013), symptoms that often coincide with addiction (Koob and Kreek, 2007). Abnormal Rac1 function has been linked to drugs of abuse. Specifically, Rac1 activity is inhibited after repeated, but not acute, cocaine administration in the nucleus accumbens (NAc) of mice (Dietz et al., 2012), and Rac1-dependent mechanisms affect the extinction of aversive opiate withdrawal memories (Wang et al., 2017). Finally, Rac1 orthologs have been shown to regulate acute alcohol sensitivity in *Drosophila melanogaster* (Peru et al., 2012).

However, Rac1's function in alcohol use disorder (AUD) has not been investigated in a mammalian system.

Previously, we found that excessive chronic alcohol consumption promotes the formation of F-actin in the NAc (Laguesse et al., 2017) and in the dorsomedial striatum (DMS) of mice (Wang et al., 2015; Laguesse et al., 2018). We further found that heavy alcohol consumption in mice results in a structural remodeling in both brain regions, leading to the maturation of dendritic spines in the NAc and in the branching of dendrites and remodeling of dendritic spines in DMS (Wang et al., 2015; Laguesse et al., 2018). Here, we examined the possibility that Rac1 controls these alcohol-dependent structural adaptations in the NAc and/or the DMS.

1.4 Results

1.4.1 Alcohol activates Rac1 in the DMS of male mice

We first tested if repeated cycles of alcohol binge drinking and withdrawal activates Rac1 in the striatum of male mice. Specifically, animals were subjected to 7 weeks of 20% alcohol or water choice for 24 hours a day, 3 days a week, with 24- or 48- (weekend) hour withdrawal periods in between during which mice had access to water only. Mice consuming water for the same duration were used as controls (**Figure 1.1A**). Striatal regions were dissected and harvested 4 hours after the beginning of a drinking session (“binge”) or 24 hours after the end of a drinking session (“withdrawal”) (**Figure 1.1A**). Rac1-GTP pulldown assay was utilized to analyze the level of active GTP-bound vs. inactive GDP-bound Rac1. We found that the activity of Rac1 was unaltered by alcohol in the NAc (**Figure 1.1B, Table 1.1**) and the DLS (**Figure 1.1C, Table 1.1**) (NAc Kruskal-Wallis test $H = 0.5731$, $p = 0.7761$; DLS One-way ANOVA: $F_{(2,15)} = 0.0139$, $p = 0.9862$). In contrast, we discovered that 7 weeks of IA20%2BC produced a robust activation of Rac1 in the DMS during both binge and withdrawal (**Figure 1.1D, Table 1.1**) (One-way ANOVA: $F_{(2, 15)} = 8.233$, $p = 0.0039$; *Post hoc*: Water vs. Binge $p = 0.0058$, W vs. WD $p = 0.0068$). The same pattern of Rac1 activation was also observed during withdrawal after 4 weeks of IA20%2BC (**Extended Figure 1.1-1, Table 1.1**) (Unpaired t-test: $t_{(6)} = 2.938$, $p = 0.0260$). In contrast, Rac1 activity was unaltered in the DMS of female mice undergoing 7 weeks of IA20%2BC (**Figure 1.1E, Table 1.1**) (Kruskal-Wallis test $H = 0.2456$, $p = 0.8968$), suggesting that there are sex differences in alcohol-dependent Rac1 activation. Together, these data suggest that chronic voluntary drinking of alcohol produces a long-lasting activation of Rac1 in the DMS of male mice.

1.4.2 Rac1 activation by alcohol in the DMS is specific

Next, we set to determine the specificity of alcohol-dependent activation of Rac1 in the DMS. The closely related small G-proteins RhoA and Cdc42 have also been linked with synaptic and structural plasticity (Francis et al., 2019; Zhang et al., 2021). We found that levels of RhoA and Cdc42 bound to GTP (**Figure 1.1F, Figure 1.1G, Table 1.1**) were unchanged in the DMS at both binge and withdrawal timepoints as compared to water-only drinking mice (RhoA One-way ANOVA: $F_{(2, 15)} = 0.472$, $p = 0.6323$; Cdc42 Kruskal-Wallis test $H = 3.310$, $p = 0.1962$). To measure if Rac1 is activated in response to moderate consumption of alcohol, we exposed mice to a 10% continuous access (10%CA) 2BC alcohol drinking paradigm in which mice were allowed to choose between 10% alcohol and water continuously for 21 days, matching the number IA20%2BC sessions. We detected no change in the activation of Rac1 in the DMS after 10%CA (**Figure 1.1H, Table 1.1**) (Unpaired t-test: $t_{(10)} = 0.3960$, $p = 0.7004$), which implies that higher concentration of alcohol and/or repeated cycles of binge and withdrawal are necessary for the alcohol-dependent activation of Rac1 in the DMS.

To examine if Rac1 is activated in the DMS by a naturally rewarding substance, mice underwent intermittent access to a 1% sucrose 2BC paradigm for 2 weeks. We found that Rac1 is not activated in the DMS of sucrose drinking mice (**Figure 1.1I, Table 1.1**) (Unpaired t-test: $t_{(12)} = 0.5345$, $p = 0.6028$), suggesting that activation of Rac1 signaling in the DMS is specific for alcohol and is not shared with natural reward. Together, these data suggest that the activation of Rac1 in the DMS observed after chronic alcohol consumption is not generalized to other closely related small G-proteins

in the Rho family, is specific to repeated cycles of binge and withdrawal of 20% alcohol and is not shared with natural reward.

1.4.3 Alcohol promotes LIM kinase activation and cofilin phosphorylation

Rac1 activation leads to the downstream phosphorylation of LIMK which in turn phosphorylates cofilin (Edwards et al., 1999). Therefore, we examined whether alcohol-mediated Rac1 stimulation promotes the activation of LIMK and cofilin phosphorylation in the DMS. To test this question, we measured the level of LIMK phosphorylation, and thus activation, as well as the phosphorylation of cofilin in the DMS after 7 weeks of IA20%2BC. We found that the phosphorylation of both LIMK and cofilin were significantly increased after alcohol binge and withdrawal in comparison to animals that drank water only (**Figure 1.1J, Table 1.1**) (One-way ANOVA: LIMK $F_{(2, 12)} = 96.40$, $p < 0.0001$; *Post hoc*: Water vs. Binge $p < 0.0001$, Water vs. Withdrawal $p < 0.0001$; Cofilin $F_{(2, 12)} = 44.14$, $p < 0.0001$; *Post hoc*: Water vs. Binge $p < 0.0001$, Water vs. Withdrawal $p < 0.0001$). Together, these data suggest that long-term alcohol consumption activates Rac1-dependent signaling.

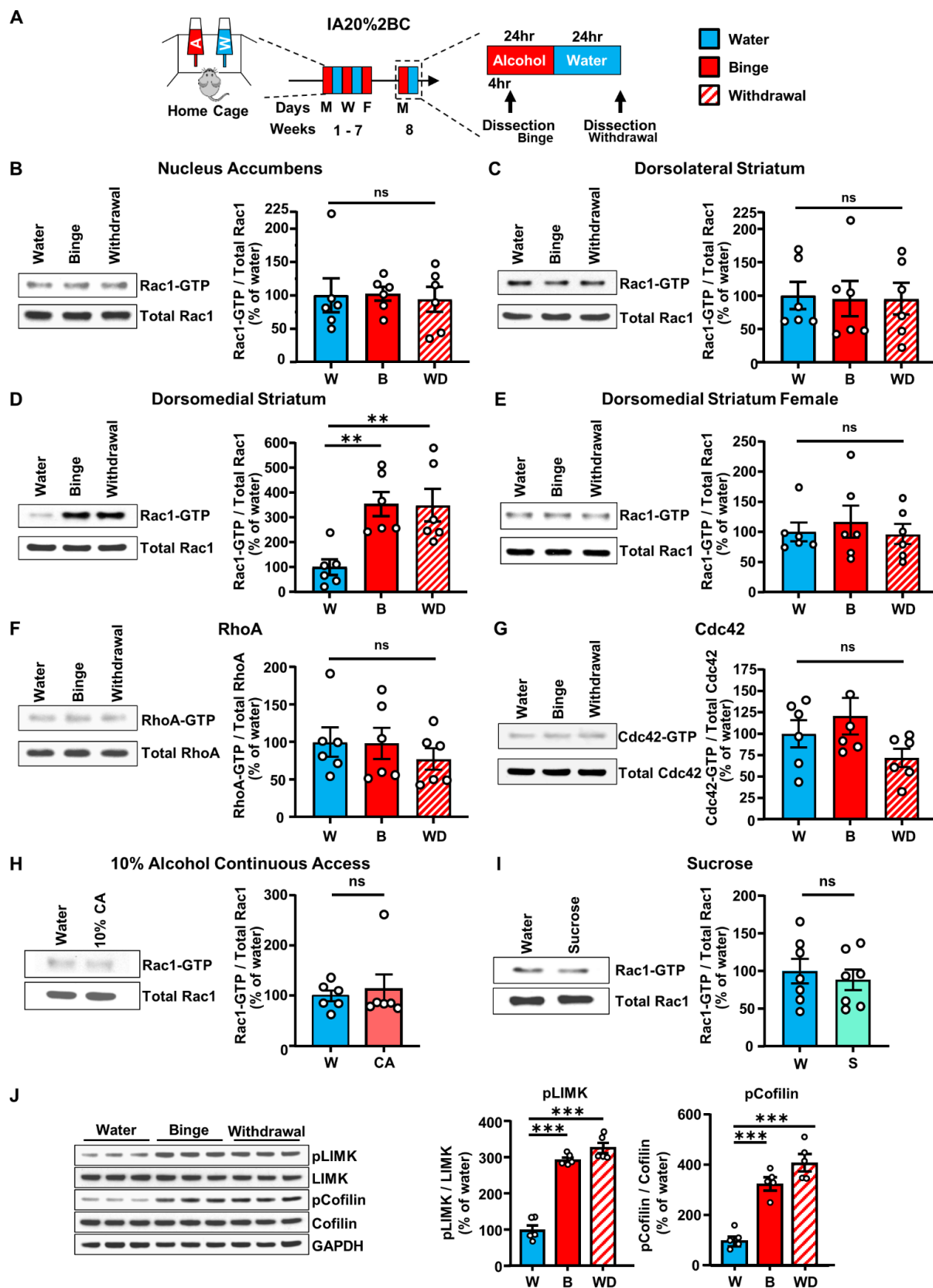
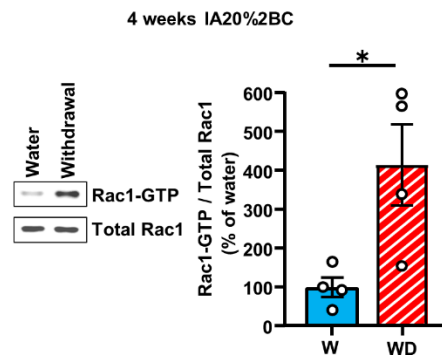


Figure 1.1. Alcohol activates Rac1 specifically in the DMS of male mice

Figure 1.1. Alcohol activates Rac1 specifically in the DMS of male mice

(A) Intermittent access to 20% alcohol in 2-bottle-choice (IA20%2BC) experimental timeline. (B-D) The NAc (B), the DLS (C), and the DMS (D) were harvested 4 hours into last drinking session (binge, B) or after 24 hours of abstinence (withdrawal, WD). Rac1-GTP pull-down assay was conducted on cell lysates. Levels of GTP-bound Rac1 were normalized to total Rac1 and presented as percentage of the average of the water values. (E) Female mice underwent IA20%2BC before the DMS was harvested and the percentage of Rac1-GTP was calculated. RhoA-GTP (F) or Cdc42-GTP (G) pull-down assay was conducted on cell lysates after IA20%2BC and quantified using western blot. Levels of GTP-bound RhoA or Cdc42 were normalized to total respective protein and presented as percentage of average of the water values. (H) Mice underwent 21 sessions of 10%CA and the DMS was harvested. Rac1-GTP pull-down assay was conducted on cell lysates and quantified using western blot. Rac1-GTP was normalized to total Rac1 and presented as percentage of average of water values. (I) Mice underwent intermittent access to 1% sucrose for 2 weeks and the DMS was harvested. Rac1-GTP pull-down assay was performed on cell lysates, and Rac1-GTP was normalized to total Rac1 and presented as average of water values. (J) Mice underwent 7 weeks of IA20%2BC and LIMK and cofilin phosphorylation in the DMS were examined using western blot analysis. The levels of phospho-LIMK (pLIMK) and phospho-Cofilin (pCofilin) were normalized to total respective protein and quantified as a percentage of the average of the water values. Data are represented as mean \pm SEM and analyzed using one-way ANOVA (C,D,F,J) with *post hoc* Šidák's multiple comparisons test, Kruskal-Wallis test (B, E, G), or unpaired two-tailed t-test (H,I). * $p < 0.05$, ** $p < 0.01$, *** $p < 0.001$; ns, non-significant. $n = 5-7$ per group.



Extended Figure 1.1-1. Rac1 is activated after 4 weeks of IA20%2BC in male mice

After 4 weeks of IA20%2BC, the DMS was harvested and Rac1-GTP pull-down assay was conducted on cell lysates. Levels of GTP-bound Rac1 were normalized to total Rac1 and presented as percentage of the average of the water values. Data are represented as mean \pm SEM and analyzed with an unpaired two-tailed t-test. * $p < 0.05$. $n = 4$ per group.

1.4.4 Alcohol activation of the LIMK/cofilin signaling pathway in the DMS depends on Rac1

The LIMK/cofilin signaling pathway can also be activated by other small G-proteins such as RhoA/B, Cdc42, and Rac3 (Edwards et al., 1999; Mira et al., 2000; Swanson et al., 2017). Thus, to confirm that the upregulation of LIMK and cofilin phosphorylation after excessive alcohol use is indeed due to the increase in Rac1 activity, we used a dominant negative Rac1 mutant to inhibit the activity of the endogenous protein. Specifically, the dominant negative mutant of Rac1 (Rac1-DN) contains a threonine to asparagine substitution at residue 17 (Worthylake et al., 2000). The Rac1 mutant forms a tight complex with Rac1-specific GEFs, but does not allow the exchange of GDP to GTP, keeping the G-protein constantly inactive (Ridley et al., 1992; Wong et al., 2006; Zhang et al., 2016) (**Figure 1.2A**). Rac1-DN was packaged into an adeno-associated virus (AAV). First, to confirm the inhibitory action of Rac1-DN, HEK293 cells were infected with AAV-Rac1-DN in media containing 1% serum (**Figure 1.2B**). Next, cells were incubated for 30 minutes with media containing 10% FBS. As shown in **Figure 1.2B**, incubation of cells with 10% FBS increased LIMK phosphorylation in non-infected cells, which was not observed in cells infected with AAV-Rac1-DN. In contrast, ERK1/2 whose phosphorylation does not depend on Rac1 was increased by 10% serum in both uninfected cells and AAV-Rac1-DN infected cells. These data suggest that AAV-Rac1-DN selectively inhibits Rac1 signaling in cultured cells.

Next, mice were bilaterally infected with AAV-Rac1-DN (3.5×10^{12} vg/ml) or an AAV-GFP (3.5×10^{12} vg/ml) control in the DMS. As shown in **Figure 1.2C-E**, intense and localized viral expression was detected in mice infected with AAV-Rac1-DN. We then

tested if Rac1 is required for alcohol-mediated LIMK and cofilin phosphorylation in the DMS. Three weeks after surgery, mice underwent 7 weeks of 1A20%2BC before dissection (**Figure 1.2F**). The DMS of mice infected with AAV-GFP or AAV-Rac1-DN were exposed to the same concentration of alcohol (**Table 1.1**). Global Rac1 protein level was significantly increased in the DMS of mice infected with AAV-Rac1-DN compared to mice infected with AAV-GFP (**Figure 1.2G**) (Two-way ANOVA: Effect of virus $F_{(1,20)} = 69.58$, $p < 0.0001$; Effect of alcohol $F_{(1,20)} = 6.774$, $p = 0.0170$; Effect of virus x alcohol $F_{(1,20)} = 0.2164$, $p = 0.6468$; *Post hoc* W+AAV-GFP vs. W+AAV-Rac1-DN $p < 0.0001$; A+AAV-GFP vs. A+AAV-Rac1-DN $p = 0.0001$). The phosphorylation of LIMK and cofilin were measured in the DMS of water- or alcohol-drinking mice infected with AAV-GFP or AAV-Rac1-DN. We observed a significant increase in the phosphorylation of LIMK and cofilin in AAV-GFP-infected animals during alcohol withdrawal (**Figure 1.2H-J, Table 1.1**) (Two-way ANOVA: pLIMK Effect of alcohol $F_{(1,20)} = 35.12$, $p < 0.0001$; *Post hoc*: Water+AAV-GFP vs. Alcohol+AAV-GFP $p < 0.0001$; pCofilin Effect of alcohol $F_{(1,20)} = 380.5$, $p < 0.0001$; *Post hoc*: Water+AAV-GFP vs. Alcohol+AAV-GFP $p < 0.0001$), which aligns with our prior results (**Figure 1.1J**). AAV-Rac1-DN overexpression had no effect on the phosphorylation of LIMK or cofilin in water-drinking animals (Two-way ANOVA: pLIMK Effect of virus $F_{(1,20)} = 58.01$, $p < 0.0001$; *Post hoc*: Water+AAV-GFP vs. Water+AAV-Rac1-DN $p = 0.3184$; pCofilin Effect of virus $F_{(1,20)} = 378.8$, $p < 0.0001$; *Post hoc*: Water+AAV-GFP vs. Water+AAV-Rac1-DN $p = 0.9679$). In contrast, overexpression of AAV-Rac1-DN significantly reduced alcohol-mediated phosphorylation of LIMK and cofilin (Two-way ANOVA: pLIMK Effect of virus x alcohol $F_{(1,20)} = 105.1$, $p < 0.0001$; *Post hoc*: Alcohol+AAV-GFP vs. Alcohol+AAV-Rac1-DN $p < 0.0001$; pCofilin Effect of virus x

alcohol $F_{(1,20)} = 423.8$, $p < 0.0001$; *Post hoc*: Alcohol+AAV-GFP vs. Alcohol+AAV-Rac1-DN $p < 0.0001$). These results suggest that the molecular consequences of Rac1 stimulation by alcohol in the DMS is the phosphorylation, and therefore activation, of LIMK and the phosphorylation of its substrate cofilin.

1.4.5 Alcohol promotes F-actin formation in the DMS via Rac1

We previously showed that chronic excessive alcohol intake increases F-actin assembly and decreases G-actin in the DMS (Laguesse et al., 2018). Phosphorylated cofilin is unable to cleave F-actin into G-actin (Bamburg, 1999). Therefore, we hypothesized that the consequence of the alcohol-mediated activation of the Rac1/LIMK/cofilin signaling is the formation of F-actin. To determine if actin remodeling in the DMS depends on Rac1 signaling, we examined the level of F-actin and G-actin in the DMS of mice that underwent 7 weeks of IA20%2BC or water and that were infected with AAV-GFP or AAV-Rac1-DN (**Figure 1.2F, Table 1.1**). Similar to previous findings (Laguesse et al., 2018), control mice infected with AAV-GFP in the DMS had a significantly higher level of F-actin after excessive chronic alcohol consumption in comparison to AAV-GFP-infected mice that drank water only (**Figure 1.2K-L, Table 1.1**) (Two-way ANOVA: Effect of alcohol $F_{(1,20)} = 101.6$, $p < 0.0001$; *Post hoc*: Water+AAV-GFP vs. Alcohol+AAV-GFP $p < 0.0001$). Conversely, mice infected with AAV-Rac1-DN had a significantly lower F-actin content in comparison to AAV-GFP mice both in the water- and alcohol-consuming groups (**Figure 1.2K-L, Table 1.1**) (Two-way ANOVA: Effect of virus $F_{(1,20)} = 105.4$, $p < 0.0001$; *Post hoc*: Water+AAV-GFP vs. Water+AAV-Rac1-DN $p = 0.0199$; Alcohol+AAV-GFP vs. Alcohol+AAV-Rac1-DN $p < 0.0001$). In addition, the

magnitude of the difference in F-actin levels is greater between alcohol-drinking AAV-GFP and AAV-Rac1-DN mice compared to water-only animals (**Figure 1.2K-L, Table 1.1**) (Two-way ANOVA: Effect of virus x alcohol $F_{(1,20)} = 30.92$, $p < 0.0001$). Overexpression of AAV-Rac1-DN had no effect on the level of G-actin in the water-only group (**Figure 1.2K, Figure 1.2M**). However, G-actin levels were reduced by alcohol in mice infected with AAV-GFP, which was reversed by overexpression of AAV-Rac1-DN (**Figure 1.2K, Figure 1.2M, Table 1.1**) (Two-way ANOVA: Effect of virus $F_{(1,20)} = 7.585$, $p = 0.0122$; Effect of alcohol $F_{(1,20)} = 12.30$, $p = 0.0022$; Effect of virus x alcohol $F_{(1,20)} = 11.73$, $p = 0.0027$; *Post hoc*: Water+AAV-GFP vs. Alcohol+AAV-GFP $p = 0.0005$; Water+AAV-Rac1-DN vs. Alcohol+AAV-GFP $p = 0.0016$; Alcohol+AAV-GFP vs. Alcohol+AAV-Rac1-DN $p = 0.0018$). Therefore, these data suggest that the alcohol-mediated increase in F-actin assembly in the DMS depends on Rac1.

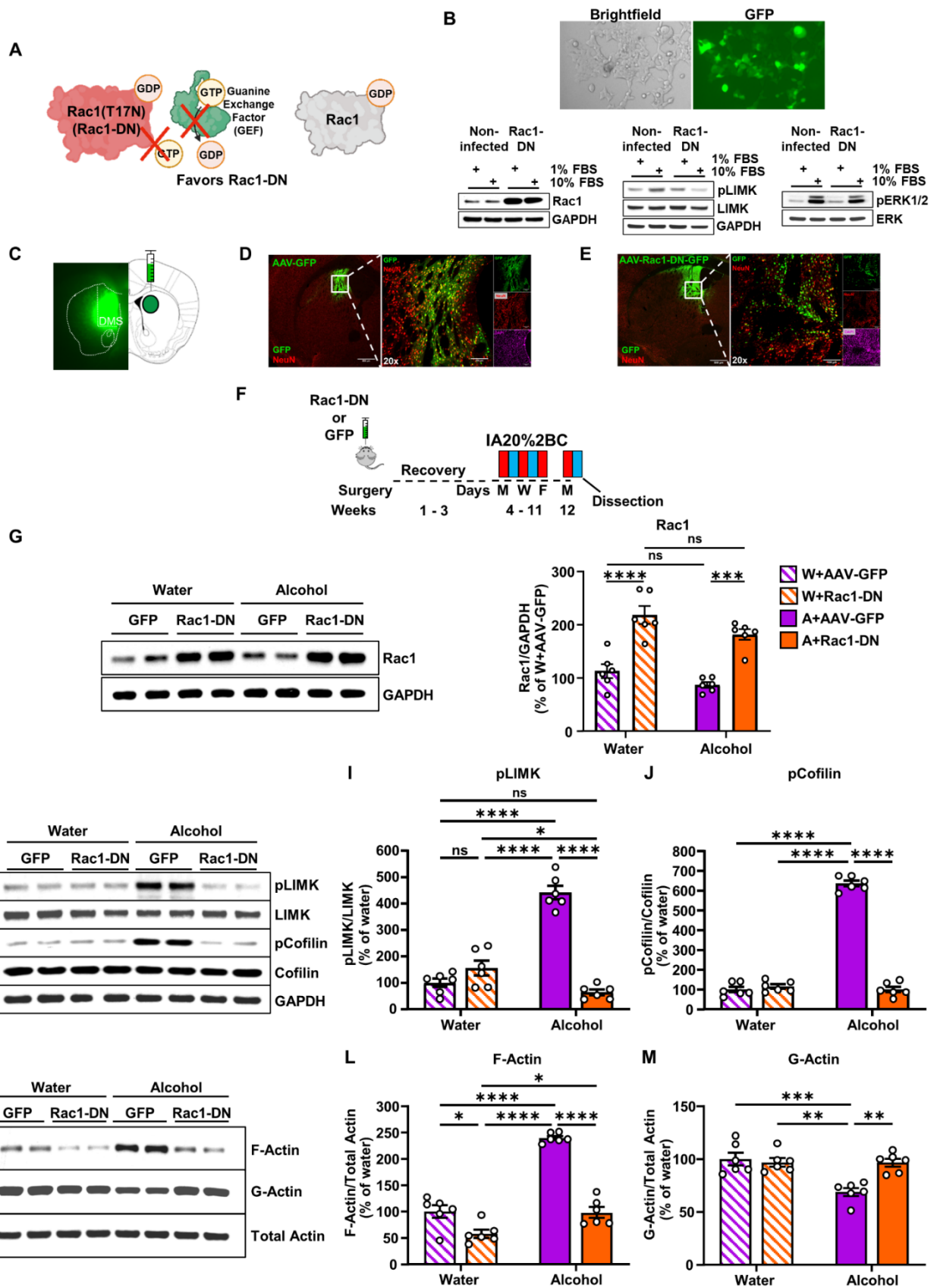


Figure 1.2. Alcohol activation of the LIMK/cofilin signaling pathway and subsequent F-actin formation in the DMS depends on Rac1

Figure 1.2. Alcohol activation of the LIMK/cofilin signaling pathway and subsequent F-actin formation in the DMS depends on Rac1

(A) Rac1-DN mechanism of action. Rac1-DN has a mutation in its P-loop and does not bind GTP. GEFs bind to Rac1-DN but are unable to exchange GDP for GTP. The GEFs remain bound to Rac1-DN and ignore endogenous Rac1. **(B)** HEK293 cells infected with AAV-Rac1-DN imaged in both brightfield and GFP to detect viral infection (2X magnification). Western blot analysis of Rac1 protein, phospho-LIMK, and phosphorylation of ERK1/2 in non-infected cells and cells infected with AAV-Rac1-DN after stimulation with 10% FBS. **(C)** Confirmation of viral overexpression during dissection on the DMS of a mouse infected with AAV-Rac1-DN. 2X image from EVOS FL tabletop fluorescent microscope. **(D-E)** Left images (4X magnification) depict the specificity of the infection site for AAV-GFP **(D)** and AAV-Rac1-DN **(E)**, scale bar 500 μ m. Right images (20X magnification) depict solely neurons infected in the DMS by both AAV-GFP **(D)** and AAV-Rac1-DN **(E)**, scale bar 100 μ m. Each slice is stained with anti-GFP (green) and anti-NeuN (red) antibodies, along with DAPI (magenta). **(F)** Experimental timeline. Mice received bilateral infusion of AAV-Rac1-DN or AAV-GFP in the DMS and were allowed 3 weeks for overexpression. After IA20%2BC or water only for 7 weeks the DMS was harvested. **(G)** Mice were infected with AAV-GFP or AAV-Rac1-DN before undergoing IA20%2BC. The DMS was harvested, and total Rac1 protein level was examined using western blot and normalized to GAPDH. Data are presented as mean \pm SEM and analyzed using two-way ANOVA with *post hoc* Šidák's multiple comparisons test. *** $p < 0.001$ **** $p < 0.0001$; ns, non-significant. $n = 6$ per group. **(H-J)** Phosphorylation of LIMK and cofilin were examined using western blot analysis. Levels of pLIMK and pCofilin were normalized to total respective protein and quantified as a percentage of AAV-GFP-infected, water-only animals. Data are represented as mean \pm SEM and analyzed by two-way ANOVA with *post hoc* Šidák's multiple comparisons test. * $p < 0.05$, **** $p < 0.0001$; ns, non-significant. $n = 6$ per group. **(K-M)** G-actin/F-actin assay was conducted on the DMS of mice after overexpression surgery and IA20%2BC or water-only drinking. The filamentous (F) or globular (G) actin contents were examined using western blot analysis and normalized to total actin and quantified as a percentage of AAV-GFP-infected, water-only animals. Data represented as mean \pm SEM and analyzed using two-way ANOVA with Šidák's multiple comparison. * $p < 0.05$, ** $p < 0.01$, *** $p < 0.001$, **** $p < 0.0001$; ns, non-significant. $n = 6$ per group.

1.4.6 Rac1 signaling is activated after voluntary and involuntary alcohol exposure in the central amygdala

After observing that the increased phosphorylation of cofilin is reliant on the alcohol-dependent activation of Rac1 in the DMS, we continued to use the phosphorylation of cofilin to examine other brain subregions where Rac1 may be involved in alcohol-induced molecular mechanisms. One region of particular interest was the amygdala. The amygdala's primary function is emotional processing, such as fear, anxiety, and reward, of sensory inputs (Duvarci and Pare, 2014; Janak and Tye, 2015). The amygdala is divided into the basolateral amygdala (BLA) and the central amygdala (CeA), which are differentiated by having principally glutamatergic (90%) neurons or GABAergic (95%) neurons, respectively (Tye et al., 2011). The CeA is the primary output region of the amygdala, mediating autonomic and behavioral responses to fear and anxiety (Tye et al., 2011). The amygdala, and specifically the CeA, plays an important role in AUD. Anxiety often co-occurs with AUD (Anker and Kushner, 2019). Subjects suffering from AUD consume alcohol to alleviate negative symptoms, including anxiety (Khantzian, 1985; Castillo-Carniglia et al., 2019). In alcohol-dependent subjects, there is a reduction in amygdala volume alongside an association with increased alcohol craving and intake (Wrase et al., 2008). This correlation has also been identified in families with a high density of alcoholism (Hill et al., 2001). The amygdala, and more specifically the CeA, is implicated in the withdrawal stage and relapse (Koob and Volkow, 2010) and is associated with compulsive drinking (Vandaele and Ahmed, 2021).

To determine whether Rac1 was activated in the amygdala of mice chronically drinking alcohol, mice underwent 7 weeks of IA20%2BC (**Figure 1.3A**) and punches of

each amygdala subregion were taken after binge and withdrawal. We observed a significant increase in the phosphorylation of cofilin in the CeA at both binge and withdrawal timepoints (**Figure 1.3B**) (One-way ANOVA: Effect of alcohol $F_{(2,6)} = 61.24$, $p = 0.0001$; *Post hoc W vs. B* $p = 0.0002$; *W vs. WD* $p = 0.0003$; *B vs. WD* $p = 0.8510$). Interestingly, there was no change in cofilin phosphorylation in the BLA (**Figure 1.3B**).

As the CeA is often associated with alcohol-associated behaviors following heavy drinking, such as withdrawal-induced anxiety (Khantzian, 1985; Castillo-Carniglia et al., 2019), we next tested if high levels of involuntary alcohol exposure elicit the same effects on Rac1 signaling in the CeA. Mice underwent chronic intermittent exposure (CIE) to alcohol vapor, being exposed to alcohol vapor concentrations between 12-18 mg alcohol/L of air for 16 hr/day followed by 8 hr withdrawal periods for 4 consecutive days/week for 2 weeks (**Figure 1.3C**). Control mice had exposure to air only for the same duration of time. Prior to being placed in the chamber, mice were injected with a dose of alcohol (1.6g/kg, i.p.) and pyrazole (1 mmol/kg, i.p) to stabilize blood alcohol concentration (BAC) within the group. The air-only group received only pyrazole. Alcohol chamber vapor concentrations were tested twice daily to ensure correct dosing and BAC was measured weekly. At time of sacrifice, after 2 weeks of CIE, the paradigm produced an average BAC of 189.14 ± 39.14 mg/dl. The CeA and BLA were dissected at the end of the final exposure session (**Figure 1.3C**) and the phosphorylation of cofilin was measured using western blot. We observed a significant increase in the phosphorylation of cofilin in the CeA, but not the BLA (**Figure 1.3D**), aligning with the IA20%2BC results (Welch's t-test: $t_{5,405} = 2.612$, $p = 0.0441$).

These results exhibit another subregion-specific activation of Rac1 signaling in response alcohol exposure. Furthermore, taken together, the analogous results after IA20%2BC and CIE suggest that alcohol exposure and subsequent withdrawal are sufficient to elicit the activation of Rac1 signaling in this region.

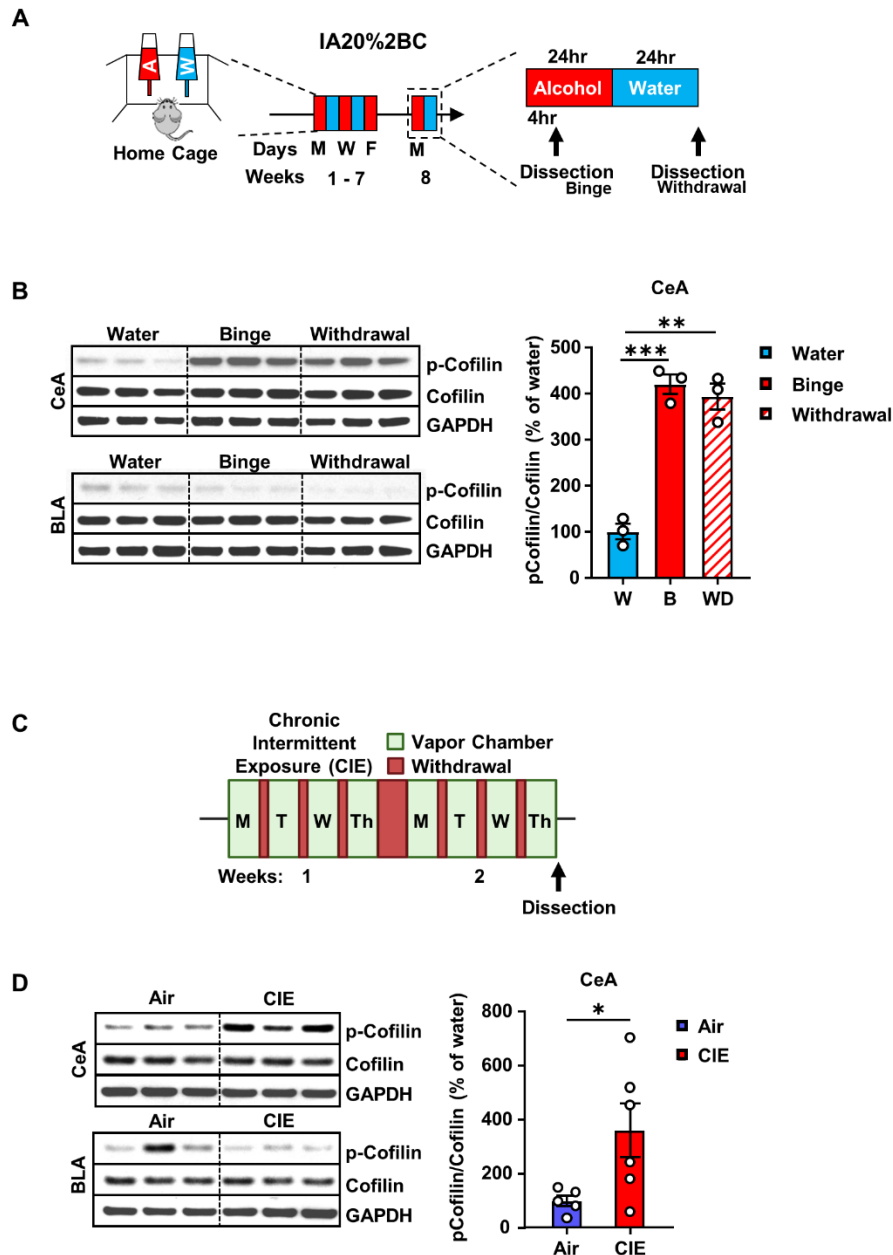


Figure 1.3. Rac1 signaling is activated after voluntary and involuntary alcohol exposure in the central amygdala

(A) Intermittent access to 20% alcohol in 2-bottle-choice (IA20%2BC) experimental timeline. (B) Phosphorylation of LIMK and cofilin in the CeA and the BLA were examined using western blot analysis. Levels of pLIMK and pCofilin were normalized to total respective protein and quantified as a percentage of water controls. Data are presented as mean \pm SEM and analyzed using one-way ANOVA with *post hoc* Šidák's multiple comparisons test. ** $p < 0.001$ *** $p < 0.001$; ns, non-significant. $n = 3$ per group. (C) Chronic intermittent exposure to alcohol (CIE) experimental timeline. Mice were exposed to (figure caption continued on next page)

(figure caption continued from previous page)

alcohol overnight for 16-hour sessions with an 8-hour withdrawal period in between for four days a week. This was repeated for 2 weeks, separated by a 72-hour withdrawal period. The CeA and BLA were harvested at the end of the final exposure.

(D) Phosphorylation of cofilin in the CeA and BLA was measured using western blot and normalized to total protein, quantified as a percentage of air controls. Data are presented as mean \pm SEM and analyzed using Welch's t-test. * $p < 0.05$. $n = 6$ per group.

1.4.7 Rac1 promotes the remodeling of dendritic arbors in the DMS

F-actin is responsible for morphological remodeling in neurons (Honkura et al., 2008; Chazeau and Giannone, 2016; Costa et al., 2020). Previously, we showed that alcohol consumption increases dendritic branch complexity in DMS medium spiny neurons (MSNs) (Wang et al., 2015; Laguesse et al., 2018). Since alcohol leads to F-actin formation via Rac1, we hypothesized that the increase in dendritic branching after alcohol use is mediated via Rac1 signaling. To test this possibility, the DMS of mice that were subjected to IA20%2BC or water only was infected with a low titer of AAV-Rac1-DN or AAV-GFP (7×10^9 - 3.5×10^{10} vg/ml). The goal was to infect a sparse population of neurons to allow for imaging of individual arbors (**Figure 1.4A**). Low-titer infection of Rac1-DN did not alter alcohol consumption (**Table 1.1**). Sholl analysis (Sholl, 1953) was then performed on the DMS of water- or alcohol-drinking mice infected with AAV-GFP or AAV-Rac1-DN (**Figure 1.4B-C**).

Similar to our prior findings (Wang et al., 2015; Laguesse et al., 2018), we found that alcohol significantly increased the complexity of dendritic trees of DMS MSNs (**Figure 1.4D**) (Three-way ANOVA: Effect of alcohol x distance $F_{(15,270)} = 5.227$, $p < 0.0001$). Specifically, DMS dendrites 30-80 μ m from the soma exhibited significantly more intersections in alcohol-drinking vs. water-only-drinking mice (**Figure 1.4D**) (Two-way ANOVA: Effect of alcohol $F_{(1, 20)} = 9.063$, $p < 0.0001$, *Post hoc Šidák's multiple comparisons test Water vs. Alcohol*). The increase in dendritic complexity was further quantified by calculating the area under the curve (AUC) (**Figure 1.4E**) (Two-way ANOVA: Effect of alcohol $F_{(1, 18)} = 7.932$, $p = 0.0114$). In addition, we observed that dendritic length (**Figure 1.4F**), the number of branching points (**Figure 1.4G**), and the

number of ending points (**Figure 1.4H**), were also increased by alcohol (Two-way ANOVA: Effect of alcohol Dendritic Length $F_{(1, 18)} = 8.247$, $p = 0.0101$; Branching points $F_{(1, 18)} = 4.050$, $p = 0.0594$; Ending points $F_{(1,18)} = 4.759$, $p = 0.0426$).

In contrast, infection of the DMS with AAV-Rac1-DN significantly reduced dendritic arborization (**Figure 1.4D**) (Three-way ANOVA: Effect of virus x distance $F_{(15, 270)} = 4.890$, $p < 0.0001$). Specifically, the number of dendritic intersections 30-80 μ m from the soma was significantly decreased when DMS neurons were infected with AAV-Rac1-DN as compared to neurons infected with AAV-GFP (**Figure 1.4D**) (Two-way ANOVA of consolidated data: Effect of virus $F_{(1, 20)} = 10.71$, $p = 0.0038$, *Post hoc Šídák's multiple comparisons test, AAV-GFP vs. AAV-Rac1-DN*). Furthermore, AAV-Rac1-DN infection significantly decreased AUC (**Figure 1.4E**), along with dendritic length, branching points, and ending points (**Figure 1.4F-H**) (Two-way ANOVA: Effect of virus AUC $F_{(1, 18)} = 8.754$, $p = 0.0084$, Dendritic length $F_{(1, 18)} = 9.186$, $p = 0.0072$, Branching points $F_{(1, 18)} = 7.551$, $p = 0.0132$, Ending points $F_{(1, 18)} = 9.030$, $p = 0.0076$). However, there was no interaction between the variables (Three-way ANOVA: Effect of alcohol x virus x distance $F_{(15,270)} = 0.2661$, $p = 0.9975$; Two-way ANOVA: Effect of alcohol x virus AUC $F_{(1,18)} = 0.0005846$, $p = 0.9810$, Dendritic length $F_{(1,18)} = 0.004819$, $p = 0.9454$, Branching points $F_{(1,18)} = 0.005694$, $p = 0.9407$, Ending points $F_{(1,18)} = 0.06334$, $p = 0.8041$).

Next, we examined the number of branches per dendritic order (**Figure 1.4I**). Three-way ANOVA showed a significant main effect of virus ($F_{(1,18)} = 7.859$, $p = 0.0117$) and a significant main effect of alcohol ($F_{(1,18)} = 4.921$, $p = 0.0396$) but no interaction between virus and alcohol ($F_{(1,18)} = 0.2476$, $p = 0.6248$). Next, the number of branches

was analyzed for each order. Two-way ANOVA showed a significant main effect of virus at 3rd and 4th order, and a significant main effect of alcohol at 4th order (**Figure 1.4I**).

Together, these data confirmed that chronic excessive alcohol use significantly increases the complexity of dendritic branching in DMS MSNs (Wang et al., 2015; Laguesse et al., 2018). Importantly, we show that Rac1 contributes to dendritic branching in DMS neurons.

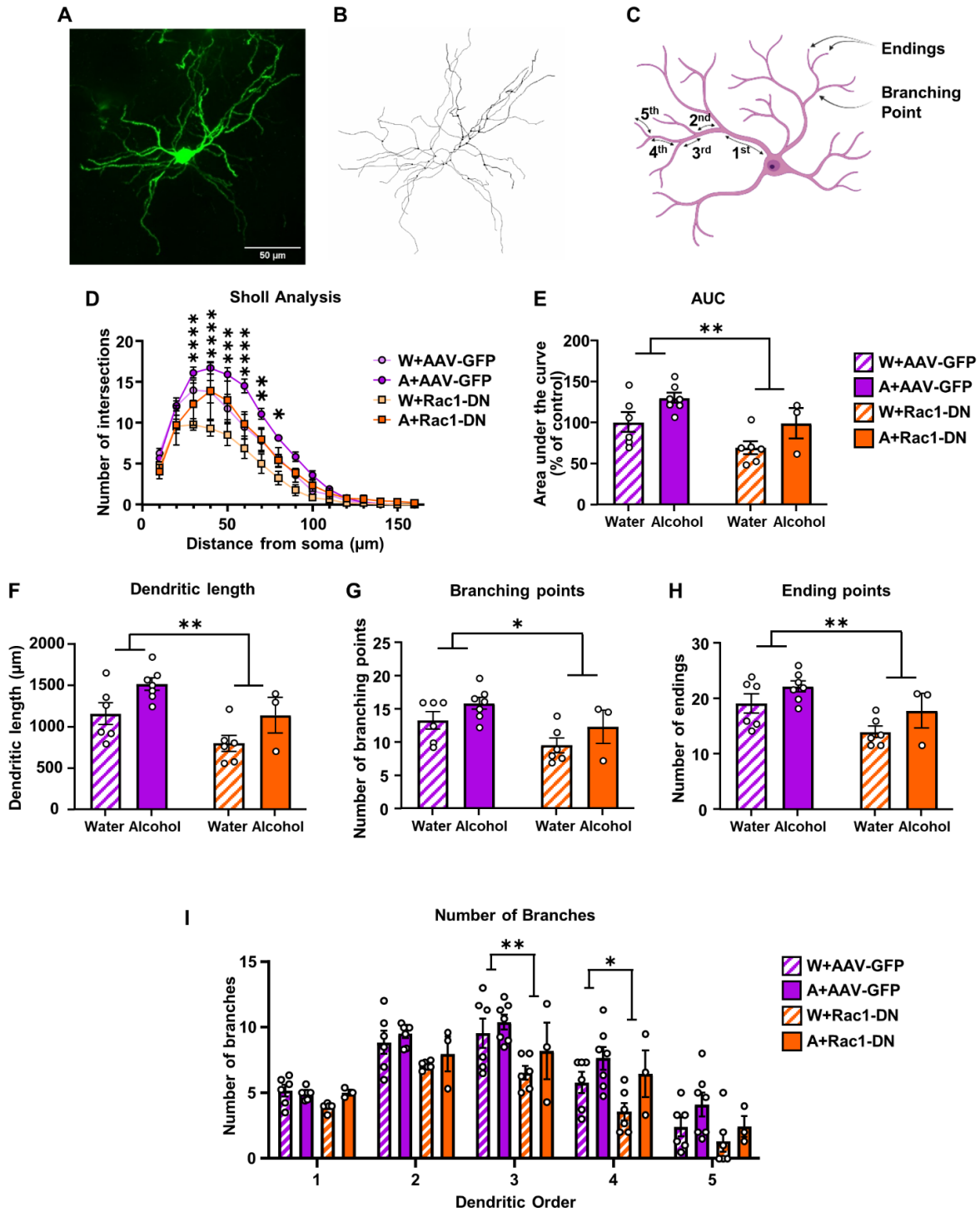


Figure 1.4. Rac1 promotes remodeling of dendritic arbors in the DMS

Low titer of AAV-GFP or AAV-Rac1-DN (7×10^9 - 3.5×10^{10} vg/ml) was infused bilaterally into the DMS. After 1 week of recovery, mice underwent 7 weeks of IA20%2BC. Mice consuming water only were used as control. Twenty-four hours after the last drinking (figure caption continued on next page)

(figure caption continued from previous page)

session, mice were perfused and brains were sliced into 100 μ m sections before MSN morphology was analyzed. **(A)** Sample image (40X magnification) of a GFP-positive DMS MSN. Scale bar, 50 μ m. **(B)** Example of the reconstruction of the GFP-positive neuron. **(C)** Scheme of the morphological parameters measured in each neuron. Dendritic order increased after each branching point, defined as a dendritic intersection. **(D, E)** Analysis of neuronal dendritic arborization. Sholl analysis was performed on reconstructed neurons. The number of intersections was analyzed for each point **(D)** and the area under the curve (AUC) **(E)** was calculated. **(F)** Measurement of total dendritic length. **(G)** Number of branching points. **(H)** Number of ending points. **(I)** Number of branches per dendritic order. Data are represented as mean \pm SEM and analyzed by two-way ANOVA. Main effect of virus is represented graphically. * $p < 0.05$, ** $p < 0.01$, *** $p < 0.001$. Water+AAV-GFP: 19 neurons from 6 mice; Alcohol+AAV-GFP: 23 neurons from 7 mice; Water+AAV-Rac1-DN: 15 neurons from 6 mice, Alcohol+AAV-Rac1-DN: 10 neurons from 3 mice.

1.4.8 Rac1 in the DMS is required for the alcohol-mediated alteration in dendritic spine morphology

Actin is the major structural protein in the post-synaptic density (PSD) (Ratner and Mahler, 1983). Actin cytoskeleton organization directly controls dendritic spine morphology (Schubert and Dotti, 2007; Hotulainen and Hoogenraad, 2010; Basu and Lamprecht, 2018). Rac1 signaling controls actin dynamics and is involved in dendritic spine morphogenesis (Bosco et al., 2009; Haditsch et al., 2009; Haditsch et al., 2013; Costa et al., 2020). Since Rac1 is activated by alcohol which in turn promotes F-actin assembly we hypothesized that the dendritic spines in the DMS are altered by alcohol in a Rac1-dependent manner.

Next, we examined the shape of individual dendritic spines on distal dendritic branches (3rd or 4th order) in mice infected with AAV-GFP and AAV-Rac1-DN in DMS and that consumed 20% alcohol or water only for 7 weeks (**Figure 1.5A**). Spine density (spine number per 10 μ m) was unaffected by alcohol drinking or AAV-Rac1-DN infection (**Figure 1.5B**) (Two-way ANOVA: Effect of virus $F_{(1,15)} = 0.1118$, $p = 0.7428$; Effect of alcohol $F_{(1,15)} = .01518$, $p = 0.9036$; Effect of virus x alcohol $F_{(1,15)} = 1.150$, $p = 0.3006$).

We found that in control mice infected with AAV-GFP, alcohol drinking significantly increased dendritic spine area, aligning with prior findings (Laguesse et al., 2018) (Two-way ANOVA: Effect of alcohol $F_{(1,15)} = 27.17$, $p = 0.0001$) (**Figure 1.5C**). Alcohol drinking also significantly increased dendritic spine volume (Two-way ANOVA: Effect of alcohol $F_{(1,15)} = 21.79$, $p = 0.0003$) (**Figure 1.5D**). Both spine length (**Figure 1.5E**) and average spine head width (**Figure 1.5F**) were significantly increased by alcohol drinking (Two-way

ANOVA: Spine Length Effect of alcohol $F_{(1,15)} = 4.617$, $p = 0.0484$; Head Width Effect of alcohol $F_{(1,15)} = 10.69$, $p = 0.0052$).

In contrast, the alcohol-mediated alterations in dendritic spine morphology were attenuated by Rac1 inhibition. Specifically, Rac1 inhibition significantly decreased dendritic spine area in alcohol-drinking animals, without affecting water-only controls. **(Figure 1.4C)** (Two-way ANOVA: Effect of virus $F_{(1,15)} = 14.86$, $p = 0.0016$; Effect of virus x alcohol $F_{(1,15)} = 6.075$, $p = 0.0263$; *Post hoc Šídák's multiple comparisons test: W+AAV-GFP vs. A+AAV-GFP* $p = 0.0003$, *A+AAV-GFP vs. W+Rac1-DN* $p < 0.0001$, *A+AAV-GFP vs. A+AAV-Rac1-DN* $p = 0.0029$, *W+AAV-Rac1-DN vs. A+AAV-Rac1-DN* $p = 0.2739$). The alcohol-mediated increase in dendritic spine volume was also prevented by Rac1-DN, without affecting water-only controls **(Figure 1.5D)** (Two-way ANOVA: Effect of virus $F_{(1,15)} = 9.634$, $p = 0.0073$; Effect of virus x alcohol $F_{(1,15)} = 6.172$, $p = 0.0253$; *Post hoc Šídák's multiple comparisons test: W+AAV-GFP vs. A+AAV-GFP* $p = 0.0005$, *A+AAV-GFP vs. W+Rac1-DN* $p = 0.0002$, *A+AAV-GFP vs. A+AAV-Rac1-DN* $p = 0.0078$, *W+AAV-Rac1-DN vs. A+AAV-Rac1-DN* $p = 0.4614$). In addition, we found that AAV-Rac1-DN slightly reduced spine length independent of drinking **(Figure 1.5E)**, and decreased spine head width **(Figure 1.5F)** (Two-way ANOVA: Spine Length Effect of virus $F_{(1,15)} = 10.99$, $p = 0.0047$; Effect of virus x alcohol $F_{(1,15)} = 0.5682$, $p = 0.4626$; Head Width Effect of virus $F_{(1,15)} = 5.064$, $p = 0.0399$; Effect of virus x alcohol $F_{(1,15)} = 3.728$, $p = 0.0726$; *Post hoc Šídák's multiple comparisons test: W+AAV-GFP vs. A+AAV-GFP* $p = 0.0086$, *W+AAV-Rac1-DN vs. A+AAV-Rac1-DN* $p = 0.7946$). Length-to-width ratio was not affected by alcohol or Rac1 inhibition alone, but a combination of these factors **(Figure 1.5G)** (Two-way ANOVA: Effect of alcohol $F_{(1,15)} = 1.285$, $p = 0.2748$; Effect of virus $F_{(1,15)}$

= 0.01974, $p = 0.8901$; Effect of virus x alcohol $F_{(1,15)} = 5.418$, $p = 0.0343$). Together, these findings suggest that Rac1 contributes to the alcohol-mediated increases in dendritic spine area, volume, and length-to-width ratio, while also directly affecting spine length and head width.

We then examined whether alcohol-mediated activation of Rac1 signaling and the increase in F-actin content was responsible for the maturation of DMS MSN dendritic spines. Dendritic spines are classed into four subtypes: filipodia, thin, stubby, and mushroom, with filopodia being the least mature form of spines and mushrooms being the most mature form (Kasai et al., 2003). Spines are characterized by different shape, with primary variables being spine length, neck, and head width (Kasai et al., 2003). Like our previous study (Laguesse et al., 2018), we found that alcohol drinking increased the maturity of dendritic spines in the DMS. Specifically, we found that in AAV-GFP infected mice, alcohol significantly increased the proportion of mushroom-shaped spines at the expense of thin spines, while not affecting filopodia or stubby spines (**Figure 1.5H**). Rac1 inhibition blocked the alcohol-mediated increase in mushroom spines and decrease in thin spines but had no effect on animals drinking water only (**Figure 1.5H**) (Three-way ANOVA: Effect of virus $F_{(1, 15)} = 2.745$, $p = 0.1183$; Effect of alcohol $F_{(1, 15)} = 0.003263$, $p = 0.9552$; Spine type $F_{(3, 45)} = 304.5$, $p < 0.0001$; Effect of virus x spine type $F_{(3, 45)} = 16.83$, $p < 0.0001$; Effect of alcohol x spine type $F_{(3, 45)} = 4.052$, $p = 0.0124$, Effect of virus x alcohol x spine type $F_{(3, 45)} = 13.08$, $p < 0.0001$; *Post hoc Šidák's multiple comparisons test: Thin: W+AAV-GFP vs. A+AAV-GFP $p = 0.0018$, A+AAV-GFP vs. W+AAV-Rac1-DN $p < 0.0001$, A+AAV-GFP vs. A+AAV-Rac1-DN $p < 0.0001$; Mushroom: W+AAV-GFP vs. A+AAV-GFP $p = 0.0082$, A+AAV-GFP vs. W+AAV-Rac1-DN $p = 0.0304$, A+AAV-GFP vs.*

A+AAV-Rac1-DN $p = 0.0123$). Together, our data suggest that Rac1 signaling is responsible for the alcohol-mediated morphological changes in dendritic spine structure and maturation in DMS MSNs.

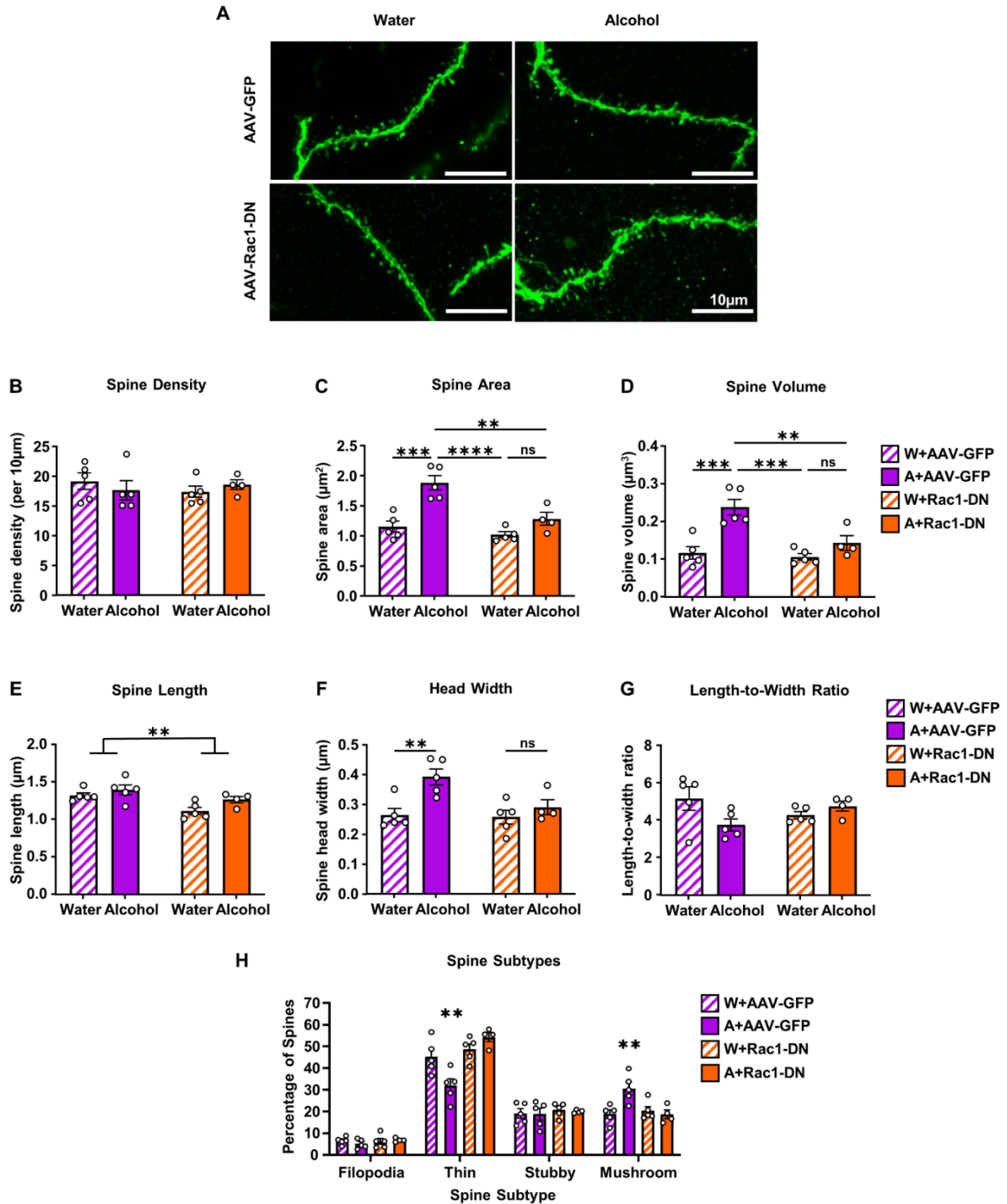


Figure 1.5. Rac1 in the DMS is required for the alcohol-mediated morphological changes in dendritic spines

Low titer of AAV-GFP or AAV-Rac1-DN (7×10^9 - 3.5×10^{10} vg/ml) was infused bilaterally into the DMS. After 1 week of recovery, mice underwent 7 weeks of IA20%-2BC. Mice consuming water only were used as control. Twenty-four hours after the last drinking (figure caption continued on next page)

(figure caption continued from previous page)

session, mice were perfused, and MSN dendritic spine morphology was analyzed. **(A)** Sample image of a GFP-positive DMS MSN (100X magnification) from each group. Scale bar, 10 μm . **(B)** Average dendritic spine density (number of spines/10 μm). **(C)** Average dendritic spine area (μm^2). **(D)** Average dendritic spine volume (μm^3). **(E)** Average dendritic spine length (μm). **(F)** Average diameter of dendritic spine heads (μm). **(G)** Dendritic spine length-to-width ratio. Data is represented as mean \pm SEM and analyzed using two-way ANOVA and Šidák's *post hoc* multiple comparisons test. * $p < 0.05$, ** $p < 0.01$, *** $p < 0.001$. **** $p < 0.0001$. **(H)** Percentage of filopodia, thin, stubby, and mushroom dendritic spines for water- and alcohol-drinking mice infected with either AAV-GFP or AAV-Rac1-DN. Three-way ANOVA and Šidák's *post hoc* multiple comparisons test. **** $p < 0.0001$. Water+AAV-GFP: 14 neurons from 5 mice; Alcohol+AAV-GFP: 13 neurons from 5 mice; Water+AAV-Rac1-DN: 14 neurons from 5 mice; Alcohol+AAV-Rac1-DN: 11 neurons from 4 mice.

1.4.9 Rac1 does not play a role in the development and maintenance of voluntary alcohol intake

Next, we set to determine if the alcohol-dependent, Rac1-mediated molecular and cellular changes have consequences on alcohol-related behaviors. First, we tested the effect of Rac1 inhibition on the development of excessive alcohol drinking. To do so, the DMS of mice was bilaterally infused with AAV-Rac1-DN or AAV-GFP (3.5×10^{12} vg/ml). After allowing for three weeks of recovery, animals underwent IA20%2BC for 7 weeks and drinking and preference were measured (**Figure 1.6A**). We found that there was no difference in alcohol consumption in the group with overexpressed AAV-Rac1-DN in the DMS compared to AAV-GFP controls (**Figure 1.6B**) (RM Two-way ANOVA: Effect of virus $F_{(1,17)} = 0.08351$, $p = 0.7761$; Effect of session $F_{(6, 102)} = 5.420$, $p < 0.0001$; Effect of virus x session $F_{(6, 102)} = 0.1339$, $p = 0.9916$). Water drinking was also unaltered (**Figure 1.6C**). RM Two-way ANOVA: Effect of virus $F_{(1,17)} = 0.4571$, $p = 0.5081$; Effect of session $F_{(6,102)} = 3.855$, $p = 0.0017$; Effect of virus x session $F_{(6,102)} = 0.8631$, $p = 0.5248$). As a result, alcohol preference was also unchanged (**Figure 1.6D**) (RM Two-way ANOVA: Effect of virus $F_{(1,17)} = 0.1798$, $p = 0.6768$; Effect of session $F_{(6, 102)} = 3.196$, $p = 0.0065$; Effect of virus x session $F_{(6, 102)} = 0.4250$, $p = 0.8608$).

Next, we determined the potential contribution of Rac1 to the maintenance of alcohol-drinking behavior. Mice were first subjected to the IA20%2BC paradigm for 7 weeks. Experimental and control groups were balanced based on drinking average. Mice underwent surgery to overexpress AAV-Rac1-DN, or AAV-GFP as a control, in the DMS. IA20%2BC was then resumed for 4 weeks and alcohol drinking was evaluated (**Figure 1.6E**). Overexpression of AAV-Rac1-DN did not alter the maintenance of alcohol drinking

(Figure 1.6F) (RM Two-way ANOVA: Effect of virus $F_{(1,14)} = 2.454$, $p = 0.1396$; Effect of session $F_{(3,42)} = 1.262$, $p = 0.2998$; Effect of virus x session $F_{(3,42)} = 0.5923$, $p = 0.6235$). Water consumption was similarly unchanged (**Figure 1.6G**) (RM Two-way ANOVA: Effect of virus $F_{(1,13)} = 0.8287$, $p = 0.3792$; Effect of session $F_{(3,39)} = 3.606$, $p = 0.0216$; Effect of virus x session $F_{(3,39)} = 0.1149$, $p = 0.9508$), leading to similar alcohol preference between the group (**Figure 1.6H**) (RM Two-way ANOVA: Effect of virus $F_{(1,14)} = 2.520$, $p = 0.1347$; Effect of session $F_{(3,42)} = 0.7839$, $p = 0.5096$; Effect of virus x session $F_{(3,42)} = 0.7518$, $p = 0.5275$). Together, these results suggest that Rac1 in the DMS does not contribute to the development or maintenance of voluntary alcohol drinking in the IA20%2BC paradigm.

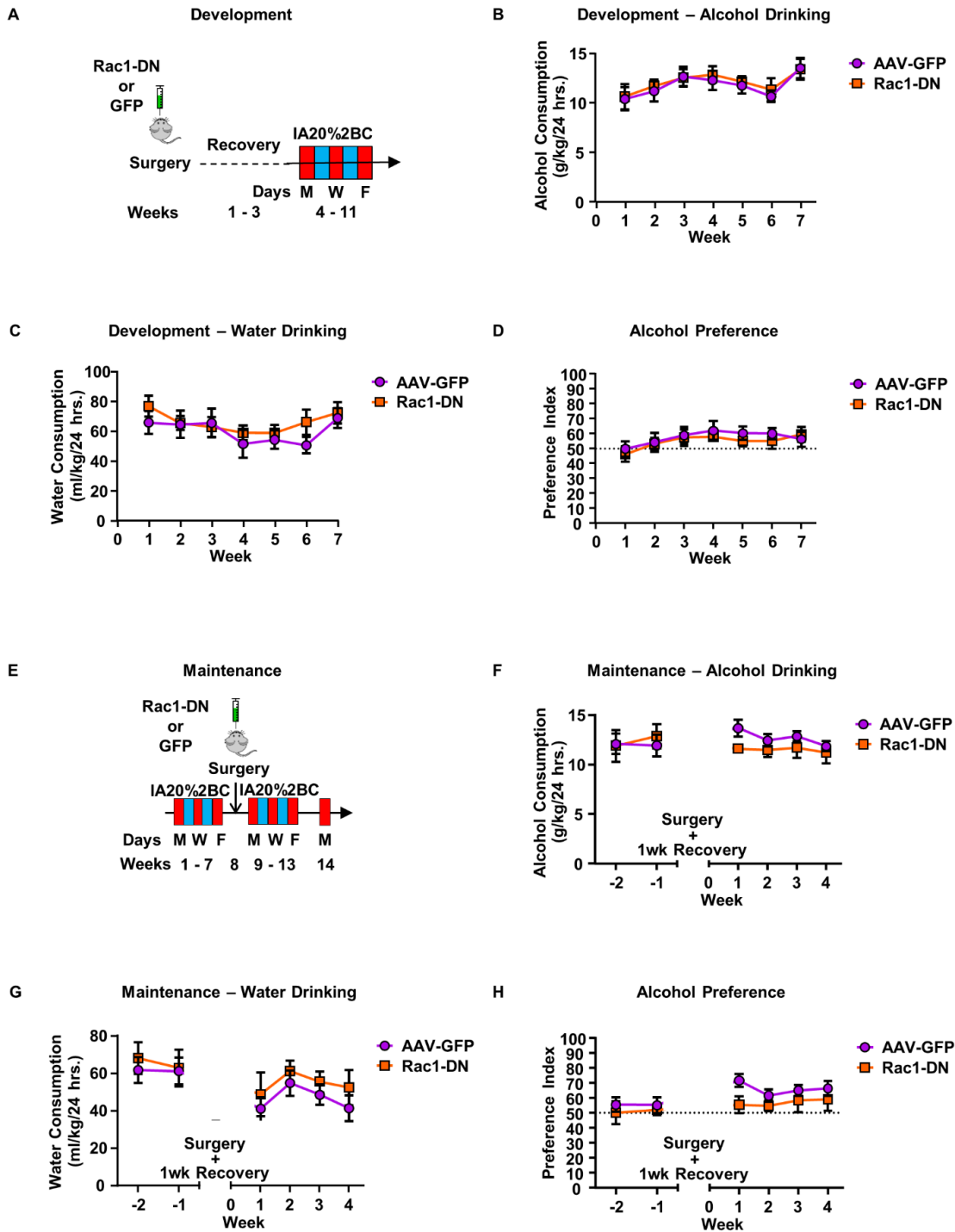


Figure 1.6. Rac1 does not play a role in the development and maintenance of voluntary alcohol intake

(A) Development: Surgery and IA20%2BC timeline. Mice received a bilateral, dual-infusion of AAV-Rac1-DN or AAV-GFP as a control. After 3 weeks of recovery, IA20%2BC began and continued for 7 weeks. (B) Weekly average alcohol consumption (g/kg/24hrs.) (figure caption continued on next page)

(figure caption continued from previous page)
of development drinking mice. **(C)** Water consumption averages for the IA20%2BC development drinking groups. **(D)** Preference for alcohol during the development IA20%2BC drinking, with an index above 50 indicating a preference for alcohol. **(E)** Maintenance: Surgery and IA20%2BC timeline. Mice first underwent IA20%2BC for 7 weeks. Groups were balanced based on average daily alcohol consumption in last 6 drinking sessions. Mice received a bilateral, dual-infusion of AAV-Rac1-DN or AAV-GFP as a control and were allowed one full week for recovery. IA20%2BC resumed for 4 weeks. **(F)** Weekly average consumption (g/kg/24hrs.) for maintenance drinking mice. **(G)** Water consumption average for maintenance drinking mice. **(H)** Preference for alcohol for maintenance-drinking mice. All data represented as mean \pm SEM and analyzed with two-way ANOVA with repeated measures. n = 9-10.

1.4.10 Rac1 in the DMS is required for alcohol-associated goal-directed learning

We observed that the activation of Rac1 signaling after chronic excessive alcohol use was specific to the DMS, a brain region that is associated with goal-directed learning (Dolan and Dayan, 2013; Shan et al., 2014). As goal-directed behavior is particularly important for drug seeking (Singer et al., 2018), we hypothesized that Rac1 in the DMS may play a role in alcohol-associated goal-directed learning.

To examine this hypothesis, the DMS of mice was bilaterally infused with AAV-Rac1-DN or AAV-GFP (3.5×10^{12} vg/ml). Mice were allowed 3 weeks to recover before undergoing IA20%2BC for 7 weeks. Mice were then trained to self-administer 20% alcohol on a fixed ratio of reinforcement 1 (FR1) schedule for 20 hours over four sessions during the first week before transitioning to 2-hour sessions. After eight 2-hour sessions of FR1, mice progressed to FR2, and alcohol-associated active lever presses and inactive lever presses were examined (**Figure 1.7A**). We found that there was no significant change in active lever presses between mice infected with AAV-Rac1-DN or AAV-GFP (**Figure 1.7B, Table 1.1**) (RM Two-way ANOVA: Effect of virus $F_{(13, 143)} = 1.522$, $p = 0.1163$; Effect of session $F_{(3.043, 33.47)} = 1.232$, $p = 0.3137$; Effect of virus x session $F_{(13, 143)} = 1.522$, $p = 0.1163$). However, mice infected with AAV-Rac1-DN pressed the inactive lever significantly more than the AAV-GFP-infected mice (**Figure 1.7C**) (RM Two-way ANOVA: Effect of virus $F_{(1, 11)} = 5.102$, $p = 0.0452$; Effect of session $F_{(13, 143)} = 0.9024$, $p = 0.5522$; Effect of virus x session $F_{(13, 143)} = 0.8569$, $p = 0.5996$). This phenotype is exemplified in the discrimination index, showing that the AAV-Rac1-DN mice exhibited significantly worse discrimination for the active lever throughout the OSA experiment in comparison to AAV-GFP controls (**Figure 1.7D**) (RM Two-way ANOVA: Effect of virus

$F_{(1, 11)} = 5.320$, $p = 0.0415$; Effect of session $F_{(13, 143)} = 2.237$, $p = 0.0107$; Effect of virus x session $F_{(13,143)} = 0.8674$, $p = 0.5886$). A similar phenotype was observed in the proportion of rewarded lever presses, which accounts for active lever presses that do not lead to a reward. Specifically, while over 50% of presses of the AAV-GFP control animals led to a reward, the AAV-Rac1-DN group failed to reach this threshold throughout the testing period (**Figure 1.7E**) (RM Two-way ANOVA: Effect of virus $F_{(1,11)} = 16.66$, $p = 0.0018$, Effect of session $F_{(13,143)} = 6.400$, $p < 0.0001$; Effect of virus x session $F_{(13,143)} = 0.5518$, $p = 0.8880$). There was no difference in alcohol consumption between groups (**Figure 1.7F**) (RM Two-way ANOVA: Effect of virus $F_{(1,11)} = 1.099$, $p = 0.3169$; Effect of session $F_{(13, 143)} = 15.18$, $p < 0.0001$; Effect of virus x session $F_{(13, 143)} = 1.156$, $p = 0.3178$), which aligns with the IA20%2BC data (**Figure 1.6**). Examination of the inter-response interval between lever presses of the final session shows that AAV-Rac1-DN mice exhibited a significantly increased proportion of lever presses in short intervals, and significantly less lever presses in the longer intervals, compared to AAV-GFP controls (**Figure 1.7G**) (RM Two-way ANOVA: Effect of virus $F_{(1,11)} = 0.5360$, $p = 0.4794$; Effect of interval $F_{(4,44)} = 64.48$, $p < 0.0001$; Effect of virus x interval $F_{(4, 44)} = 6.145$, $p = 0.0005$; *Post hoc* 0-5 $p = 0.0034$, >20 $p < 0.001$). These phenotypes can be visualized in the behavioral trace of individual mouse profiles from the OSA session with the greatest discrimination difference (**Figure 1.7H**). As the DMS plays an important role in movement (Kravitz and Kreitzer, 2012), we examined the consequence of Rac1 inhibition in the DMS on locomotion using an open field paradigm. As shown in **Figure 1.7I**, attenuation of Rac1 activity in the DMS had no effect on locomotion (Unpaired t-test: $t_{(16)} = 0.06783$, $p = 0.9468$). Therefore, this behavioral difference is not due to changes in motor behavior. Together, these data

suggest that Rac1 in the DMS plays a role in discrimination of alcohol-associated rewarded lever presses.

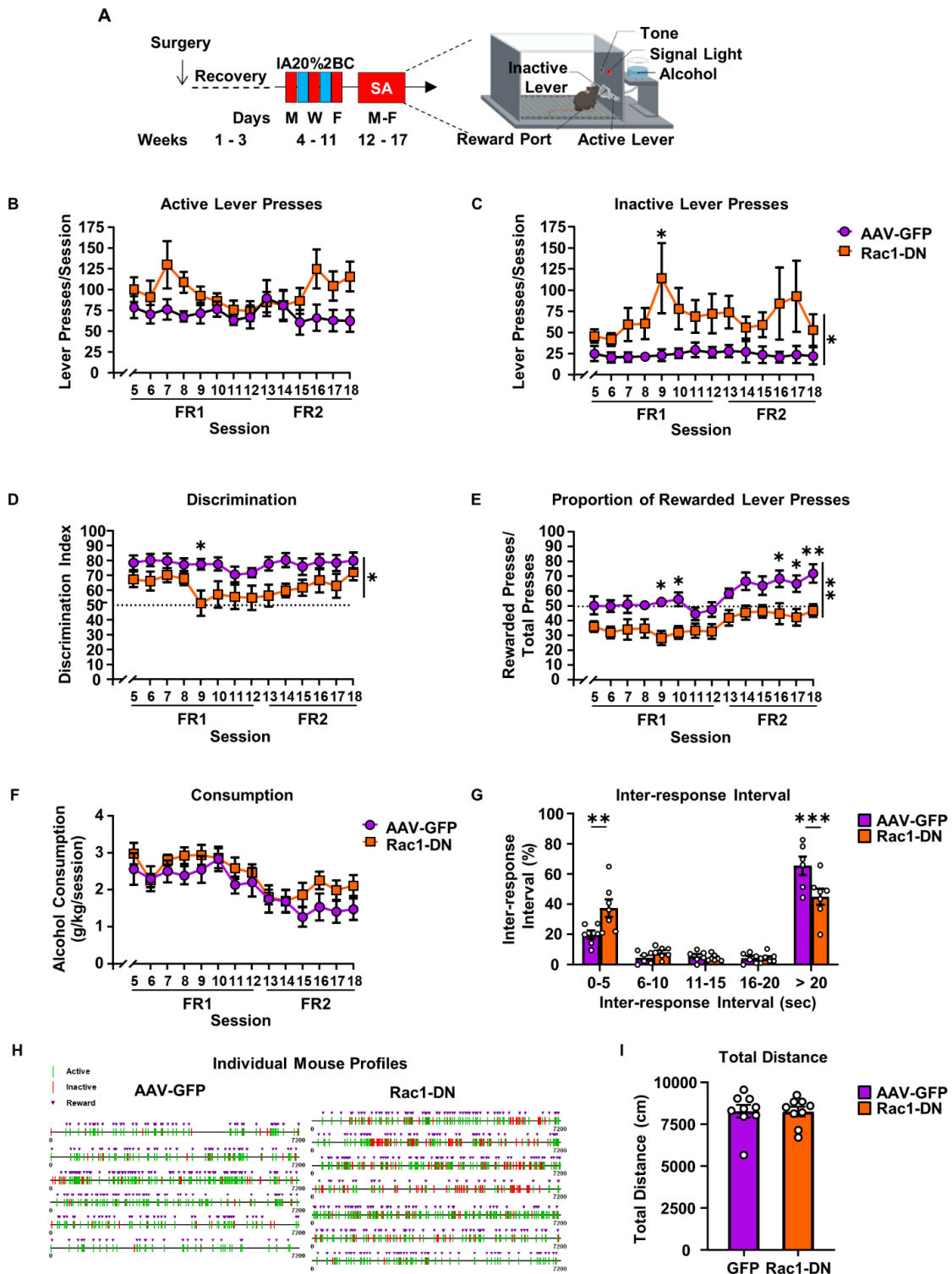


Figure 1.7. Rac1 in the DMS is required for alcohol-associated goal-directed learning

(A) Operant self-administration of 20% alcohol paradigm. Mice underwent surgery to overexpress AAV-Rac1-DN or AAV-GFP in the DMS. After 3 weeks of recovery, mice (figure caption continued on next page)

(figure caption continued from previous page)

underwent 7 weeks of IA20%2BC to develop a preference for alcohol before transitioning to 20% alcohol OSA for 1 week of training and 4 experimental weeks. **(B-C)** The group average of active **(B)** and inactive **(C)** lever presses during the 2-hour sessions. **(D)** Discrimination index for the active lever. Calculated as proportion of active lever presses compared to total lever presses. **(E)** Proportion of rewarded lever presses. Calculated as rewarded lever presses compared to total lever presses.

(F) Alcohol consumption during each session. **(G)** Proportion of inter-response interval between lever presses during the final session. Data are presented as mean \pm SEM and analyzed using RM Two-way ANOVA and Šidák's *post hoc* multiple comparisons test. * $p < 0.05$, ** $p < 0.01$, *** $p < 0.001$. $n = 6, 7$. **(H)** Individual mouse behavioral profiles from OSA session 9. Each line corresponds with an active (green) or inactive (red) lever press, and triangles represent reward (purple). **(I)** Total distance moved in an open field. Mice were placed in an open field and locomotion was recorded for 20 minutes. Data represented as mean \pm SEM and analyzed using an unpaired t-test. $n = 9$ per group.

Next, we examined if the reduction in discrimination as a result of Rac1-DN is related to deficits in goal-directed behavior. Goal-directed behavior is reliant on an association between response and outcome (Yin et al., 2005; Balleine and O'Doherty, 2010). We used a contingency degradation model to test the hypothesis that Rac1 in the DMS is involved in alcohol-associated goal-directed behavior. Mice were first infected with AAV-Rac1-DN or AAV-GFP in the DMS before undergoing IA20%2BC for 7 weeks. Mice were then trained to operant self-administer alcohol as described in (Morisot et al., 2019a) (**Figure 1.8A**). To bias mice towards goal-directed behavior, mice were trained on a random ratio (RR) schedule of reinforcement, which is known to promote goal-directed actions (Yin et al., 2005) (**Figure 1.8A**). AAV-GFP-infected mice significantly reduced active lever pressing during degraded sessions compared to non-degraded sessions (**Figure 1.8B**) However, AAV-Rac1-DN-infected mice pressed similarly during non-degraded and degraded sessions indicating a disruption in alcohol-associated, goal-directed learning (**Figure 1.8B**) (Two-way ANOVA: Effect of virus $F_{(1,12)} = 4.863$, $p = 0.0477$; Effect of degradation $F_{(1,12)} = 17.98$, $p = 0.0011$; Effect of virus x degradation $F_{(1,12)} = 11.38$, $p = 0.0055$; *Post hoc* ND vs. D: AAV-GFP $p = 0.0003$, AAV-Rac1-DN $p = 0.7989$). As shown in **Figure 1.8C**, the port entries during non-degraded and degraded sessions were unchanged (Two-way ANOVA: Effect of virus $F_{(1,2)} = 1.060$, $p = 0.3236$; Effect of degradation $F_{(1,12)} = 4.732$, $p = 0.0503$; Effect of virus x degradation $F_{(1,12)} = 0.4249$, $p = 0.5268$). Together, these data suggest that Rac1 in the DMS plays a role in alcohol-associated, goal-directed learning.

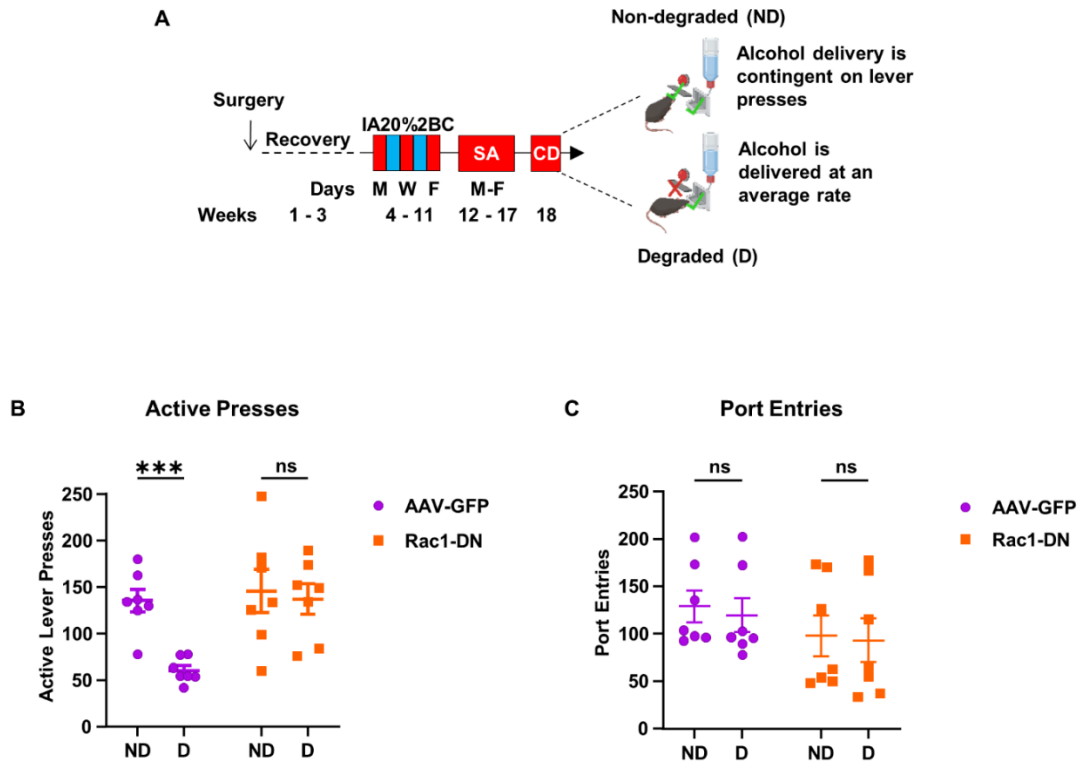


Figure 1.8. Rac1 in the DMS is required for alcohol action-outcome associations

(A) Contingency degradation paradigm. Mice received a dual-infusion of AAV-GFP or AAV-Rac1-DN into the DMS. After a recovery period, mice underwent IA20%2BC for 7 weeks before being trained to operant self-administer alcohol. Mice were first trained on an FR1 schedule before progressing to a random ratio (RR) schedule of reinforcement. Under RR, mice received a reward after a random number of active lever presses within a range (e.g. RR2 1-3 presses, RR3 2-4 presses, RR4 3-5 presses). Mice were trained for 5 sessions at each reinforcement step and spent 10 sessions at RR4 before testing. During the contingency degradation test, there were two types of sessions: non-degraded (ND) and degraded (D). During non-degraded sessions, rewards were delivered on an RR4 schedule. During degraded sessions, rewards were delivered at a rate equal to the average of the last week of training, but active lever presses had no effect. Testing consisted of a ND session followed by a D session, repeated three times. **(B)** Average active lever presses during ND and D testing sessions for AAV-GFP and AAV-Rac1-DN mice. **(C)** Average port entries during ND and D testing sessions for AAV-GFP and AAV-Rac1-DN mice. Data represented as mean \pm SEM and analyzed using two-way ANOVA with Šidák's *post hoc* multiple comparisons test. *** $p < 0.001$. $n = 7$ per group.

1.4.11 Rac1 in the DMS is not required for sucrose goal-directed learning

Alcohol is often distinct from natural reward (Alhadeff et al., 2019; Nall et al., 2021; Martins et al., 2022), and Rac1 in the DMS is not activated in response to sucrose consumption (**Figure 1.1I**). We hypothesized that Rac1 in the DMS does not play a role in sucrose-dependent goal-directed learning. To test this hypothesis, the DMS of mice was first bilaterally infused with AAV-Rac1-DN or AAV-GFP (3.5×10^{12} vg/ml). Mice underwent IA20%2BC for 7 weeks to match the condition of alcohol self-administration. The mice were then trained to operant self-administer 1% sucrose, initially starting with an FR1 reinforcement schedule for 20 hours of training over four sessions before transitioning to 2-hour sessions. After 8 2-hour sessions of FR1, mice were advanced to an FR2 schedule (**Figure 1.9A**). We observed no difference between mice with AAV-Rac1-DN and AAV-GFP overexpression in active lever pressing (**Figure 1.9B**), inactive lever pressing (**Figure 1.9C**), discrimination (**Figure 1.9D**), or proportion of rewarded lever presses (**Figure 1.9E**) (RM Two-way ANOVA: **1.9B** Effect of virus $F_{(1,11)} = 4.651$, $p = 0.0540$; Effect of session $F_{(3.905, 42.36)} = 5.335$, $p = 0.0015$; Effect of virus x session $F_{(13,141)} = 0.9458$, $p = 0.5079$; **1.9C** Effect of virus $F_{(1,11)} = 0.2087$, $p = 0.6566$; Effect of session $F_{(2.224, 24.12)} = 0.8833$, $p = 0.4364$; Effect of virus x session $F_{(13,141)} = 0.6457$, $p = 0.8119$; **1.9D** Effect of virus $F_{(1,11)} = 0.007081$, $p = 0.9344$; Effect of session $F_{(3.161, 34.29)} = 1.888$, $p = 0.1475$; Effect of virus x session $F_{(13,141)} = 0.7552$, $p = 0.7057$; **1.9E** Effect of virus $F_{(1,11)} = 0.0001974$, $p = 0.9890$; Effect of session $F_{(3.512, 38.10)} = 6.534$, $p = 0.0007$; Effect of virus x session $F_{(13,141)} = 0.7314$, $p = 0.7298$). These data suggest that Rac1 in the DMS does not affect learning of natural-reward-associated goal-directed behavior and

that the learning deficiency exhibited by AAV-Rac1-DN overexpression in the DMS is specific to alcohol-associated goal-directed learning.

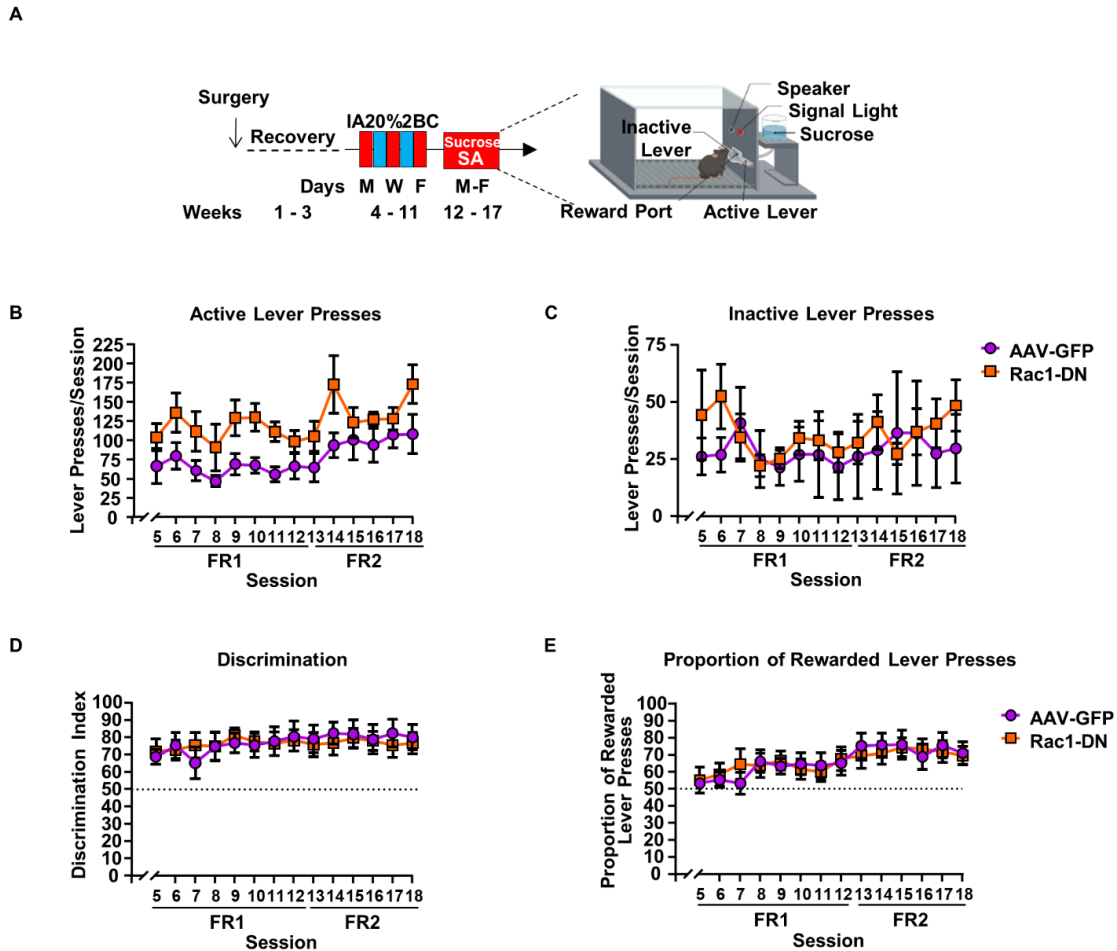


Figure 1.9. Rac1 in the DMS is not required for sucrose goal-directed learning

(A) Operant self-administration of 1% sucrose paradigm. Mice underwent surgery to overexpress AAV-Rac1-DN or AAV-GFP in the DMS. After 3 weeks of recovery, mice underwent IA20%2BC for 7 weeks. 1% sucrose OSA began with 1 week of training and 4 weeks of experimental tracking. Variables tracked during the session include **(B)** active lever presses and **(C)** inactive lever presses. **(D)** Discrimination and **(E)** proportion of rewarded lever presses were calculated. Data are represented as mean \pm SEM and analyzed using RM Two-Way ANOVA. $n = 7, 6$.

1.4.12 Systemic Rac1 inhibition reduces binge alcohol drinking in male and female mice

Inhibition of Rac1 specifically in the DMS did not lead to a reduction in voluntary drinking, although it disrupted alcohol-associated goal-directed learning. However, we have shown that Rac1 signaling is activated after alcohol drinking in at least one other region associated with AUD, the CeA, and it is likely activated in others. Therefore, we tested whether systemic Rac1 inhibition would reduce voluntary drinking in the IA20%2BC paradigm.

Mice first underwent IA20%2BC for 7 weeks (**Figure 1.10A**). One hour before the first drinking session of the eighth week, mice were injected with Rac1 inhibitor NSC23766 (10mg/kg) (Gao et al., 2004) or saline as a control (**Figure 1.10A**). Alcohol drinking was measured 4 hours into the drinking session (binge) and at the end of the session. Groups were balanced by average alcohol consumption and the treatment was repeated within-subject one week later. We found that systemic Rac1 inhibition significantly reduced binge drinking in both male and female mice (**Figure 1.10B, 1.10E**) (Paired t-test: Male $t_{(17)} = 4.782$, $p = 0.0002$; Female $t_{(18)} = 3.210$, $p = 0.0049$). While male mice showed no reduction in total drinking after the 24-hour session (**Figure 1.10C**) (Paired t-test: $t_{(17)} = 1.975$, $p = 0.0648$), female mice significantly reduced total drinking throughout the session after Rac1 inhibition (**Figure 1.10F**) (Paired t-test: $t_{(18)} = 3.598$, $p = 0.0021$). In both male and female mice, total water drinking was unchanged by systemic Rac1 inhibition (**Figure 1.10D, 1.10G**) (Paired t-test: Male $t_{(17)} = 0.4487$, $p = 0.6593$; Female $t_{(18)} = 0.4064$, $p = 0.6890$). As systemic, but not intra-DMS, Rac1 inhibition

significantly reduced alcohol drinking, there is likely a region or combination of regions in male and females where Rac1 is contributing to voluntary alcohol-drinking behaviors.

We next examined whether systemic Rac1 inhibition would significantly reduce sucrose consumption. Mice first underwent intermittent access to 0.3% sucrose two-bottle choice for 2 weeks. Mice were then injected with Rac1 inhibitor NSC23766 (10mg/kg) or saline one hour before the first session of the third week. The treatment was repeated within subject one week later. Male mice did not reduce binge or 24-hour sucrose drinking after systemic Rac1 inhibition (**Figure 1.10H, 1.10I**) (Paired t-test: Binge $t_{(17)} = 2.026$, $p = 0.0588$; 24-hour $t_{(18)} = 1.821$, $p = 0.0852$). Together, these results suggest the reduction in alcohol drinking as a result of Rac1 inhibition is controlled by a mechanism not shared with natural reward.

Finally, we examined the effect of Rac1 inhibitor NSC23766 on open-field locomotion. Male mice were injected with NSC23766 or saline and placed in a novel open-field and allowed to explore for 20 minutes. The experiment was repeated within subject one week later. Total locomotion was unchanged in mice that received NSC23766 (**Figure 1.10J**) (Paired t-test: $t_{(15)} = 1.297$, $p = 0.2143$). These results lead us to conclude that systemic Rac1 inhibition is not affecting motor activity, and therefore the reduction in alcohol drinking is not due to hypolocomotion.

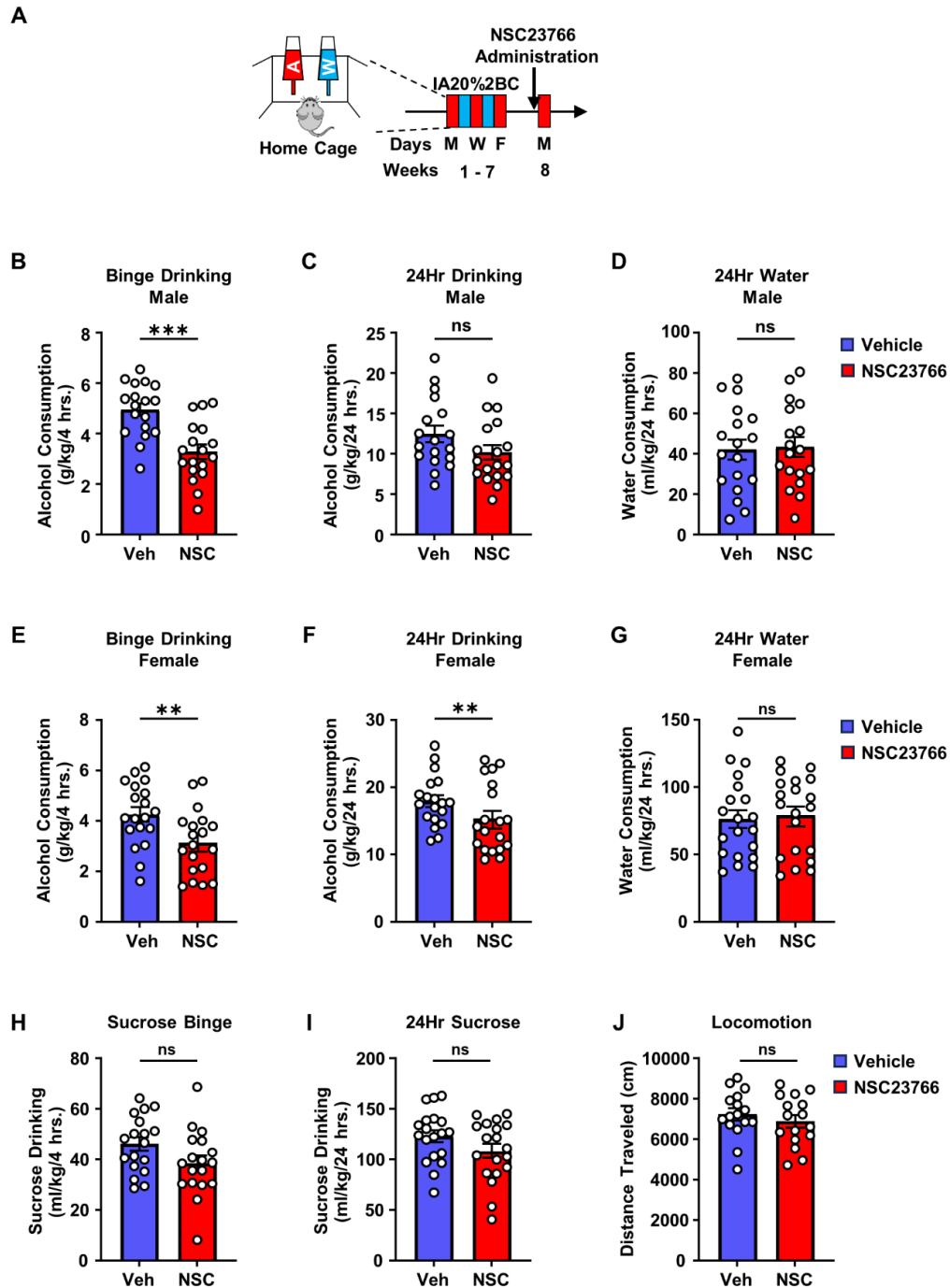


Figure 1.10. Systemic Rac1 inhibition reduces binge alcohol drinking in male and female mice

(A) Experimental timeline. Rac1 inhibitor NSC23766 was administered systemically via an i.p. injection one hour before the first session of the eighth week of IA20%2BC. The experiment was repeated within subject one week later. Alcohol drinking was measured 4 hours into the session (binge) or at the end of the session (B) Male mice significantly (figure caption continued on next page)

(figure caption continued from previous page)

reduced alcohol binge drinking after Rac1 inhibition. **(C)** Male mice total session drinking was unaffected by Rac1 inhibition. **(D)** Male water consumption throughout the session was unaffected by Rac1 inhibition. **(E-G)** Rac1 inhibition significantly reduced both binge **(E)** and total **(F)** alcohol drinking in female mice, without affecting total water drinking **(G)**. **(H-I)** Male mice did not reduce binge **(H)** or 24-hr **(I)** consumption of 0.3% sucrose in response to systemic Rac1 inhibition. **(J)** Locomotion of male mice in the open field test was unaffected by Rac1 inhibition. Data are represented as mean \pm SEM and analyzed using paired two-tailed t-test. ** $p < 0.01$, *** $p < 0.001$, ns, non-significant. $n = 16-19$.

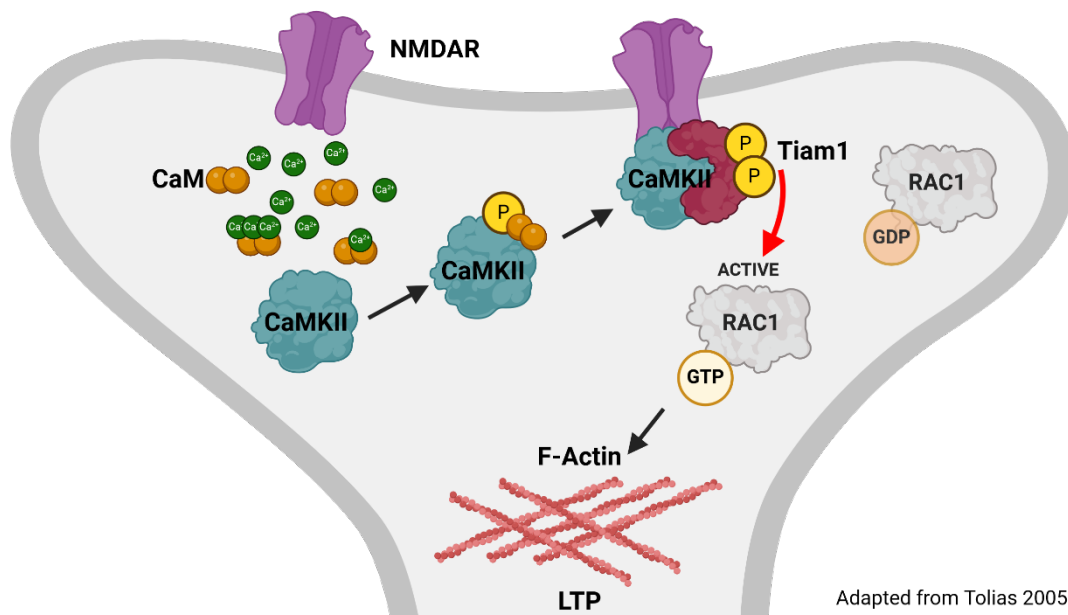
1.5 Discussion

We show herein that Rac1 signaling is activated in the DMS in response to long term excessive alcohol drinking of male mice. We further show that the consequences of alcohol-mediated Rac1/LIMK/cofilin signaling in the DMS are the formation of F-actin and the alteration of dendritic spine morphology. Finally, we present data to suggest that Rac1 in the DMS plays a role in alcohol-associated goal-directed learning. Together, our results suggest that Rac1 in the DMS plays an important role in molecular and morphological adaptations that promote alcohol-dependent learning behavior.

1.5.1 Rac1 is activated in the DMS after alcohol consumption

We found that Rac1 signaling is activated specifically in the DMS of male mice in response to long-term drinking of alcohol which was observed during the 4-hour binge drinking session and was still detected after 24 hours of withdrawal. The mechanism by which alcohol activates Rac1 in the DMS is unknown, and the sequence of events is unclear, e.g. is the binge or withdrawal session that initiates the activation of Rac1? Rac1 is activated by NMDA receptor stimulation in rat cortical and hippocampal neurons (Tolias et al., 2005; Xiao et al., 2013). Previously, we found that *ex vivo* and *in vivo* exposure to, and withdrawal from, alcohol induces long-term facilitation of GluN2B-containing NMDA receptor activity specifically in the DMS (Wang et al., 2007; Wang et al., 2010). Glutamatergic tone is increased in cortical regions that project to the striatum of humans and rats during acute alcohol withdrawal (Hermann et al., 2012; Hwa et al., 2017). Therefore, it is very plausible that Rac1 is first activated during withdrawal through the activation of GluN2B receptors in the DMS, and that its activity is maintained during the

alcohol drinking session. The long-lasting activation of Rac1 in the DMS in response to alcohol could be due to increased level and/or activity of one or both of its specific GEFs, Tiam1 and/or Karilin-7 (Tolias et al., 2005; Xie et al., 2007) or because of a reduction of the level and/or activity of its specific GAPs (Toure et al., 1998; Garcia-Mata et al., 2006; Peru et al., 2012; Nakamura, 2013).



Model 2. Upstream activation of Rac1 by NMDAR signaling

Model 2 is the proposed mechanism of Rac1 activation during long-term excessive alcohol drinking, adapted from (Tolias et al., 2005). The NMDAR is a major target of alcohol (Kumari and Ticku, 2000; Ron, 2004). Initially, alcohol consumption facilitates the inhibitory actions of GABA and inhibits the excitatory effects of glutamate, leading to well-known behavioral phenotypes, such as disinhibition, hyperlocomotion, and anxiolysis (Becker and Mulholland, 2014; Dharavath et al., 2023). Repeated alcohol exposure leads to compensatory changes in these systems, reducing GABA release, altering postsynaptic GABA receptor composition, enhancing glutamate release, and increasing

NMDAR function (Lovinger and Roberto, 2013; Becker and Mulholland, 2014). These compensatory changes lead to a hyperglutamatergic state during withdrawal, which alters synaptic plasticity (Chandler et al., 2006; Zorumski et al., 2014). This proposed mechanism of Rac1 activation relies on this hyperglutamatergic state. CaMKII is activated in response to NMDAR stimulation (Lisman et al., 2002), and CaMKII phosphorylates Tiam1, leading to Tiam1-dependent Rac1 activation (Fleming et al., 1999) (**Model 2**). Tolias et al. confirm that calcium influx through the NMDAR induces both Tiam1 phosphorylation and Rac1 activation (Tolias et al., 2005). This process contributes to actin cytoskeletal remodeling and dendritic spine maturation (Tolias et al., 2005).

Another plausible explanation for alcohol-mediated Rac1 activation in the DMS is that withdrawal from IA20%2BC might trigger activation of a DMS-specific circuit by activating only neurons projecting to the DMS. For example, Ma et al. observed an increase in glutamatergic transmission from mPFC neurons projecting to the DMS in alcohol- but not water-drinking rats (Ma et al., 2017). In addition, chronic IA20%2BC drinking was shown to alter instrumental learning by affecting the thalamus-to-DMS circuit (Ma et al., 2022). Further work is required to unravel the specificity of inputs and their interaction with alcohol.

Furthermore, ~95% of the DMS MSNs express either dopamine D1 receptors (D1) or dopamine D2 receptors (D2) (Gerfen and Surmeier, 2011; Calabresi et al., 2014; Cheng et al., 2017). Alcohol increases the complexity of dendritic branching and maturation of dendritic spines selectively in D1 but not D2 DMS MSNs (Wang et al., 2015). Since the inhibition of endogenous Rac1 attenuates alcohol-dependent re-structuring of

DMS MSNs, we speculate that alcohol-mediated Rac1 signaling is specifically localized to D1 neurons. This possibility will be determined in future studies.

Interestingly, we did not detect Rac1 activation in response to alcohol drinking in the DMS of female mice. While Rac1 is not activated in the DMS of female mice in response to alcohol drinking, this does not exclude Rac1 from being activated by alcohol in other brain regions, such as the amygdala or hippocampus, where Rac1 is involved in learning and memory (Martinez et al., 2007; Haditsch et al., 2009; Wu et al., 2014; Gao et al., 2015). Further investigation is required to unravel the mechanisms controlling sex-specificity in Rac1 signaling.

1.5.2 Rac1 in the DMS promotes alcohol-dependent morphological adaptations

We previously showed that the complexity of dendritic branching is increased by alcohol (Wang et al., 2015; Laguesse et al., 2018). Here, we replicated the data of both studies and showed that Rac1 is responsible for DMS MSNs dendritic complexity. However, because Rac1-DN significantly decreased dendritic arborization in both water- and alcohol-drinking animals, we cannot definitively conclude that Rac1 contributes to alcohol-dependent alteration of dendritic tree complexity, but based on the finding that Rac1 inhibition significantly alters F-actin content, this possibility is highly likely.

Rac1 is involved in the maturation and morphogenesis of dendritic spines (Nakayama et al., 2000; Tashiro et al., 2000; Pennucci et al., 2019; Costa et al., 2020). In addition to the DMS, (Wang et al., 2015; Laguesse et al., 2018) and data herein, alcohol exposure affects dendritic spine morphology in cortical regions such as the medial prefrontal cortex (mPFC) (Cannady et al., 2021), and the orbitofrontal cortex (OFC)

(McGuier et al., 2015). Therefore, it is plausible that the activation of Rac1 may also be the molecular mediator of alcohol-dependent structural plasticity in cortical regions.

Interestingly, Rac1 was reported to play a role in cocaine-dependent neuroadaptations in other striatal regions. Specifically, Dietz et al. reported that cocaine-dependent increase in NAc thin spine density was mediated by Rac1 (Dietz et al., 2012), whereas Li et al. showed that the cocaine-dependent increase of Rac1 signaling in the dorsal striatum leads to dendritic spine maturation (Li et al., 2015). Cocaine also increases actin cycling through LIMK/cofilin signaling in the NAc (Toda et al., 2006). Tu et al. observed that decreased Rac1 signaling is required for METH-mediated spine density and maturation in the NAc (Tu et al., 2019). Here, the increase in dendritic maturation after alcohol drinking in the DMS is shown to be Rac1-dependent. These findings suggest that drugs of abuse are altering Rac1 signaling in a drug- and subregion-dependent manner.

1.5.3 Rac1 and alcohol-associated behaviors

We found that Rac1 in the DMS does not play a role in voluntary drinking behavior. It is not unusual that alcohol-mediated signaling controls a specific behavior without affecting voluntary drinking. For example, inhibition of mTORC1 activity in the OFC attenuates habitual alcohol seeking without affecting IA20%2BC consumption (Morisot et al., 2019b). Furthermore, lack of toll-like receptor 4 (TLR4) does not alter alcohol consumption or preference (Blednov et al., 2017a), but does significantly reduce the duration of loss of righting reflex and recovery from alcohol-induced motor incoordination

(Blednov et al., 2017b). Although Rac1 signaling in the DMS does not mediate voluntary drinking behavior, its activation may be involved in other alcohol-related behaviors.

The DMS primarily mediates goal-directed behaviors (Yin et al., 2005; Balleine and O'Doherty, 2010; Everitt and Robbins, 2013; Gremel and Costa, 2013), which play a major role in the addiction cycle (Hogarth, 2020). Here, we showed that Rac1 inhibition in the DMS impairs active lever discrimination and leads to a reduction in the proportion of lever presses leading to a reward, suggesting a failure to learn the association between an active lever press and alcohol reward. The elevated inactive lever presses are unlikely to have resulted from increased locomotor activity, as Rac1 inhibition did not affect locomotion. However, we found that AAV-Rac1-DN mice are insensitive to contingency degradation, implying a failure to learn the goal-directed behavior of pressing the active lever to receive an alcohol reward. Therefore, Rac1 in the DMS is required for alcohol-specific goal-directed action-outcome contingency or outcome value learning. While the debate persists regarding the role of goal-directed vs. habitual behavior in addiction, a large body of evidence suggest that drug seeking is driven by goal-directed behavior (Hogarth, 2020; Vandaele and Ahmed, 2021). The loss of goal-directed behavior in response to Rac1 inhibition in the DMS does not necessarily imply a transition to habitual behavior, which requires additional tests such as assessment of stimulus-response association (Turner and Balleine, 2024). Further work is required to investigate Rac1's role in goal-directed behavior.

Interestingly, this learning deficit is specific for alcohol, as Rac1 inhibition in the DMS did not affect the learning of active lever association with sucrose reward. This phenotype could be the result of disrupting the Rac1 signaling reinforcing active lever

preference (“GO”) or the avoidance of undesired action (“NO-GO”) (Cheng et al., 2017). The normal physiological role of Rac1 in the DMS is unknown. Rac1 has been linked with learning and memory in other regions such as the hippocampus, where it is required for spatial learning (Haditsch et al., 2009). Rac1 in the hippocampus also mediates reversible forgetting (Lv et al., 2019), contributing to the long-term maintenance of memory behaviors like contextual-fear conditioning and object recognition (Lv et al., 2019).

To our knowledge, this is the first study unveiling a molecular mechanism involved in alcohol-specific goal-directed learning. Prior studies have investigated the mechanisms of goal-directed learning in the context of food and sucrose seeking in the rodent striatum (Hart et al., 2018; Matamales et al., 2020; Peak et al., 2020). For example, using chemogenetics, Peak et al. found that D1R MSNs in the posterior DMS were critical for sucrose goal-directed learning (Peak et al., 2020), and Matamales et al. have shown that striatal-dependent goal-directed learning for food involves ensembles of D1R MSNs, controlled and modified by D2R MSNs (Matamales et al., 2020). It is tempting to speculate that specific sucrose or alcohol ensembles exist within the DMS. With Rac1 signaling contributing to alcohol but not sucrose self-administration, our results provide support to the notion that natural reward and alcohol drug reward mechanisms are different (Alhadeff et al., 2019).

In summary, in this study we unraveled that alcohol drinking increases Rac1 signaling in the DMS, leading to the alcohol-mediated maturation of dendritic spines and to alcohol-dependent goal-directed behavior learning processes. As goal-directed behavior is a major contributor to the cycle of addiction (Hogarth, 2020), unraveling the molecular foundation of goal-directed behavior, as explored in this study, bears profound

importance for both basic science and the discovery of novel medications aimed at treating AUD.

1.6 Future Directions

In this chapter, we discovered that Rac1 is activated in response to chronic alcohol drinking specifically in the DMS of male mice, but not female mice. Related, we noticed an activation of Rac1 after alcohol exposure in the CeA of male mice, showcasing the subregion-specific activation of alcohol-dependent Rac1 signaling. Therefore, the primary direction of future studies is to investigate which other subregions have increased Rac1 signaling in response to excessive alcohol drinking in both male mice and female mice.

Discovering subregions where Rac1 is active in response to alcohol drinking will likely have implications for alcohol-associated behaviors. We observed that systemic Rac1 inhibition reduces alcohol drinking in both male and female mice. Also, we show that Rac1 in the DMS is contributing to alcohol-associated goal-directed behavior in male mice. However, this activation does not control voluntary drinking. Together, these data imply that Rac1 signaling in another subregion, or perhaps a combination of regions, is reinforcing voluntary drinking behaviors in both male and female mice. Similarly, perhaps Rac1 signaling is associated with other alcohol-associated behaviors. For example, its activation in the CeA may be contributing to the symptoms associated with withdrawal, like increased anxiety. Indirectly, Rac1 signaling in the CeA may lead to increased binge drinking to alleviate these withdrawal symptoms.

Additionally, the upstream activation of Rac1 must be examined. Although it is proposed that increased NMDAR signaling during withdrawal is leading to Rac1 activation, this must be examined directly. Furthermore, it would be interesting to explore the specific GEF and GAP profile leading to Rac1 activation and inactivation, respectively. The inhibition methods utilized here, NSC23766 and Rac1-DN, both affect the activation

of Rac1 by disrupting GEF binding. However, if Rac1 is being activated during withdrawal, and this activation is long-lasting, the inhibition of inactivation of Rac1 may be a significant factor in Rac1's role in the progression of AUD. This question requires investigation into the profile of GAPs inactivating Rac1. The subregion-specificity of GAPs may also explain the specific activation profile of Rac1 signaling in response to long-term drinking.

Table 1.1. Average Alcohol Consumption for biochemical experiments

Figure	Average Consumption (g/kg/24hr)	SEM (\pmg/kg/24hr)
1.1B NAc	13.38	1.025
1.1C DLS	13.38	1.060
1.1D DMS	14.53	0.982
1.1E Female DMS	19.59	0.979
1.1F RhoA	12.31	0.4461
1.1G Cdc42	13.67	0.7354
1.1H 10%CA	8.787	0.2611
1.1J pLIMK pCofilin	15.34	0.5169
1.2H-M AAV-GFP	14.00	0.7264
1.2H-M AAV-Rac1-DN	13.68	0.4589
1.3,4 AAV-GFP	10.63	0.5058
1.3,4 AAV-Rac1-DN	10.88	1.223
1.6 AAV-GFP	12.10	0.7463
1.6 AAV-Rac1-DN	12.36	1.046
E1.1-1 4wk DMS	12.560	1.678
1.1I Sucrose	174.81 (ml/kg)	17.87 (ml/kg)

1.7 Materials and Methods

Antibodies

Rabbit anti-pLIMK (#ab38508) antibodies were purchased from Abcam (Waltham, MA). Chicken anti-GFP (#A10262) antibodies were purchased from Life Technologies (Carlsbad, CA). Rabbit anti-LIMK1 (#3842S), Cofilin (#3312S), pCofilin Ser3 (#3311S), RhoA (#6789S), Cdc42 (#2246S) antibodies were purchased from Cell signaling technology (Danvers, MA). Mouse anti-GAPDH (#G8795) antibodies, anti-actin (#A2228) antibodies, phosphatase inhibitor Cocktails 2 and 3 were from Sigma Aldrich (St. Louis, MO). Mouse anti-Rac1 antibodies (#ARC03), the G-Actin/F-Actin assay kit (BK037), the Rac1 pull-down activation assay kit (#BK035), the RhoA pull-down activation assay kit (#BK036), and the Cdc42 pull-down activation assay kit (#BK034) were purchased from Cytoskeleton, Inc. (Denver, CO). Nitrocellulose membranes and Enhance Chemiluminescence (ECL) were purchased from Millipore (Burlington, MA). EDTA-free complete mini-Protease Inhibitor Cocktails were from Roche (Indianapolis, IN). Pierce bicinchoninic acid (BCA) protein assay kit was purchased from Thermo Scientific (Rockford, IL). Ethyl alcohol (190 proof) was purchased from VWR (Radnor, PA). NuPAGE Bis-Tris precast gels were purchased from Life Technologies (Carlsbad, CA). Donkey anti-rabbit horseradish peroxidase (HRP) and donkey anti-mouse HRP conjugated secondary antibodies were purchased from Jackson ImmunoResearch (West Grove, PA). The donkey anti-mouse IgG AlexaFluor 564 and donkey anti-chicken AlexaFluor 488 antibodies were purchased from Life Technologies (Carlsbad, CA).

Animals

Male and female C57BL/6J mice (Jackson Laboratory, Bar Harbor, ME) arrived at 6-8 weeks old and were allowed one week of habituation before experiments began. Mice were housed individually in a reversed 12-hour light-dark cycle room (lights on at 22:00/off at 10:00) that was temperature- and humidity-controlled. Unrestricted amounts of food and water were provided. Animal procedures were approved by the UCSF Institutional Animal Care and Use Committee (IACUC).

Preparation of solutions

Alcohol solution was prepared from an absolute anhydrous alcohol solution (190 proof) diluted to 20% (v/v) in tap water for alcohol-drinking experiments. Sucrose solution (1%) was dissolved in tap water (w/v).

Collection of brain samples for biochemical analyses

Mice were euthanized 4 hours after the beginning of the last drinking session (“binge” timepoint) or 24 hours after the last drinking session (“withdrawal” timepoint). Brains were removed and dissected on an ice-cold platform into 1mm sections, and specific subregions were dissected based on Allen Brain Atlas anatomy.

Western blot analysis

Tissue was homogenized in ice-cold radio immunoprecipitation assay (RIPA) buffer (in mM: 50 Tris-HCL, 5 EDTA, 120 NaCl, and 1%NP-40, 0.1% deoxycholate, 0.5% SDS, proteases and phosphatases inhibitors). Samples were homogenized using a sonic

dismembrator. Protein content was determined using BCA™ protein assay kit. Thirty µg of each tissue lysate was loaded for separation by SDS-PAGE then transferred onto nitrocellulose membrane at 300mA for 2 hours. Membranes were blocked with 5% milk-PBS containing 0.1% Tween 20 at room temperature (RT) for 30 minutes and then probed with the appropriated primary antibodies overnight at 4°C. The membranes were washed and probed with HRP-conjugated secondary antibodies for one hour at room temperature. Membranes were developed using the enhanced chemiluminescent reagent (ECL) and band intensities were quantified using ImageJ software (NIH).

Small G-protein activation assay

Small G-protein activity was determined using the Rac1, RhoA, or Cdc42 activation *in vivo* assay biochemical kits for the respective protein (Cytoskeleton Inc., Denver, CO). The tissues were lysed in lysis buffer (50mM Tris-HCl pH7.4, 450mM NaCl, 1% Triton X-100) containing protease and phosphatase inhibitor cocktail. Thirty µg of each lysate was incubated with 10 µL PAK Rac1/Cdc42 binding domain (PAK-PBD)-agarose beads for Rac1 and Cdc42, or 15 µL Rhotekin Rho binding domain (Rhotekin-RBD)-agarose beads for RhoA, for 16 hours. For the control, the same amount of lysate was incubated with GDP or GTP for 15 minutes followed by incubation with PAK-PBD or Rhotekin-RBD-agarose beads for 16 hours. The beads were washed twice with washing buffer followed by boiling in 30 µL 2X sample loading buffer. The samples were analyzed by western blot.

F-actin/G-actin assay

F-actin and G-actin content was measured using the G-actin/F-actin in vivo assay biochemical kit (Cytoskeleton Inc., Denver, CO) as previously described in (Laguesse et al., 2018) with slight modification. Tissue punches were homogenized in 250 μ L cold LAS02 buffer containing protease and phosphatases inhibitors and centrifuged at 350g for 5 minutes at 4°C to remove cellular debris. Protein concentrations were determined in the supernatant using BCA™ protein assay kit. Supernatant was centrifuged at 15,000g for 30 minutes at 4°C and the new supernatant contained soluble globular actin (G-actin). The insoluble filamentous actin (F-actin) in the pellet was then resuspended and incubated on ice for 1 hour in 250 μ L F-actin depolymerization buffer, with gently mixing every 15 minutes. Samples were centrifuged at 15,000g for 30 minutes at 4°C and this supernatant was used to measure F-actin content by western blot. Twenty μ L of the G-actin fraction and 40 μ L of the F-actin fractions were loaded and analyzed by western blot.

Adeno-associated viruses

AAV2-Rac1-DN-GFP (AAV-Rac1-DN; 3.5×10^{12} vg/ml) was produced by the Duke Viral Vector Core (Durham, North Carolina). The plasmid containing the T17N Rac1 mutation (plasmid #22784, pCyPet-Rac1(T17N)) and AAV-GFP (pAAV.CMV.PI.EGFP.WPRE.bGH; 1.6×10^{13} vg/ml) were purchased from Addgene. AAV-GFP was diluted to match the concentration of AAV-Rac1-DN.

Confirmation of AAV-Rac1-DN in cells

HEK293 cells were plated at 120,000 cells per well on a 12-well-plate. The media was changed to 1% FBS-DMEM 24 hours prior to the infection. The cells were then infected with 2 μL of AAV-Rac1-DN virus (3.5×10^{12} vg/ml). Seventy-two hours after the infection, cells were incubated with 10% FBS for 30 minutes. The cells were lysed and analyzed by western blot.

Stereotaxic surgery

Mice were anesthetized using vaporized isoflurane and were fixed in a stereotaxic frame (David Kopf Instruments). To overexpress the virus in the entirety of the DMS, bilateral microinfusions were accomplished using stainless steel injectors (33 gauge; Small Parts Incorporated) connected to Hamilton syringes (10 μL , 1701) at two sites in the DMS (anteroposterior (AP) +1.1 mm, mediolateral (ML) \pm 1.2 mm, dorsoventral (DV) -3 mm and AP +0.66 mm, ML \pm 1.2 mm, DV -2.8 mm measured from bregma). Animals received a 1 μL bilateral infusion of AAV-GFP or AAV-Rac1-DN-GFP (3.5×10^{12} vg/ml) at an infusion rate of 0.1 $\mu\text{L}/\text{min}$ controlled by an automatic pump (Harvard Apparatus). The injectors were left at the infusion site for 10 minutes after the conclusion of the infusion to allow the virus to diffuse.

To image single neurons, a low-titer (7×10^9 - 3.5×10^{10} vg/ml) of AAV-GFP or AAV-Rac1-DN-GFP was infused into the DMS (AP +1.1 mm, ML \pm 1.2 mm, DV -2.8 mm). 0.5 μL of each virus was infused bilaterally at a rate of 0.1 $\mu\text{L}/\text{min}$. Injectors were left in place for 10 minutes for viral diffusion.

***In vivo* confirmation of viral expression**

After the conclusion of an experiment, animals were euthanized by cervical dislocation and the brains were removed. The brain was dissected on ice into 1-mm-thick coronal sections and green fluorescent protein (GFP) was visualized and imaged using an EVOS FL tabletop fluorescent microscope (ThermoFisher Scientific, Waltham, MA). Mice with surgeries that failed to elicit viral overexpression were excluded from the study.

Immunostaining

Mice were euthanized by transcardial perfusion with 0.01M PBS followed by 4% paraformaldehyde (PFA) in phosphate buffer, for 5 minutes each step. Brains were removed and postfixed in 4% PFA for 24 hours before being transferred to a 30% sucrose solution for 3 days. Brains were then frozen rapidly on dry ice before being coronally sectioned into 100 μm sections using a Leica CM3050 cryostat (Leica Biosystems, Richmond, IL). Slices were placed in 0.01M PBS and the ones containing the site of infection were selected to be stained. Sections were blocked with 5% normal donkey serum for 4 hours. Slices were incubated in the primary antibody over 48 hours at 4°C on an orbital shaker. After primary antibody incubation, slices were washed 3 times for 45 minutes each in PBS before secondary antibody incubation overnight at 4°C on an orbital shaker. There was another cycle of washing before placing the slices onto Superfrost Plus microscope slides (Fisher Scientific, Hampton, NH) and mounting slides using Prolong Gold mounting medium (ThermoFisher Scientific, Waltham, MA). Slides were allowed 24 hours to dry before the edges were sealed to prevent dehydration.

Morphological analysis

Low titer of AAV-GFP or AAV-Rac1-DN (7×10^9 - 3.5×10^{10} vg/ml) was infused bilaterally into the DMS. After 1 week of recovery, mice underwent 7 weeks of IA20%2BC. Twenty-four hours after the last drinking session, mice were euthanized, perfused, processed, and 100 μm coronal sections were collected. Images of GFP-stained DMS neurons were acquired with a spinning disk confocal microscope with a 40x objective and a Z-interval of 1 μm (Nikon, Tokyo, Japan). Images were deconvoluted using AutoQuantX (v3.1.3, Media cybernetics, Inc, Rockville, MD), and GFP neurons were traced using NeuroLucida software (MBF Biosciences, Williston, VT).

Scholl analysis: Dendritic branches were quantified using Sholl analysis (Sholl, 1953). Starting radius of dendritic branches was 10 μm and end radius was 160 μm from the center of the soma with an interval of 10 μm between radii. Cell body area was measured using Fiji software (NIH).

Spine Analysis: Images of GFP-stained DMS neurons were acquired with a spinning disk confocal microscope with a 100x objective and a Z-interval of 0.1 μm (Nikon, Tokyo, Japan). Only distal dendrites (3rd or 4th order) were analyzed. Morphological properties were analyzed using Imaris software (Oxford Instruments, Concord, MA). Dendritic spines were classified based on a combination of length and head and neck morphology. Spines were classified into four subtypes as in (Laguesse et al., 2018): filipodia (>2 μm length, indiscernible head), stubby (<1 μm length, no visible neck), mushroom (>0.4 μm head width, short neck), thin (head width <0.4 μm , long neck).

Behavioral paradigms

2-bottle choice drinking paradigms

Intermittent access to 20% alcohol (IA20%2BC): The paradigm was conducted as described in (Laguesse et al., 2017). Mice were given 24-hour access to one bottle of 20% alcohol (v/v) in tap water or one bottle of water. Drinking sessions started at 11:30AM Monday, Wednesday, and Friday with 24- or 48-hour (weekend) withdrawal periods in between during which only water was available. The bottles were alternated each session to prevent a side preference from developing. The bottles were weighed at the end of each session and adjusted for spill. Mice were weighed once a week. Animals that drank over 7g/kg/24hr were included in the study. See **Table 1** for average values in each of the experiments. Percentile of alcohol preference (preference index) was calculated by dividing the amount of alcohol drank to the amount of water+alcohol X100.

Intermittent access to 1% sucrose: Mice had access to a 2-bottle choice between water and 1% sucrose three days a week for 24-hour periods for two weeks (Laguesse et al., 2017). Bottles were weighed at the end of each session and switched in between. Between sessions, only water was available. The bottle weights were spill-adjusted after each session. Mice were weighed weekly, and 1% sucrose consumption was measured in milliliters per kilogram of bodyweight (ml/kg). Food was available *ad libitum*.

Continuous access to 10% alcohol: Mice had access to a bottle of 10% alcohol (v/v) in tap water and a bottle of water for 24 hours a day for 3 weeks (21 drinking sessions) (Laguesse et al., 2017) Bottles were removed and weighed daily. Bottle positions were alternated to reduce side preference development. The bottle weights were spill-adjusted

after each session. Mice were weighed weekly and alcohol consumption was calculated for each in grams per kilogram.

Chronic Intermittent Exposure (CIE): CIE was conducted based on protocols previously established in (Becker and Lopez, 2004). Alcohol (95%) was volatilized and mixed with air before being delivered to Plexiglass inhalation chambers (60 x 36 x 60 cm) at a rate of 10 liters/minute. The rate of alcohol delivery maintained an ethanol concentration in the chamber in the range of 15-20 mg/L of air, which was measured via breathalyzer before placing mice in the chamber and removing mice from the chamber. Before mice were added to the CIE chamber, intoxication was initialized with an i.p. injection of alcohol (1.6g/kg) and blood alcohol concentration (BAC) was stabilized with administration of alcohol dehydrogenase inhibitor pyrazole (1mmol/kg). “Air” control mice received identical handling, but received a saline and pyrazole injection, and alcohol vapor in the chamber was replaced with water vapor. Mice were placed in the chambers at 17:00 for a 16-hour exposure period and removed at 9:00 the next day. After an 8-hour withdrawal period, the process was repeated. Mice underwent 72-hour withdrawal periods during weekends. BAC was measured weekly and at the end of the experimental exposure.

Operant self-administration (OSA) paradigms

Alcohol operant self-administration: OSA was conducted as described in (Laguesse et al., 2017). Mice underwent stereotaxic surgery and IA20%2BC for 7-8 weeks as described above. Prior to training, animals were handled for 1-2 minutes per day for 3 consecutive days. OSA was conducted during the dark phase of the reverse light/dark cycle in operant chambers (length: 22 cm, width: 20 cm, height: 14 cm). OSA boxes were

connected to a computer running MED-PC to control and record session activity. The operant chambers (Med-Associates; Georgia, VT) had two levers (length: 1.5 cm, distance between: 11 cm, height above floor: 2.5 cm) on one wall. The operant chambers were also equipped with a reward port between the levers (height above floor: 0.5 cm) that included a photo-beam to track port entries. Upon reward delivery, a 3-second tone (2900Hz) and a cue-light above the reward port was activated. To receive a reward, the mouse must press the active lever in a fixed-ratio 1 (FR1) schedule, where one active-lever press leads to one reward. A successful completion of this condition resulted in a delivery of 10 μ L of 20% alcohol to the reward port. The mouse must enter the reward port twice to reactivate the active lever, ensuring consumption of the reward. Animals received a total of 20 hours of training time in the paradigm in the first week (two 6-hour and two 4-hour sessions) before transitioning to 2-hour afternoon sessions that began consistently at 13:00. After 8 2-hour FR1 sessions, the complexity of the task was increased to FR2, where two active lever presses were required for one reward. Active lever presses, inactive lever presses, port entries, and reward deliveries were measured. Consumption was normalized based on mouse body weight and rewards administered. Discrimination index was calculated as the percentage of active lever presses divided by total presses. The proportion of reward lever presses statistic was calculated by comparing lever presses that led to a reward to total lever presses, including inactive lever presses. Mice with low viral expression were excluded from the study.

Contingency degradation: The contingency degradation experiment was conducted as previously described in (Morisot et al., 2019a). Mice were first trained in the OSA boxes on an FR1 schedule of reinforcement with 20% alcohol. Mice completed three 6-hour

sessions and three 4-hour sessions before transitioning to 2-hour sessions starting at 13:00. After two 2-hour sessions under the FR1 schedule, mice progressed to random ratio (RR) training. During RR OSA, rewards were delivered following a random number of lever presses. Mice completed five sessions under RR2 (one reward delivery following an average of two lever presses with number of presses ranging from one to three), followed by five sessions of RR3 (number of presses ranged from two to four), and ten sessions of RR4 (number of presses ranged three to five). After completion of training, mice underwent two types of contingency degradation testing sessions, non-degraded (ND) and degraded (D). During ND sessions, active lever pressing led to the same cue and reward delivery as RR4 training. However, during D sessions, active lever pressing had no outcome, and rewards were delivered regularly throughout the session, determined by the average reward delivery rate of the last five RR4 training sessions. One mouse was excluded due to low viral expression.

Sucrose operant self-administration: OSA of 1% sucrose was slightly modified from conditions described in (Laguesse et al., 2017). Specifically, mice underwent stereotaxic surgery to overexpress AAV-GFP or AAV-Rac1-DN-GFP in the DMS. After allowing for viral overexpression, mice began 1% sucrose self-administration training in the chambers previously described with two 6-hour and two 4-hour training sessions in the first week. Animals were handled for 1-2 minutes daily for 3 consecutive days before training began. They then transitioned to 2-hour afternoon sessions that began consistently at 13:00. After 8 2-hour FR1 sessions, the mice transitioned to FR2. Mice with low viral expression were excluded from the study.

Open-field test

Mice infected with either AAV-GFP or AAV-Rac1-DN were placed in an open field (43cm x 43cm) in low-light conditions and allowed to explore for 20 minutes (Warnault et al., 2016). Locomotor activity was tracked using EthoVision XT software (Noldus, Leesburg, VA), and total movement (cm) was reported.

Data analysis

GraphPad Prism 9 and MATLAB were used for statistical analysis.

Biochemical analysis: Data were analyzed using the appropriate statistical test, including one-way ANOVA, two-way ANOVA, three-way ANOVA, or two-tailed t-test for normal populations, or Kruskal-Wallis for non-normal populations. *Post hoc* testing was done using Šidák's multiple comparisons test. For data represented in Figures 1.3 and 1.4, statistical analysis was separated by independent variable.

IA20%2BC numbers are expressed as the mean \pm SEM consumption over the final two weeks (**Table 1.1**). Data was first tested for normality using the Shapiro-Wilk normality test with accompanying QQ plot. Parametric tests were performed on data samples deemed to be derived from normal populations. The results were determined to be statistically significant if the resulting p-value was less than 0.05.

Behavioral analysis: IA-2BC and OSA data were analyzed using a two-way repeated-measures ANOVA, followed by *post hoc* Šidák's multiple comparisons test. A two-tailed t-test was performed on the open-field locomotion. The results were determined to be statistically significant if the resulting p-value was less than 0.05.

Introduction to Chapter 2

Chapter 2 of this dissertation examines the physiological role of a protein that has been previously identified in mechanisms underlying AUD, Prosapip1. Our lab previously investigated Prosapip1 in the NAc, where it was found to control synaptic adaptations that drive alcohol intake, seeking, and reward (Laguesse et al., 2017). Laguesse et al. found that translation of Prosapip1 was significantly increased in an mTORC1-dependent manner in the NAc in response to alcohol drinking. This increase in translation led to an increase in synaptic protein levels that was sustained through withdrawal. The elevated levels of Prosapip1 protein led to the formation of F-actin which, in turn, caused the maturation of dendritic spines. Finally, it was shown that Prosapip1 drives alcohol self-administration and seeking. While this important work ties Prosapip1 in the NAc to mechanisms underlying AUD, nothing is known about the normal physiological role of Prosapip1. Here, we provide evidence that physiological role of Prosapip1 is to control PSD scaffolding, LTP, and learning and memory processes in the dorsal hippocampus.

Chapter 2

Prosapip1 in the dorsal hippocampus mediates long-term potentiation and spatial memory

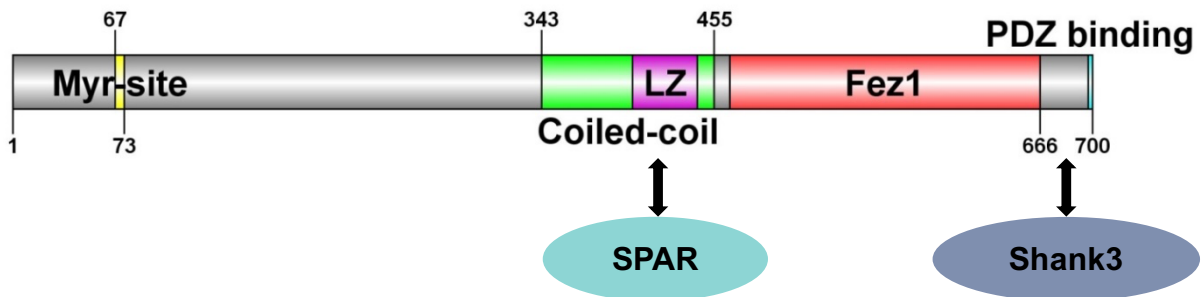
Contributing Authors: Zachary W. Hoisington, Himanshu Gangal, Khanhky Phamluong, Gregg E. Homanics, Jun Wang, and Dorit Ron

2.1 Abstract

Prosapip1 is a brain-specific protein localized to the post-synaptic density, where it has been shown to affect dendritic spine maturation. However, nothing is known about the physiological role of Prosapip1. To examine this, we utilized the Cre LoxP system to develop a Prosapip1 neuronal knockout mouse. We show that Prosapip1 is directly controlling the synaptic localization of proteins SPAR, PSD-95, and the GluN2B subunit of the NMDA receptor. Prosapip1 is also shown to play a role in NMDA-receptor-mediated transmission and long-term potentiation in the CA1 region of the dorsal hippocampus. While the Prosapip1 neuronal knockout mouse performed normally in developmental, locomotor, and anxiety tasks, it showed a spatial memory deficit in multiple behavioral paradigms. Using viral administration of Cre, Prosapip1 was knocked out specifically in the dorsal hippocampus, and the deficit in spatial memory was replicated. Taken together, the physiological role of Prosapip1 in the dorsal hippocampus is to facilitate long-term potentiation resulting in spatial learning and memory.

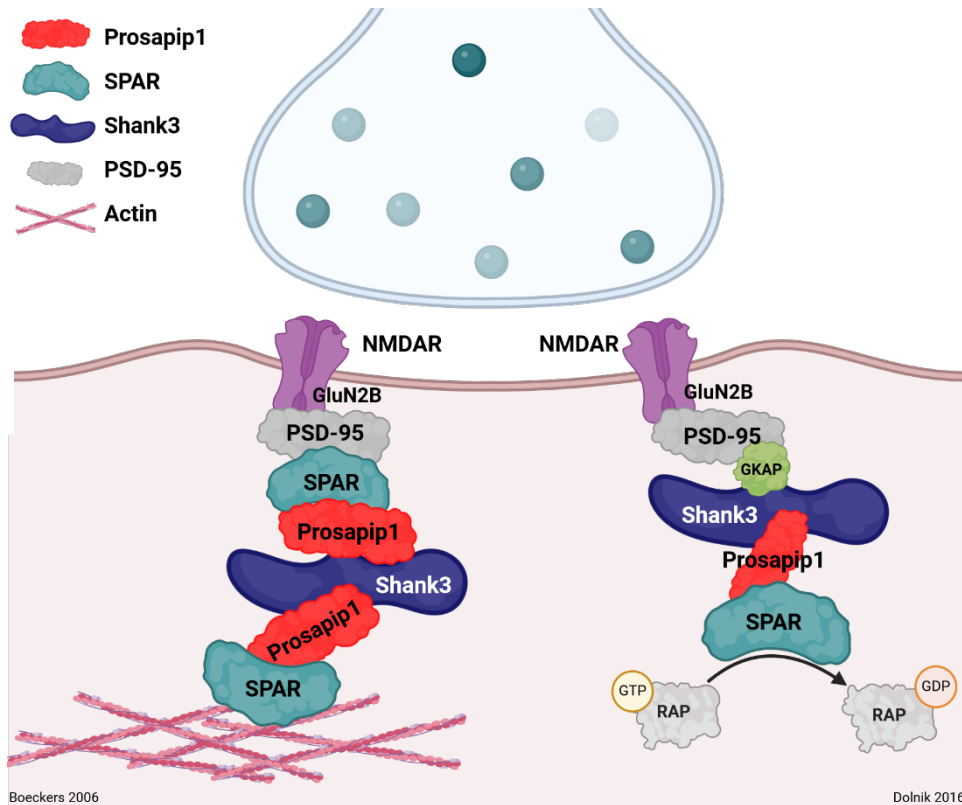
2.2 Introduction

ProSAP-interacting protein 1 (Prosapip1), encoded by the gene *LZTS3*, is a brain-specific protein that shows particularly high expression in the cortex, cerebellum, and the hippocampus (CA1, CA3, dentate gyrus (DG)) (Wendholt et al., 2006). It is highly enriched in the postsynaptic density (PSD) of excitatory synapses (Wendholt et al., 2006; Dolnik et al., 2016).



Model 3. Prosapip1 domains

Prosapip1 is characterized by a coiled-coil domain (CC) with an internal leucine zipper (LZ), a C-terminal Fez1 domain, and a C-terminal type I PDZ-domain-binding motif (STEI) (**Model 3**) (Wendholt et al., 2006). Its leucine zipper domain is known to be involved in protein-protein dimerization via the leucines, which provide a hydrophobic interaction environment (Vinson et al., 2002). Its central coiled-coil domain binds the spine-associated Rap GTPase-activating protein (SPAR) (Wendholt et al., 2006). Prosapip1 shares its C-terminal Fez1 domain with the other members of the Fezzin family (LAPSER1, PSD-Zip70, N4BP3) (Wendholt et al., 2006). The protein Fez1 (fasciculation and elongation protein zeta 1) is essential for neural circuit establishment and axon outgrowth (Razar et al., 2022). These Fezzins interact with the PDZ (PSD-95/Dlg1/ZO-1) domain of Shank family proteins.



Model 4. Prosapip1 is a key protein in the PSD

Prosapip1 specifically interacts with the well-known PSD protein Shank3 (Wendholt et al., 2006) (**Model 4**), whose role is to interconnect multiple proteins to provide structural and functional stability in the PSD (Sheng and Kim, 2000; Boeckers et al., 2002; Grabrucker et al., 2011; Sala et al., 2015). Through this interaction, Prosapip1 regulates the levels of SPAR (Wendholt et al., 2006; Dolnik et al., 2016; Reim et al., 2016), an essential modulator of spine morphology (Pak et al., 2001; Richter et al., 2007). Prosapip1 has been confirmed to interact with SPAR *in vivo* in the nucleus accumbens, where it leads to synaptic and structural modifications (Laguesse et al., 2017). Consequently, Prosapip1 is hypothesized to directly contribute to synaptic function (Dolnik et al., 2016), and has been shown to control the maturation of dendritic spines (Reim et al., 2016). However, nothing is known about the basal physiological role of Prosapip1 *in vivo*. Here, we report that

Prosapip1 in the dorsal hippocampus mediates long-term potentiation and spatial memory.

2.3 Results

2.3.1 Generation and characterization of Prosapip1(flx/flx) mice

To elucidate the role of Prosapip1 in the CNS, we first developed a mouse line with flox sites flanking the Prosapip1 gene. Guide RNA binding sites were identified in intron 2 and in the 3' UTR of exon 5 of Prosapip1 (*Lzts3*) (**Figure 2.1A**). PAGE purified Ultramer single stranded DNA oligos that were homologous to the target loci in intron 2 and exon 5 (**Figure 2.1B**) were used as repair templates.

To construct a conditional knockout of Prosapip1 in neurons, we crossed the homozygous Prosapip1 floxed (Prosapip1(flx/flx)) mouse with a mouse line expressing Cre recombinase under the control of a synapsin promoter (Syn1-Cre(+)). Male Prosapip1(flx/flx);Syn1-Cre(-/-) mice were mated with female Prosapip1(flx/flx);Syn1-Cre(+/-) mice (**Figure 2.1C**), which generated Prosapip1(flx/flx);Syn1-Cre(+) and Prosapip1(flx/flx);Syn1-Cre(-) mice, which were used as controls. The neuronal knockout was confirmed via western blot (**Figure 2.1D**). Prosapip1(flx/flx);Syn1-Cre(-) mice have protein levels of Prosapip1 comparable to a C57BL/6 mouse, while Prosapip1(flx/flx);Syn1-Cre(+) show a complete removal of Prosapip1 protein in the dorsal hippocampus. Body weight of male and female mice was monitored every 2 weeks from birth to assess potential developmental effects. While males were significantly heavier than females throughout development, there was no significant effect of the genotype on weight over time (**Figure 2.1E**) (Three-way ANOVA: Effect of genotype $F_{(1,33)} = 0.7842$, $p = 0.3823$; Effect of sex $F_{(1,33)} = 23.94$, $p < 0.0001$; Effect of time $F_{(5,158)} = 588.4$, $p = < 0.0001$; Effect of genotype x sex $F_{(1,33)} = 1.345$, $p = 0.2545$; Effect of

genotype x time $F_{(5,158)} = 0.1476$, $p = 0.9805$; Effect of sex x time $F_{(5,158)} = 2.345$, $p = 0.0437$; Effect of genotype x sex x time $F_{(5,158)} = 0.3764$, $p = 0.8643$).

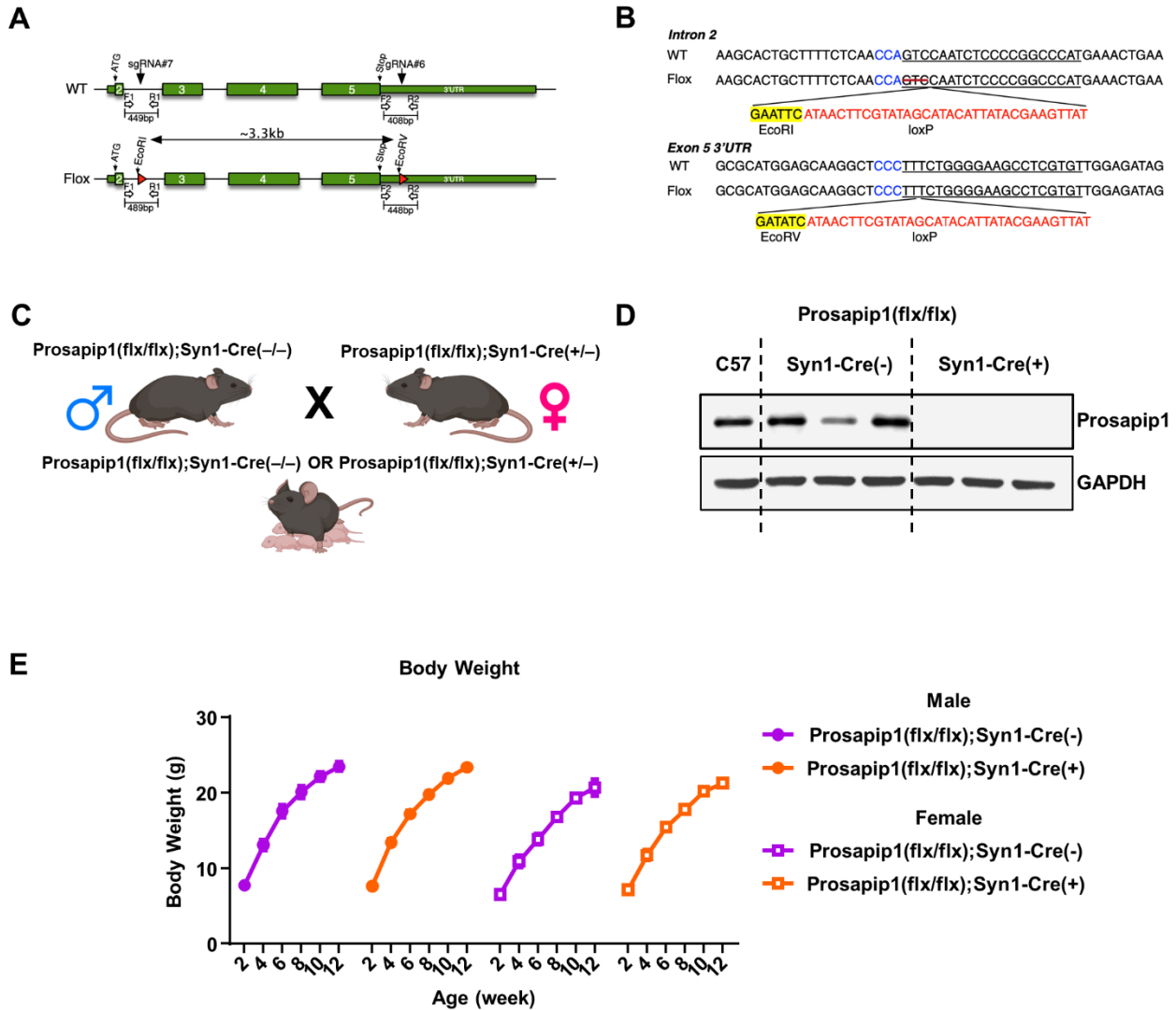


Figure 2.1. Generation and characterization of Prosapip1(flx/flx) mice

(A) Identification of guide RNA binding sites in intron 2 and the 3' UTR of exon 5 of Prosapip1. (B) PAGE purified Ultramer single stranded DNA oligos that were homologous to the target loci in intron 2 and exon 5 were used as repair templates. (C) Genetic crossing scheme of the Prosapip1(flx/flx);Syn1-Cre mice. Male Prosapip1(flx/flx);Syn1-Cre(-/-) mice were mated with female Prosapip1(flx/flx);Syn1-Cre(+/-) mice, leading to litters of Prosapip1(flx/flx);Syn1-Cre(+/-) (experimental) and (figure caption continued on next page)

(figure caption continued from previous page)

Prosapip1(flx/flx);Syn1-Cre(-/-) (control) mice. **(D)** Western blot analysis of the dorsal hippocampus of Prosapip1(flx/flx);Syn1-Cre(-) and Prosapip1(flx/flx);Syn1-Cre(+) mice. Prosapip1(flx/flx);Syn1-Cre(+) mice have a complete knockout of Prosapip1, while Prosapip1(flx/flx);Syn1-Cre(-) mice are comparable to a C57BL/6 control. **(E)** Body weight of male and female Prosapip1(flx/flx);Syn1-Cre(-) and Prosapip1(flx/flx);Syn1-Cre(+) mice was measured biweekly from birth. There was no effect of Prosapip1 neuronal knockout on body weight over time. Data are represented as mean \pm SEM and analyzed using three-way ANOVA. n = 5-11 per group.

2.3.2 Prosapip1 is required for synaptic localization of PSD proteins

Prosapip1 is a scaffolding protein that recruits SPAR to the PSD and interconnects it with Shank3 (Wendholt et al., 2006; Reim et al., 2016). Therefore, we first examined how the synaptic localization of SPAR and Shank3 were affected by Prosapip1 neuronal knockout. We analyzed the total (**Figure 2.2A**) and synaptic (**Figure 2.2B**) levels of SPAR and Shank3 in the dorsal hippocampus of Prosapip1(flx/flx);Syn1-Cre(-) and Prosapip1(flx/flx);Syn1-Cre(+) mice. We did not detect a change in total SPAR between groups (**Figure 2.2C**) (Welch's t-test: $t_{(6.963)} = 1.427$, $p = 0.1968$), but saw a significant reduction in synaptic SPAR in Prosapip1(flx/flx);Syn1-Cre(+) mice (**Figure 2.2D**) (Welch's t-test: $t_{(5.880)} = 5.183$, $p = 0.0022$). The total and synaptic levels of Shank3 were similar between groups (**Figure 2.2E-F**) (Welch's t-test: Total $t_{(6.923)} = 1.345$, $p = 0.2210$, Synaptic $t_{(6.720)} = 0.1306$, $p = 0.8999$). Collectively, these results imply that Prosapip1 in the dorsal hippocampus is necessary for synaptic localization of SPAR, but not Shank3.

After observing a reduction in synaptic levels of SPAR resulting from Prosapip1 knockout, we hypothesized further disruption to PSD complexes. As SPAR and Shank3 are known to interact with NMDAR and AMPAR (Naisbitt et al., 1999; Tu et al., 1999; Boeckers et al., 2002; Arons et al., 2012; Ross and Aizenman, 2023), we examined the synaptic levels of NMDAR subunits GluN2A and GluN2B, along with AMPAR subunit GluA1. In addition, we examined synaptic levels of PSD-95, a protein known to interact with SPAR and stabilize NMDAR surface expression (Naisbitt et al., 1999; Tu et al., 1999; Pak et al., 2001; Boeckers, 2006; Won et al., 2016; Coley and Gao, 2019). Protein levels were measured through western blot analysis in both the total homogenate and crude synaptosomal fraction (**Figure 2.2G-H**). While we observed no change in the overall

levels of GluN2B (**Figure 2.2I**) (Welch's t-test: $t_{(6.700)} = 1.675$, $p = 0.1398$), we saw a significant reduction in the synaptic levels in Prosapip1(flx/flx);Syn1-Cre(+) mice compared to Prosapip1(flx/flx);Syn1-Cre(-) controls (**Figure 2.2J**) (Welch's t-test: $t_{(6.332)} = 5.524$, $p = 0.0012$). In contrast, the total and synaptic levels of NMDAR subunit GluN2A were unchanged in the Prosapip1(flx/flx);Syn1-Cre(+) mice (**Figure 2.2K-L**) (Welch's t-test: Total $t_{(4.429)} = 0.1050$, $p = 0.9210$; Synaptic $t_{(6.689)} = 0.1758$, $p = 0.8656$). Total and synaptic levels of GluA1 were also unchanged in Prosapip1(flx/flx);Syn1-Cre(+) mice (**Figure 2.2M-N**) (Welch's t-test: Total $t_{(6.956)} = 0.1831$, $p = 0.8599$; Synaptic $t_{(6.060)} = 0.8548$, $p = 0.4252$). When examining the protein levels of PSD-95, we saw Prosapip1(flx/flx);Syn1-Cre(+) exhibited a reduction in total PSD-95 (**Figure 2.2O**) and a drastic reduction in synaptic PSD-95 (**Figure 2.2P**) (Welch's t-test: Total $t_{(4.740)} = 3.174$, $p = 0.0266$; Synaptic $t_{(5.693)} = 8.136$, $p = 0.0002$). Together, Prosapip1 is involved in the synaptic localization of NMDAR subunit GluN2B and total and postsynaptic protein level of PSD-95 in the dorsal hippocampus.

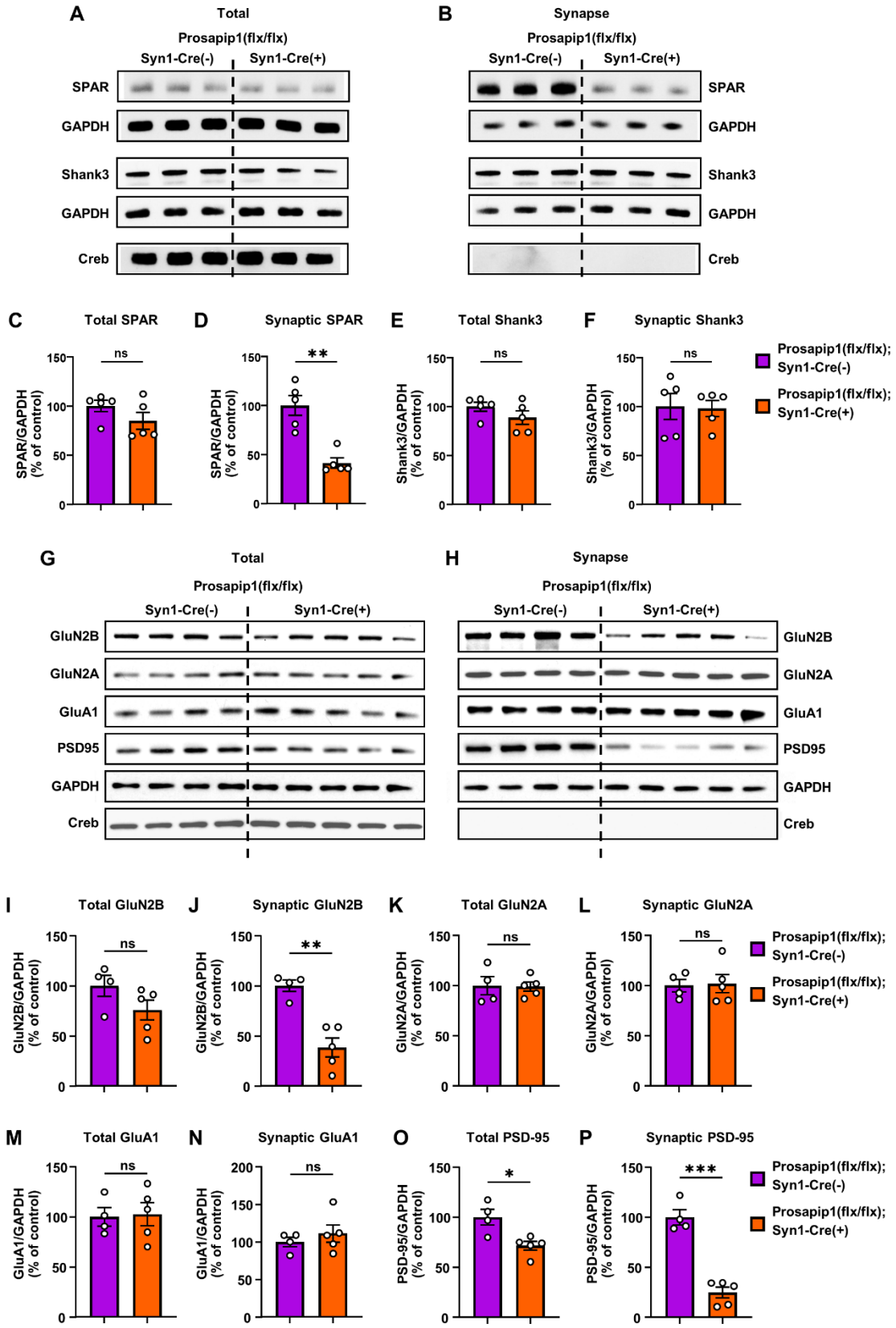


Figure 2.2. Prosapip1 is required for synaptic localization of PSD proteins

Figure 2.2. Prosapip1 is required for synaptic localization of PSD proteins

(A-B) The dorsal hippocampus was harvested from Prosapip1(flx/flx);Syn1-Cre(-) and Prosapip1(flx/flx);Syn1-Cre(+) mice, and western blot analysis was performed on the total homogenate **(A)** and crude synaptic fraction **(B)**. **(C)** Total SPAR levels were unchanged between groups. **(D)** Synaptic SPAR was significantly reduced in Prosapip1(flx/flx);Syn1-Cre(+) mice compared to controls. **(E-F)** Neither the total **(E)** nor synaptic **(F)** protein levels of Shank3 were affected by the Prosapip1 knockout. Data are represented as mean \pm SEM and analyzed using unpaired two-tailed t-test with Welch's correction. ** $p < 0.01$; ns, non-significant. $n = 5$ per group. **(G-H)** Western blot on the total **(G)** and synaptic fraction **(H)** of the dorsal hippocampus of Prosapip1(flx/flx);Syn1-Cre(-) and Prosapip1(flx/flx);Syn1-Cre(+) mice. **(I)** Total levels of NMDAR subunit GluN2B were similar in Prosapip1(flx/flx);Syn1-Cre(-) and Prosapip1(flx/flx);Syn1-Cre(+) mice. **(J)** Synaptic levels of GluN2B were significantly reduced in Prosapip1(flx/flx);Syn1-Cre(+) mice. **(K-L)** Both total **(K)** and synaptic **(L)** levels of NMDAR subunit GluN2A were unchanged between Prosapip1(flx/flx);Syn1-Cre(-) and Prosapip1(flx/flx);Syn1-Cre(+) mice. **(M-N)** Total and synaptic levels of AMPAR subunit GluA1 were unchanged in Prosapip1(flx/flx);Syn1-Cre(-) compared to Prosapip1(flx/flx);Syn1-Cre(+) mice. **(O-P)** The level of total and synaptic PSD-95 protein was significantly reduced in the dorsal hippocampus of Prosapip1(flx/flx);Syn1-Cre(+) mice compared to controls. Data are represented as mean \pm SEM and analyzed using unpaired two-tailed t-test with Welch's correction. * $p < 0.05$, ** $p < 0.01$, *** $p < 0.001$; ns, non-significant. $n = 4-5$ per group.

2.3.3 Prosapip1 in the dorsal hippocampus plays a role in NMDA receptor-mediated transmission and long-term potentiation

Given the altered synaptic protein composition in Prosapip1 neuronal knockout mice, we explored potential impairments in hippocampal long-term potentiation (LTP). To examine this, hippocampal slices from both Prosapip1(flx/flx);Syn1-Cre(-) and Prosapip1(flx/flx);Syn1-Cre(+) mice were prepared for electrophysiology recordings. Bipolar stimulating electrodes were positioned in the CA1 region of the dorsal hippocampal slices. Simultaneously, the recording electrode was placed approximately 100-150 μm away from the stimulating electrode (**Figure 2.3A**). The administration of a single electrical pulse (2 ms) elicited a fiber volley, followed by a field excitatory postsynaptic potential response (fEPSPs) (**Figure 2.3B**). Before inducing LTP, a stable baseline of fEPSPs was established for 10 minutes. Following this, high-frequency stimulation (HFS) was applied at 100 Hz for 1 second, repeated four times at 20-second intervals, to trigger LTP. In the control mice, there was a significant increase in the fEPSP amplitude following HFS, indicating successful LTP induction, and this potentiation persisted for at least 30 minutes. Conversely, in the Prosapip1(flx/flx);Syn1-Cre(+) mice, such potentiation was notably absent. A comparative analysis of the normalized fEPSPs, conducted 20-30 minutes post-HFS, revealed a significantly reduced fEPSP amplitude in the Prosapip1(flx/flx);Syn1-Cre(+) group compared to the Prosapip1(flx/flx);Syn1-Cre(-) controls (**Figure 2.3D**) (Unpaired t-test: $t_{(17)} = 3.933$, $p < 0.01$). These findings strongly suggest Prosapip1 plays a role in the induction of hippocampal LTP.

The LTP induction in the hippocampus is known to rely on the functioning of postsynaptic NMDARs. Therefore, we aimed to discern if there were any differences

between Prosapip1(flx/flx);Syn1-Cre(-) and Prosapip1(flx/flx);Syn1-Cre(+) mice in terms of NMDAR-mediated excitatory postsynaptic currents (EPSCs) in CA1 pyramidal neurons. A whole-cell voltage-clamp recording technique was employed for this purpose. First, a low concentration of external Mg^{2+} was used to facilitate the removal of the magnesium block from the NMDAR channel. Concurrently, AMPARs and GABA_A receptors (GABA_ARs) were pharmacologically inhibited. NMDAR-EPSCs were recorded in response to an escalating series of stimulus intensities. The amplitude of NMDAR-EPSCs was significantly reduced in the Prosapip1(flx/flx);Syn1-Cre(+) mice compared to the controls (**Figure 2.3E**) (Two-way ANOVA: Effect of intensity $F_{(1,3)} = 9.441$, $p < 0.001$; Effect of genotype $F_{(1,23)} = 4.565$, $p = 0.044$; Effect of intensity x genotype $F_{(1,3)} = 1.376$, $p = 0.258$). To determine whether this change in NMDAR-EPSCs resulted from pre- or postsynaptic alterations, we investigated postsynaptic changes by measuring NMDA-induced currents. This was done by bath application of NMDA (20 μ M for 30 seconds). We observed that the peak current in the Prosapip1(flx/flx);Syn1-Cre(+) mice was markedly lower than that in their control counterparts (**Figure 2.3F**) (Unpaired t-test: $t_{(22)} = 3.094$, $p = 0.00529$). This suggests a decrease in postsynaptic NMDAR responsiveness in Prosapip1(flx/flx);Syn1-Cre(+) mice.

Our research then focused on determining the presence of any presynaptic alterations in glutamatergic transmission affecting CA1 neurons. We pursued this by measuring the paired-pulse ratio (100 ms interval) of electrically evoked EPSCs in these neurons. Our findings revealed that this ratio was significantly higher in the Prosapip1(flx/flx);Syn1-Cre(+) group as compared to the controls, indicating a probable reduction in presynaptic glutamate release onto CA1 neurons in the

Prosapip1(flx/flx);Syn1-Cre(+) mice (**Figure 2.3G**) (Unpaired t-test: $t_{(22)} = 2.099$, $p = 0.0475$) (Zucker and Regehr, 2002).

In summary, the data collectively imply that the absence of Prosapip1 impairs the induction of hippocampal LTP. This impairment is likely attributed to the downregulation of NMDAR function in these mice.

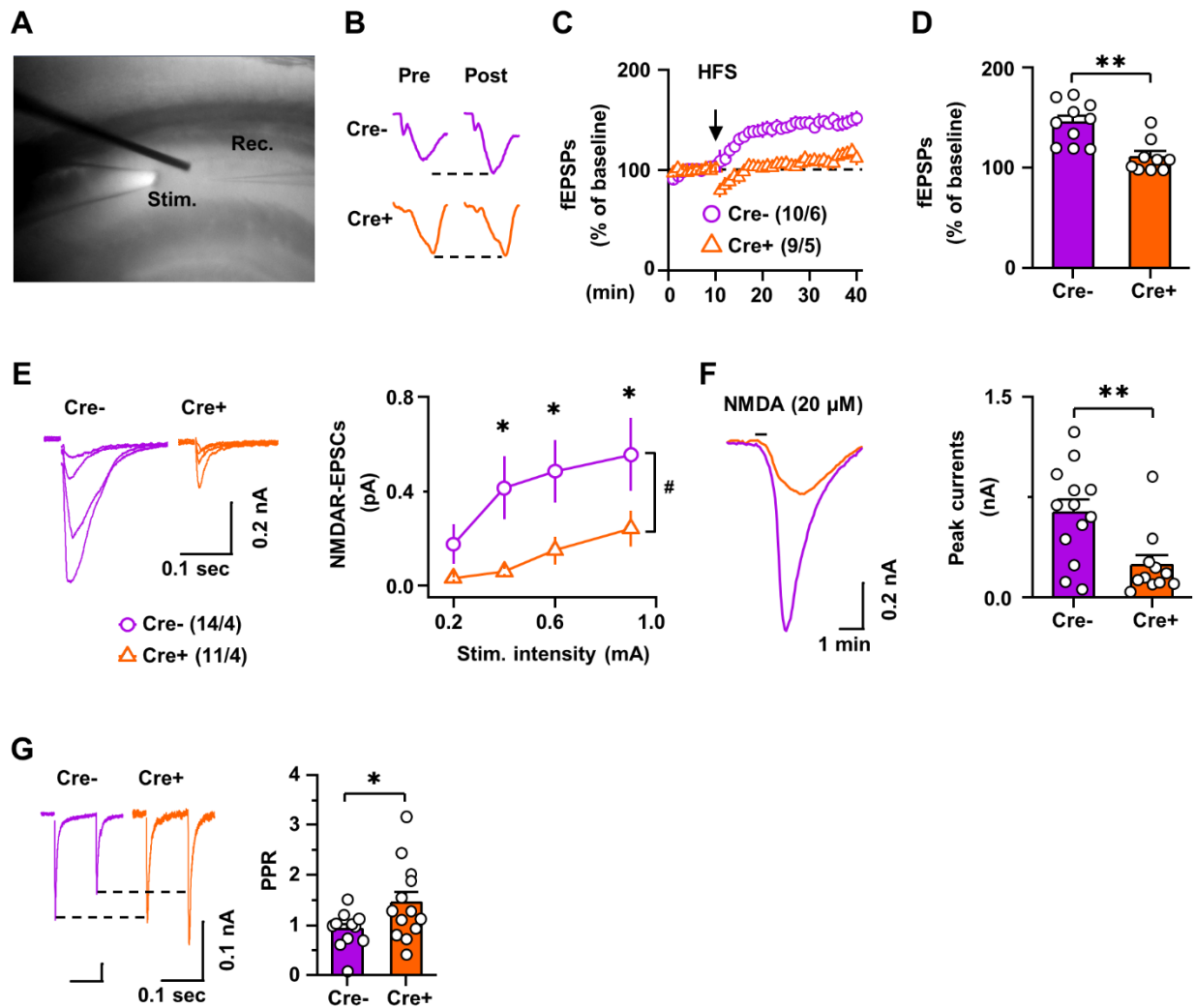


Figure 2.3. Prosapip1 in the dorsal hippocampus plays a role in NMDA receptor-mediated transmission and long-term potentiation

(A) Arrangement of stimulating and recording electrodes within the hippocampal CA1 region. (B) Sample field excitatory postsynaptic potential (fEPSP) traces recorded before (figure caption continued on next page)

(figure caption continued from previous page)

(pre) and after (post) administering high-frequency stimulation (HFS) in both Prosapip1(flx/flx);Syn1-Cre(-) (Cre-) and Prosapip1(flx/flx);Syn1-Cre(+) (Cre+) groups. The HFS was 100 Hz, with 100 pulses, repeated four times every 20 seconds. **(C)** The time course of fEPSPs before and after HFS is graphically depicted. n = 10 slices from 6 mice (10/6) for Cre- and 9/5 for Cre+. **(D)** fEPSP amplitudes, measured between 30-40 minutes, were significantly lower in the Cre+ group than Cre- controls; **p < 0.01 by unpaired t-test. **(E)** Electrically-evoked NMDAR-EPSC amplitudes in CA1 neurons were lower in the Cre+ mice than Cre- controls; #p < 0.05; *p < 0.05 versus Cre+ at the same stimulating intensities by two-way RM ANOVA followed by post-hoc Tukey test; n = 14 neurons from 4 mice (14/4, Cre-) and (11/4, Cre+). **(F)** The peak currents induced by NMDA (20 μ M for 30 seconds) in CA1 neurons were significantly smaller in Cre+ mice than in Cre- controls; **p < 0.01 by unpaired t-test; n = 13/4 (Cre-) and 11/4 (Cre+). **(G)** Paired-pulse ratios for EPSCs in CA1 neurons were higher in the Cre+ mice than in the Cre- controls; *p < 0.05 by unpaired t-test; n = 11/3 (Cre-) and 13/4 (Cre+).

2.3.4 Prosapip1 knockout does not affect locomotion or anxiety

As Prosapip1 knockout is affecting neuronal PSD scaffolding and LTP, we next performed a behavioral battery to assess the consequences of these molecular changes. Upon reaching adulthood, mice were placed in an open field and allowed to explore for 20 minutes, where locomotor and exploratory activity were measured. The Prosapip1 neuronal knockout did not alter locomotor activity (**Figure 2.4A**) (Unpaired t-test: $t_{(41)} = 1.460$, $p = 0.1518$). Furthermore, there were no differences between genotypes when assessing the time spent in the center of the open field (**Figure 2.4B**) (Two-way ANOVA: Effect of genotype $F_{(1,19)} = 0.05615$, $p = 0.8152$; Effect of sex $F_{(1,20)} = 0.07505$, $p = 0.7869$; Effect of genotype x sex $F_{(1,19)} = 1.224$, $p = 0.2823$).

Next, the light/dark box and elevated plus maze paradigms were used to assess anxiety-like behavior. The light/dark box consists of two chambers where the subject may choose to explore the well-lit (“light”) or visible-light-blocked (“dark”) side of a chamber. Spending more time in the dark side of the chamber implies an increase in anxiety. Both Prosapip1(flx/flx);Syn1-Cre(-) and Prosapip1(flx/flx);Syn1-Cre(+) mice spent significantly more time in the dark side of the light/dark box, but there was no significant difference between the genotypes (**Figure 2.4C**) (Two-way ANOVA: Effect of chamber $F_{(1,29)} = 92.69$, $p < 0.0001$; Effect of genotype $F_{(1,29)} = 0.9504$, $p = 0.3377$; Effect of chamber x genotype $F_{(1,29)} = 0.09645$, $p = 0.7584$). Mice also underwent the elevated plus maze test. The elevated plus maze is elevated above the floor and consists of two “closed” arms with opaque walls and two “open” arms with no railing. Time exploring the open arm is used to assess anxiety. Prosapip1(flx/flx);Syn1-Cre(-) and Prosapip1(flx/flx);Syn1-Cre(+) mice spent a similar amount of time exploring the open arm (**Figure 2.4D**) (Mann Whitney Test:

$p = 0.2878$). Taken together, it does not appear that neuronal Prosapip1 is involved in anxiety-related behavior.

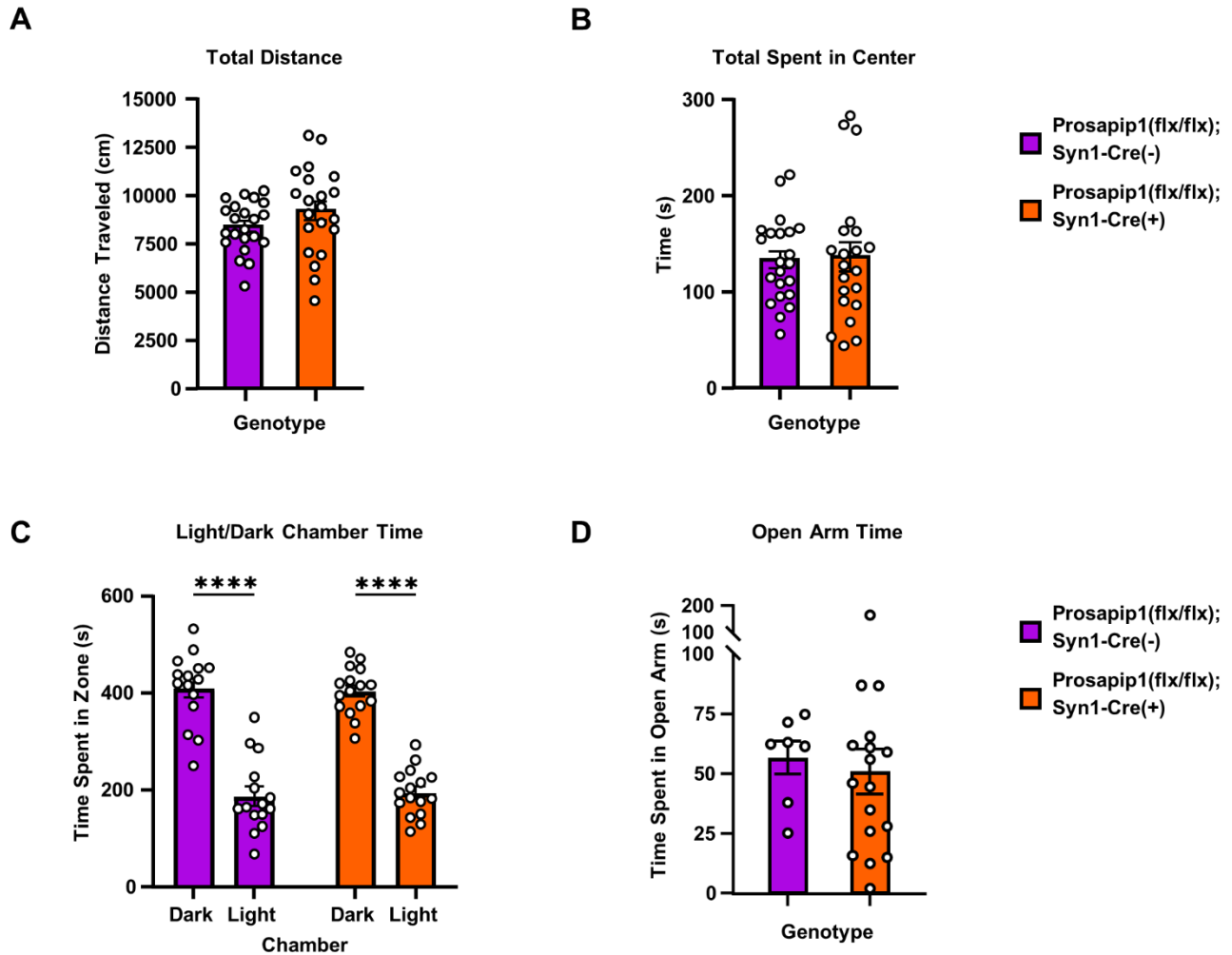


Figure 2.4. Prosapip1 knockout does not affect locomotion or anxiety

(A) Total distance traveled during the open field test. Prosapip1(flx/flx);Syn1-Cre(-) and Prosapip1(flx/flx);Syn1-Cre(+) mice traveled a similar distance in the open field. **(B)** Time spent in the center of the open field. There was no difference between genotypes in time spent in center. **(C)** Light/dark box chamber time. Both Prosapip1(flx/flx);Syn1-Cre(-) and Prosapip1(flx/flx);Syn1-Cre(+) mice spent significantly more time in the dark chamber, and there was no difference between the genotypes. **(D)** Exploratory behavior of mice in the elevated plus maze. Prosapip1(flx/flx);Syn1-Cre(-) and Prosapip1(flx/flx);Syn1-Cre(+) mice spent a similar amount of time exploring the open arm of the maze. Data are represented as mean \pm SEM and analyzed using unpaired two-tailed t-test (A, B, D) or two-way ANOVA (C). **** $p < 0.0001$. $n = 7-21$.

2.3.5 Prosapip1 contributes to spatial memory

Prosapip1 was originally identified in hippocampal neurons (Wendholt et al., 2006; Reim et al., 2016), a brain region associated with memory (Broadbent et al., 2004). Given the altered PSD composition and subsequent loss of LTP in this region after Prosapip1 knockout, we assessed the effect of the knockout on memory-related behaviors in mice. First, mice performed the novel object recognition (NOR) test (Leger et al., 2013; Lueptow, 2017) with an inter-trial interval of 24 hours to assess long-term spatial memory. Prosapip1(flx/flx);Syn1-Cre(-) animals showed a significant preference for the novel object, indicating long-term recognition memory of the familiar object and its spatial location (**Figure 2.5A**). Contrarily, Prosapip1(flx/flx);Syn1-Cre(+) mice spent a similar amount of time exploring both objects, performing at chance levels (**Figure 2.5A**) (Two-way ANOVA: Effect of object $F_{(1,40)} = 34.32$, $p < 0.0001$; Effect of genotype $F_{(1,40)} = 0.3079$, $p = 0.5821$; Effect of object x genotype $F_{(1,40)} = 18.37$, $p = 0.0001$). The lack of novel object recognition implies a loss of object characteristic acquisition or long-term spatial memory.

To further assess the role of Prosapip1 in spatial learning and memory, the mice performed a novelty T-maze test (Sanderson et al., 2009). Mice are allowed to explore two arms of a “T”-shaped maze during training trials while the third arm is blocked. All three arms are available during the test. The experiment utilized a 1-minute inter-trial interval, which is reliant on hippocampal LTP (Sanderson et al., 2009). During the test trial, Prosapip1(flx/flx);Syn1-Cre(-) mice primarily explored the novel arm of the T-maze, indicated by a positive difference score (time spent in novel arm – time spent in familiar arm) (**Figure 2.5B**). Prosapip1(flx/flx);Syn1-Cre(+) mice explored the arms at chance levels, performing significantly worse than control animals, and indicating a lack of spatial

memory for the familiar arm of the maze (**Figure 2.5B**) (Welch's t-test: $t_{(26.08)} = 5.434$, $p < 0.0001$).

Next utilized was the 3-chamber social interaction (3CSI) test. The 3CSI test has two stages. The first part measures the preference for social interaction with a juvenile interaction partner. The *Prosapip1* interaction partner, *Shank3*, is a protein associated with autism spectrum disorder, and mice deficient in *Shank3* display dysfunctional social behavior in this test (Peca et al., 2011). We found that *Prosapip1(flx/flx);Syn1-Cre(-)* and *Prosapip1(flx/flx);Syn1-Cre(+)* mice behave similarly, with both significantly preferring the interaction partner over the empty chamber (**Figure 2.5C**) (Two-way ANOVA: Effect of social $F_{(1,29)} = 34.30$, $p < 0.0001$; Effect of genotype $F_{(1,29)} = 5.419$, $p = 0.0271$, Effect of social x genotype $F_{(1,29)} = 0.05655$, $p = 0.8137$; *post hoc* Empty vs. Social: *Prosapip1(flx/flx);Syn1-Cre(-)* $p = 0.0006$, *Prosapip1(flx/flx);Syn1-Cre(+)* $p = 0.0005$). In the second stage of the 3CSI, the mouse has the choice between interacting with a familiar partner (partner from part 1) or a novel interaction partner. This assesses the social novelty recognition of the subject. *Prosapip1(flx/flx);Syn1-Cre(-)* mice displayed a preference for the novel interaction partner, exhibited by the increase in chamber time (**Figure 2.5D**) (Two-way ANOVA: Effect of social novelty $F_{(1,29)} = 17.60$, $p = 0.0002$; Effect of genotype $F_{(1,29)} = 1.463$, $p = 0.2362$, Effect of social novelty x genotype $F_{(1,29)} = 2.947$, $p = 0.0967$; *post hoc* Familiar vs. Novel: *Prosapip1(flx/flx);Syn1-Cre(-)* $p = 0.0008$). *Prosapip1(flx/flx);Syn1-Cre(+)* mice spent a similar amount of time with the familiar and novel interaction partners (**Figure 2.5D**) (*post hoc* Familiar vs. Novel: *Prosapip1(flx/flx);Syn1-Cre(+)* $p = 0.1451$). The lack of discrimination from

Prosapip1(flx/flx);Syn1-Cre(+) mice implies an abated recognition of social novelty or loss of social memory.

While the Prosapip1(flx/flx);Syn1-Cre(+) mice show impaired performance in the NOR and novelty T-maze tests, these results may be attributed to the learning/acquisition process or storage of memory. For a more detailed investigation into the role of Prosapip1 on spatial learning and memory, we employed the Barnes maze (Barnes, 1979; Pitts, 2018). The Barnes maze is a white plastic platform with holes evenly drilled around the perimeter. Underneath one of these holes is an exit tunnel. The protocol has a training and testing phase, where spatial learning and memory, respectively, are specifically examined. When originally habituated the maze, there was no difference in baseline exploratory profile between Prosapip1(flx/flx);Syn1-Cre(-) and Prosapip1(flx/flx);Syn1-Cre(+) mice (**Extended Figure 2.5A**) (Unpaired t-test: $t_{(16)} = 0.2635$, $p = 0.7955$). The primary variable examined during training trials was the path to escape, which tracked the distance traveled from the starting point to the exit compartment. A shorter path to escape is more efficient and indicates learning of the paradigm objective and exit location. Prosapip1(flx/flx);Syn1-Cre(-) mice immediately improve performance, with a significant decrease in path to escape observed as soon as the third trial (**Figure 2.5E**) (Two-way ANOVA: Effect of trial $F_{(15,285)} = 7.899$, $p < 0.0001$, *post hoc* Prosapip1(flx/flx);Syn1-Cre(-), Trial 1 vs. Trial 3: $p = 0.0465$). Prosapip1(flx/flx);Syn1-Cre(+) mice improved performance over time but more gradually, and performed significantly worse than control mice over the entirety of training (**Figure 2.5E**) (Two-way ANOVA: Effect of genotype $F_{(1,19)} = 102.0$, $p < 0.0001$; Effect of trial x genotype $F_{(15,285)} = 1.401$, $p = 0.1454$). The performance was significantly different by the second trial (*post hoc* Trial 2,

Prosapip1(flx/flx);Syn1-Cre(-) vs. Prosapip1(flx/flx);Syn1-Cre(+) $p < 0.0001$). In addition, Prosapip1(flx/flx);Syn1-Cre(+) mice committed significantly more primary (incorrect hole visit) and secondary (incorrect hole revisit) errors throughout training (**Figure 2.5F**) (Three-way ANOVA: Effect of trial $F_{(15,289)} = 7.289$, $p < 0.0001$; Effect of genotype $F_{(1,19)} = 100.7$, $p < 0.0001$; Effect of error type $F_{(0.4468, 8.489)} = 4.554$, $p = 0.0772$; Effect of trial x genotype $F_{(15,289)} = 1.529$, $p = 0.0940$; Effect of trial x error type $F_{(6.157, 117)} = 2.865$, $p = 0.0115$; Effect of genotype x error type $F_{(1,19)} = 15.09$, $p = 0.0010$; Effect of trial x genotype x error type $F_{(15,285)} = 1.831$, $p = 0.0303$).

Differences in training performance can be explained by examining the search strategy of each mouse. There are three defined search strategies: random, serial, and spatial, which correspond to an increase in task efficiency (**Figure 2.5G**). Prosapip1(flx/flx);Syn1-Cre(-) mice searched randomly during the first trial before quickly switching to a serial search strategy. Spatial searching appeared as early as trial 3, and its ratio increased until it had become a majority on the last day of training (**Figure 2.5H**). In the Prosapip1(flx/flx);Syn1-Cre(+) mice, randomly searching was a much more prevalent strategy throughout training (**Figure 2.5I**). Some, and eventually a majority, of mice switched to serial search strategy, which also explains the gradual decrease in path to escape. Few Prosapip1(flx/flx);Syn1-Cre(+) mice utilized the spatial search strategy. Comparing these differences, both groups associate the context of the Barnes maze with the objective to escape, but Prosapip1(flx/flx);Syn1-Cre(+) mice fail to learn or remember the spatial location of the exit.

The probe trial of the Barnes maze specifically assesses the spatial memory of the mouse. During the probe trial, the exit is removed, and the mouse is allowed to explore

the platform for 5 minutes. If the mouse remembers the location of the exit, it will spend significantly more time exploring the exit quartile compared to chance alone. Control mice performed above chance value, spending an average of 116.84 seconds in the exit quartile (**Figure 2.5J**). *Prosapip1(flx/flx);Syn1-Cre(+)* mice, contrarily, performed around chance, spending an average of 68.52 seconds in the exit quartile (**Figure 2.5J**). This was significantly less than control mice (Mann-Whitney test, $p = 0.0004$). *Prosapip1* is required for spatial memory in the Barnes maze.

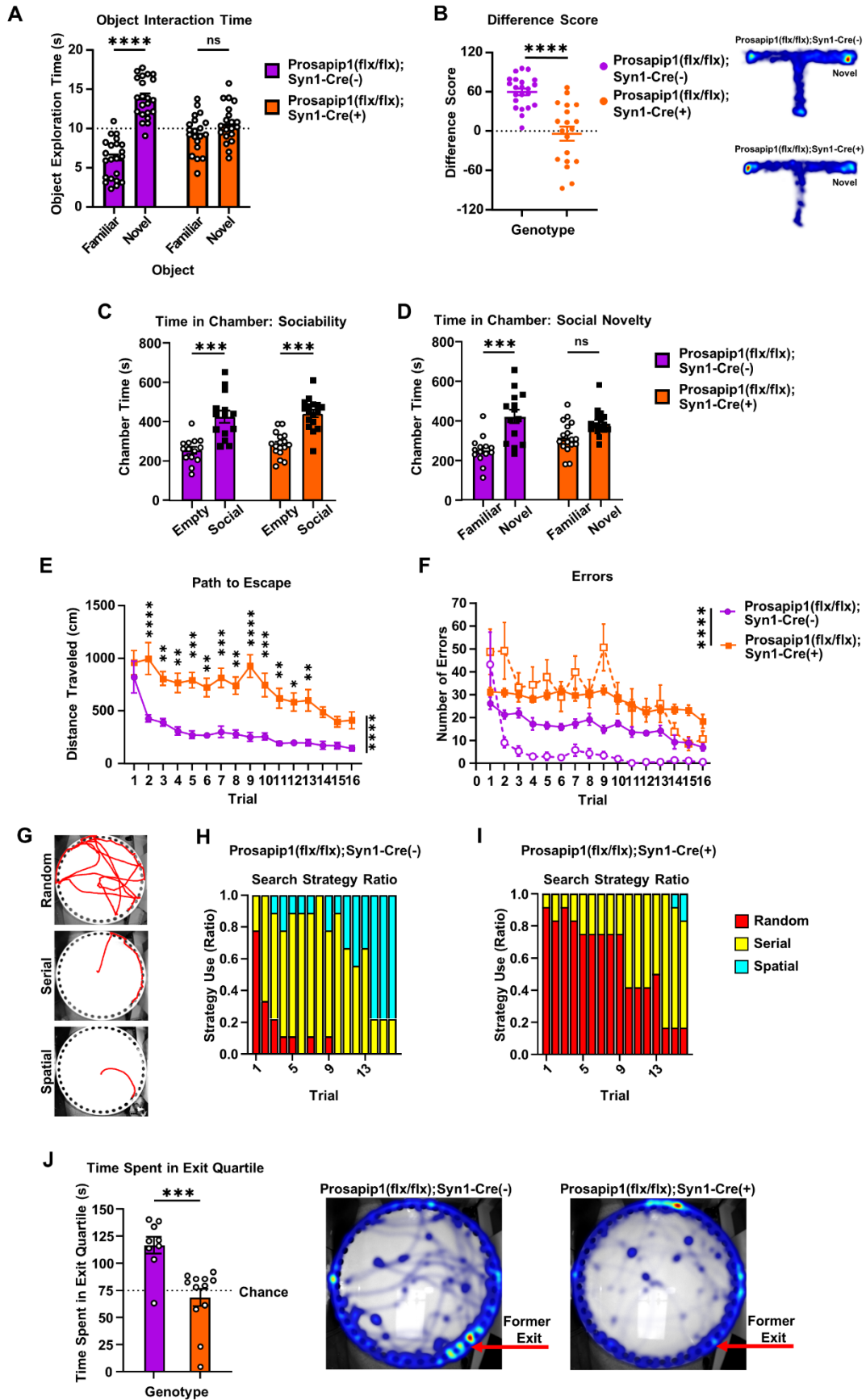
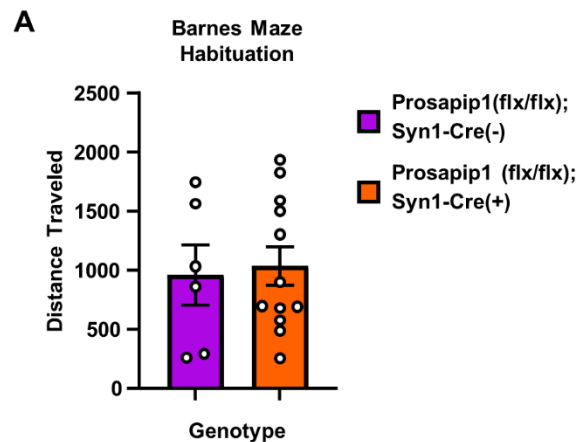


Figure 2.5. Prosapip1 contributes to spatial memory

Figure 2.5. Prosapip1 contributes to spatial memory

(A) Time spent exploring the familiar and novel objects in the novel object recognition test. *Prosapip1(flx/flx);Syn1-Cre(-)* mice significantly preferred the novel object, while *Prosapip1(flx/flx);Syn1-Cre(+)* mice showed no preference. **(B)** Difference score of time spent exploring the novel arm of the T-maze. *Prosapip1(flx/flx);Syn1-Cre(-)* had a significantly higher difference score than *Prosapip1(flx/flx);Syn1-Cre(+)* mice. **(C)** Time spent in the empty and social-paired chamber in the 3-chamber social interaction test. *Prosapip1(flx/flx);Syn1-Cre(-)* and *Prosapip1(flx/flx);Syn1-Cre(+)* mice preferred the social chamber. **(D)** Time spent in the familiar and novel chamber of the 3-chamber social interaction test. *Prosapip1(flx/flx);Syn1-Cre(-)* mice significantly preferred the chamber containing the novel partner. **(E)** Distance traveled during Barnes maze training. *Prosapip1(flx/flx);Syn1-Cre(-)* mice had a significantly shorter path throughout the training. **(F)** Primary (filled circles) and secondary (hollow circles) errors committed during Barnes maze training. *Prosapip1(flx/flx);Syn1-Cre(-)* mice committed significantly less primary and secondary errors throughout training than *Prosapip1(flx/flx);Syn1-Cre(+)* mice. **(G)** Example path from mice exhibiting random, serial, and spatial search strategies. **(H-I)** Ratio of search strategy used by *Prosapip1(flx/flx);Syn1-Cre(-)* and *Prosapip1(flx/flx);Syn1-Cre(+)* mice during Barnes maze training. **(J)** Time spent in exit quartile during the probe trial and associated heatmap. *Prosapip1(flx/flx);Syn1-Cre(-)* mice spent significantly more time in the correctly paired exit quartile than *Prosapip1(flx/flx);Syn1-Cre(+)* mice. Data are represented as mean \pm SEM and analyzed using two-way ANOVA (A,C,D,E), Welch's t-test (B), three-way ANOVA (F), or Mann-Whitney test (J). * $p < 0.05$, ** $p < 0.01$, *** $p < 0.001$, **** $p < 0.0001$. $n = 9-20$.



Extended Figure 2.5. Prosapip1 knockout did not affect Barnes maze habituation

(A) Distance traveled during the Barnes maze habituation trial. *Prosapip1(flx/flx);Syn1-Cre(-)* and *Prosapip1(flx/flx);Syn1-Cre(+)* mice traveled a similar distance to find the exit for the first time in the Barnes maze.

2.3.6 Prosapip1 in the dorsal hippocampus contributes to spatial memory

The neuronal knockout of Prosapip1 caused a loss of spatial memory. We next aimed to determine the region specificity of these effects. Spatial memory is often associated with the dorsal hippocampus (Pilly and Grossberg, 2012), so we delivered Cre locally to the dorsal hippocampus of Prosapip1(flx/flx) mice using an adeno-associated virus (AAV). An AAV expressing GFP was used as a control (**Figure 2.6A**). Western blot analysis of the AAV-Cre-infected dorsal hippocampus of Prosapip1(flx/flx) mice shows efficient elimination of Prosapip1 protein (**Figure 2.6B**).

We repeated the experimental battery performed on the genetically manipulated mice on the mice infused with AAV-GFP or AAV-Cre in the dorsal hippocampus. In the open field, AAV-GFP- and AAV-Cre-infected mice exhibited similar levels of locomotion (**Figure 2.6C**) (Welch's t-test: $t_{(29.59)} = 1.961$, $p = 0.0594$) and spent a similar amount of time in the center of the field (**Figure 2.6D**) (Welch's t-test: $t_{(29.72)} = 1.066$, $p = 0.2951$). The region-specific knockout of Prosapip1 did not affect exploratory behavior. We also directly assessed anxiety-like behavior using the light/dark box. Mice infected with AAV-GFP and AAV-Cre both spent comparable amounts of time in the light and dark chamber, preferring the dark (**Figure 2.6E**) (Two-way ANOVA: Effect of chamber $F_{(1,32)} = 46.74$, $p < 0.0001$; Effect of treatment $F_{(1,32)} = 2.361$, $p = 0.1342$; Effect of chamber x treatment $F_{(1,32)} = 0.1588$, $p = 0.6929$). Therefore, Prosapip1 in the dorsal hippocampus does not control anxiety-like behavior.

Next, we examined the role of Prosapip1 in the dorsal hippocampus on spatial memory. We first assessed spatial memory using the novel object recognition test. The AAV-GFP-infected mice showed a significant preference for the novel object, indicating

functioning spatial memory (**Figure 2.6F**) (Two-way ANOVA: Effect of object $F_{(1,31)} = 36.30$, $p < 0.0001$; *post hoc* Familiar vs. Novel (AAV-GFP): $p < 0.0001$). Mice infected with AAV-Cre, however, showed no significant preference for either object (**Figure 2.6F**) (Two-way ANOVA: Effect of treatment $F_{(1,31)} = 3.069$, $p = 0.0897$; Effect of object x treatment $F_{(1,31)} = 35.05$, $p < 0.0001$; *post hoc* Familiar vs. Novel (AAV-Cre): ns). Similarly, in the novelty T-maze test, AAV-GFP-infected mice spent much of the test exploring the novel arm of the maze, indicated by a positive difference score (**Figure 2.6G**). This was significantly more than the AAV-Cre-infected mice that explored the maze at chance levels (**Figure 2.6G**) (Welch's t-test: $t_{(26.04)} = 3.777$, $p = 0.0008$). Together, these results suggest that *Prosapip1* in the dorsal hippocampus specifically contributes to spatial memory.

We also assessed the effects of region-specific *Prosapip1* knockout on sociability and social memory using the 3-chamber social interaction test. Both AAV-GFP- and AAV-Cre-infected mice showed a significant preference for interacting with a social partner over the empty cage (**Figure 2.6H**) (Two-way ANOVA: Effect of social $F_{(1,31)} = 31.60$, $p < 0.0001$; Effect of treatment $F_{(1,31)} = 0.0003957$, $p = 0.9843$; Effect of social x treatment $F_{(1,31)} = 0.7781$, $p = 0.3845$). When a novel interaction partner was introduced, AAV-GFP mice significantly preferred interacting with the novel partner (**Figure 2.6I**) (Two-way ANOVA: Effect of social novelty $F_{(1,31)} = 9.777$, $p = 0.0038$; Effect of treatment $F_{(1,31)} = 0.2045$, $p = 0.6543$; Effect of social novelty x treatment $F_{(1,31)} = 0.1131$, $p = 0.7389$; *post hoc* Familiar vs. Novel (AAV-GFP): $p = 0.0303$). AAV-Cre-infected mice did not show a significant preference (**Figure 2.6H**) (*post hoc* Familiar vs. Novel (AAV-Cre): ns).

Finally, AAV-GFP and AAV-Cre mice underwent the Barnes maze procedure to directly assess spatial learning and memory. During training trials, AAV-Cre-infected mice

performed significantly worse when examining path to escape (**Figure 2.6J**) (Two-way ANOVA: Effect of trial $F_{(15,180)} = 6.246$, $p < 0.0001$; Effect of treatment $F_{(1,12)} = 22.95$, $p = 0.0004$; Effect of trial x treatment $F_{(15,180)} = 2.033$, $p = 0.0153$). While AAV-GFP-infected mice quickly improved exit strategy, AAV-Cre-infected mice were more variable and took a longer path, on average. After training, when we performed the probe trial, we found that AAV-GFP-infected mice spent significantly more time in the exit quartile compared to AAV-Cre mice (**Figure 2.6K**) (Mann-Whitney test: $p = 0.0047$). Based on this, we conclude that *Prosapip1* in the dorsal hippocampus is specifically involved in the formation and retrieval of spatial memory.

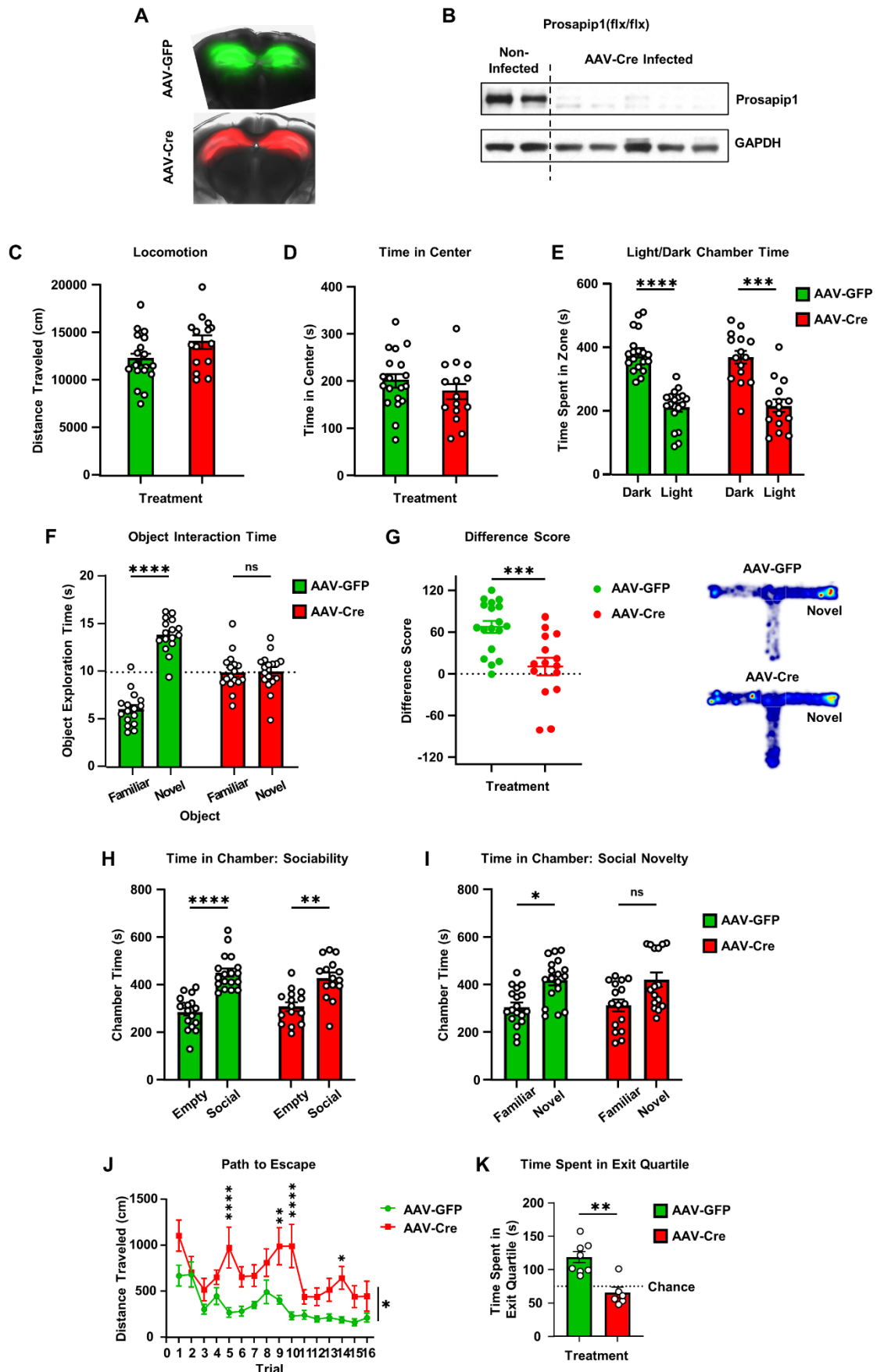


Figure 2.6. Prosapip1 in the dorsal hippocampus contributes to spatial memory

Figure 2.6. Prosapip1 in the dorsal hippocampus contributes to spatial memory

(A) Images of AAV-GFP and AAV-Cre overexpression in the dorsal hippocampus of Prosapip1(flx/flx) mice. **(B)** Western blot analysis of Prosapip1 in the dorsal hippocampus in non-infected mice compared to mice infected with AAV-Cre. **(C)** Total distance traveled during the open field test. AAV-GFP and AAV-Cre mice exhibited similar locomotion. **(D)** Time in center during the open field test. Treatment had no effect on time spent in center. **(E)** Time spent in the dark and light chamber during the light/dark box test. AAV-GFP and AAV-Cre mice both significantly preferred the dark side of the chamber. **(F)** Time spent exploring the familiar and novel object during the novel object recognition test. AAV-GFP mice significantly preferred the novel object, while AAV-Cre mice showed no preference. **(G)** Difference score of time spent exploring the novel arm of the T-maze. AAV-GFP mice had a significantly higher difference score than AAV-Cre mice. **(H)** Time spent in the empty and social chamber of the 3-chamber social interaction test. Both AAV-GFP and AAV-Cre mice significantly preferred the social-paired chamber. **(I)** Time spent in the familiar and novel chambers in the 3-chamber social interaction test. AAV-GFP mice significantly preferred the novel partner. **(J)** Distance travelled during escape during Barnes maze training trials. AAV-GFP mice performed significantly better than AAV-Cre mice. **(K)** Time spent in the exit quartile during the probe trial. AAV-GFP mice spent significantly more time in the correctly paired exit quartile than AAV-Cre mice. Data are represented as mean \pm SEM and analyzed using two-way ANOVA (E, F, H, I, J), Welch's t-test (C, D, G), or Mann-Whitney test (K). * $p < 0.05$, ** $p < 0.01$, *** $p < 0.001$, **** $p < 0.0001$. n = 6-18.

2.4 Discussion

Our findings suggest that Prosapip1 in the dorsal hippocampus is responsible for the synaptic localization of SPAR and PSD-95, and consequently, for the membranal localization of GluN2B. Furthermore, our data suggest that Prosapip1 in the dorsal hippocampus plays an important role in LTP as well as spatial learning and memory.

2.4.1 Prosapip1 is a key protein in the PSD

The PSD is a complex protein network located at the postsynaptic membrane of excitatory neurons (Boeckers et al., 2002; Boeckers, 2006; Kaizuka and Takumi, 2018). The PSD is crucial for synaptic transmission and plasticity, and abnormalities in the PSD network are linked to various neuropsychiatric disorders (Vyas and Montgomery, 2016; Kaizuka and Takumi, 2018), such as schizophrenia, autism spectrum disorder (ASD), and intellectual disorder (Coley and Gao, 2019). The two major families of proteins in the PSD are membrane associated guanylate kinases (MAGUKs), such as PSD-95, and Src homology 3 domain and ankyrin repeat proteins (Shanks) (Vyas and Montgomery, 2016; Kennedy, 2018). Actin, which recycles between globular (G-actin) and filamentous (F-actin), is also crucial in reorganizing and stabilizing the PSD (Adam and Matus, 1996; Qualmann et al., 2004; Boeckers, 2006; Kuriu et al., 2006).

We found that conditional knockout of Prosapip1 leads to a significant reduction in the synaptic levels of SPAR, PSD-95, and GluN2B. Prosapip1 is highly enriched in the PSD of excitatory synapses (Wendholt et al., 2006; Reim et al., 2016), and these results suggest it could be crucial to the formation and stability of PSD complexes. Prosapip1

scaffolds SPAR to Shank3 in the PSD (Wendholt et al., 2006; Dolnik et al., 2016; Reim et al., 2016). Both SPAR and Shank3 interact with PSD-95 (Naisbitt et al., 1999; Tu et al., 1999; Pak et al., 2001; Boeckers, 2006). SPAR binds PSD-95 directly (Pak et al., 2001), and Shank3 associates with Guanylate kinase-associated protein (GKAP), which binds PSD-95 (Naisbitt et al., 1999; Tu et al., 1999; Boeckers, 2006). PSD-95 binds to NMDAR subunits GluN2A and GluN2B and stabilizes NMDAR surface expression (Won et al., 2016; Coley and Gao, 2019). We previously found that Prosapip1 binds SPAR *in vivo* (Laguesse et al., 2017). Reim et al. previously showed that Prosapip1 is directly regulating SPAR levels in the PSD in primary hippocampal neurons, but knockdown of Prosapip1 does not lead to reduced postsynaptic Shank3 or PSD-95 (Reim et al., 2016). Our data supports this study, as Prosapip1 knockout *in vivo* led to a reduction of synaptic SPAR but did not affect synaptic Shank3. In contrast to Reim et al. we found that the loss of Prosapip1 also led to a reduction in synaptic PSD-95. Studies have shown PSD-95 deficiency causes an imbalance of NMDAR and AMPAR presence, altering glutamatergic transmission (Elias et al., 2006; Zhang et al., 2013; Chen et al., 2015). In this study, the level of synaptic GluA1 in the dorsal hippocampus is unchanged after knockout of Prosapip1. Pak et al. showed that SPAR binds PSD-95 and GluN2B, but not GluA1 (Pak et al., 2001). However, PSD-95 and Shank3 do interact with GluA1 (Jeyifous et al., 2016; Ross and Aizenman, 2023). Based on our results and these studies, the complex controlling AMPAR synaptic localization is different, and likely independent of Prosapip1 in the dorsal hippocampus. Together our data suggest that Prosapip1 is necessary for the formation and maintenance of the NMDAR-associated PSD network.

Prosapip1 also controls the formation of F-actin in dendritic spines (Laguesse et al., 2017), and may be acting through SPAR localization, although the mechanism by which SPAR leads to F-actin formation is still unclear. SPAR reorganizes the actin cytoskeleton and recruits PSD-95 to F-actin (Pak et al., 2001). Alternatively, SPAR is a Rap-GAP, downregulating activity of Rap-GTPases (primarily Rap1A, Rap2A) (Pak et al., 2001; Pak and Sheng, 2003; Seeburg et al., 2008; Hoe et al., 2009; Herrick et al., 2010). Active Rap reduces dendritic complexity, leads to spine loss, and causes formation of thin spines (Zhu et al., 2002; Xie et al., 2005; Ryu et al., 2008). The termination of Rap activity may be an indirect mechanism by which SPAR and Prosapip1 are forming actin filaments. The F-actin structure in the PSD reliant on Prosapip1 could be crucial for stability of the Shank/NMDA/PSD-95 complex.

2.4.2 Prosapip1 and LTP

LTP is a persistent increase in synaptic strength between neurons that can last for months in vivo (Abraham et al., 2002; Cooke and Bliss, 2006). LTP has been studied in a variety of species from rodents (Romero-Barragan et al., 2021) to non-human primates (Urban et al., 1996). The insights gained in these model systems can be applied to humans (Cooke and Bliss, 2006). Therefore, understanding the mechanisms of LTP are crucial to furthering understanding of human neuroanatomy and unraveling the pathophysiology of neurological disease. LTP is often induced by HFS, which causes extensive glutamate release and significant AMPAR activity, resulting in large membrane depolarization (Ma et al., 2018). This depolarization facilitates the removal of Mg²⁺ blockage in NMDARs, thereby activating them and leading to calcium influx. This influx

triggers the calmodulin/CaMKII pathway, initiating a series of cascades that enhance AMPAR phosphorylation and trafficking, culminating in sustained synaptic strengthening (Huganir and Nicoll, 2013; Herring and Nicoll, 2016). Therefore, the induction of hippocampal LTP heavily relies on NMDAR activation, with alterations in NMDAR function significantly affecting the establishment of hippocampal LTP and its associated learning and memory processes. In our study, we discovered that mice lacking Prosapip1 exhibited markedly diminished NMDAR-mediated synaptic transmission. This reduction in NMDAR functionality likely results in decreased calcium influx during high-frequency stimulation and diminished activation of calmodulin/CaMKII, leading to weaker synaptic strengthening. Indeed, we observed substantially smaller LTP in Prosapip1-deficient mice compared to wild-type controls. Notably, the knockout of Prosapip1 led to reduced NMDA-induced currents, indicating that Prosapip1 plays a critical role in regulating NMDAR function.

2.4.3 Behavioral consequences of loss of Prosapip1

We found that neuronal knockout of Prosapip1 led to significant deficits in spatial learning and memory. Memory consists of three primary processes: encoding, consolidation, and retrieval (Straube, 2012). In this study, the defect in memory function may be attributed to a failure to encode new information (Spangler et al., 1991; Walker and Gold, 1991; Bye and McDonald, 2019) or consolidate this “short-term” into “long-term” memory (Kim et al., 1992; Kim et al., 1993; Yang et al., 2022; Rossato et al., 2023). The spatial T-maze experiment utilized a short inter-trial interval of one minute, and Prosapip1 knockout mice showed a loss of spatial learning and memory, which implies a

failure to encode new information. Similarly, the Barnes maze training trials were separated by an ITI of 30 minutes, but *Prosapip1* knockout mice did not acquire spatial memory between training trials, nor during the longer consolidation periods between days, again implying a failure to encode spatial information. It is unlikely that NMDAR dysfunction is affecting the retrieval of memory, as studies have exhibited rats' ability to use previously acquired spatial information during NMDAR blockage (Bast et al., 2005; Mackes and Willner, 2006; Bye and McDonald, 2019).

It is highly likely that the altered composition of the PSD and subsequent loss of hippocampal LTP are leading to the observed behavioral changes. LTP is considered the cellular mechanism underlying learning and memory (Bliss and Collingridge, 1993; Frey and Morris, 1998; Malenka and Nicoll, 1999; Collingridge et al., 2004). In vivo studies showed that LTP strength is directly correlated to long-term memory storage (Abel et al., 1997; Pastalkova et al., 2006; Sacktor, 2008), and loss of hippocampal LTP has also been shown to impair spatial, but not contextual memory (Bach et al., 1995). This distinction can be observed in the Barnes maze experiment, where *Prosapip1* knockout mice do significantly reduce distance traveled to exit, but do not switch to spatial searching. In this example, *Prosapip1* knockout mice are retaining the contextual understanding to escape the platform, but do not recall the spatial location of the exit. The link between NMDAR function and learning and memory is well established (Newcomer et al., 2000; Li and Tsien, 2009). For example, blockage of hippocampal NMDA receptors impairs spatial learning in rats (Spangler et al., 1991; Walker and Gold, 1991; Davis et al., 1992; Bye and McDonald, 2019). The GluN2B subunit of the NMDAR is specifically important for learning and memory (Al Abed et al., 2020; Nachtigall et al., 2024), and its

age-related decline in expression is strongly associated with age-related declines in memory (Brim et al., 2013). Prosapip1 is likely controlling the reinforcement of learning and memory by PSD scaffolding, stabilization, and GluN2B synaptic localization, leading to LTP.

We observed that Prosapip1 knockout in the dorsal hippocampus replicated the spatial learning and memory deficits exhibited by the neuronal knockout mice, suggesting that Prosapip1 is controlling these learning and memory processes specifically in the dorsal hippocampus. The dorsal hippocampus primarily controls memory formation and recall (Eichenbaum, 1997; Broadbent et al., 2004; Squire et al., 2004; Pilly and Grossberg, 2012). We found that LTP in the CA1 subregion of the dorsal hippocampus was reliant on Prosapip1. The CA1 subregion is critically involved in consolidating and retrieving contextual memory (Lee and Kesner, 2004; Daumas et al., 2005). The CA3 and DG are also involved in memory processes (Broadbent et al., 2004; Lee and Kesner, 2004; Daumas et al., 2005). As our conditional knockout strategy resulted in Prosapip1 deletion from the entire dorsal hippocampus, it is plausible that Prosapip1 is contributing to LTP and memory acquisition and consolidation in these subregions as well, although further studies are required.

It is also important to note that other Fezzins do not compensate for the loss of Prosapip1 in the dorsal hippocampus. Knockout of other Fezzins, like PSD-Zip70, also lead to cognitive deficits (Mayanagi et al., 2015). However, these deficits were attributed to the action of PSD-Zip70 in the PFC. Therefore, one could hypothesize that proteins in this family enact their function in specific brain subregions. Also, Fezzin LAPSER1, similarly proposed to scaffold SPAR to the PSD (Schmeisser et al., 2009), is increased in

primary hippocampal neurons after Prosapip1 overexpression (Reim et al., 2016). Proteins in the Fezzin family may be reliant on each other, which could explain the lack of compensatory mechanisms.

Unraveling the physiological role of Prosapip1 may lead to a better understanding of neuropsychiatric disease. Abnormalities with PSD proteins are associated with disorders such as ASD and schizophrenia (Vyas and Montgomery, 2016; Kaizuka and Takumi, 2018). Dysfunction of the hippocampus contributes to many neuropsychiatric diseases, including Alzheimer's disease (Anand and Dhikav, 2012; Rao et al., 2022), characterized by memory loss. Interestingly, recent genome wide association studies (GWAS) correlate mutations in the gene encoding Prosapip1 with Parkinson's disease (Nalls et al., 2014; Chang et al., 2017; Nalls et al., 2019; Kim et al., 2024). This study provides a foundation for future exploration of Prosapip1 and its involvement in postsynaptic processes.

2.5 Future Directions

In this chapter, Prosapip1 is shown to control PSD scaffolding, LTP, and hippocampus-dependent learning and memory. The future directions of this work include a continuation of the biomolecular investigation. Prosapip1 is shown here to reduce the synaptic localization of SPAR, but there are three SPAR proteins (SPAR1-3) that have different interaction partners and physiological roles. Prosapip1 interacts with all the SPAR proteins (Wendholt et al., 2006; Spilker et al., 2008; Dolnik et al., 2016; Reim et al., 2016). SPAR1 also interacts with Fezzins PSD-Zip70 and LAPSER1 (Maruoka et al., 2005; Schmeisser et al., 2009). SPAR1 is unique in that it interacts directly with F-actin (Pak et al., 2001). In hippocampal neurons, it localized to dendritic spines and leads to spine head enlargement (Pak et al., 2001). This mechanism is regulated by down-regulation of Rap-GTPases (primarily Rap1A, Rap2A) and its interaction with actin (Pak et al., 2001; Pak and Sheng, 2003; Seeburg et al., 2008; Hoe et al., 2009; Herrick et al., 2010). Its loss leads to behavioral impairments in memory and social behavior (Matsuura et al., 2022). SPAR1 level in spines is regulated by neuronal activity (Pak and Sheng, 2003; Seeburg et al., 2008). Specifically, phosphorylation of SPAR1 following excitatory synaptic transmission leads to its degradation, consequently leading to transformation of mature spines into immature filopodia (Pak and Sheng, 2003; Seeburg et al., 2008). SPAR1 transcripts are predominantly expressed in the forebrain and increase throughout development (Spilker et al., 2008). SPAR2 is similar to SPAR1, showing significant sequence homology and interaction with Prosapip1 (Spilker et al., 2008). SPAR2 also shows GAP activity for all five Rap GTPases, but GTPase activation by SPAR2 is generally weaker than SPAR1 (Spilker et al., 2008). However, SPAR2 does not bind to

actin (Spilker et al., 2008). Also, overexpression of SPAR2 in hippocampal neurons does not affect spine morphology like SPAR1 (Spilker et al., 2008). SPAR2 is constantly expressed, and primarily localized in the dentate gyrus (Spilker et al., 2008). SPAR3 is the most recently investigated protein in the family (Dolnik et al., 2016). SPAR3 also does not contain an actin-binding domain, like SPAR2. Interestingly, SPAR3 transcripts are found in all major brain regions, but decrease between 1-3 months of age (Dolnik et al., 2016). Investigating the entire family of SPAR proteins may increase understanding of the physiological role of Prosapip1.

Similarly, the investigation of Rap activity is an important to understand the cellular mechanism of Prosapip1. There are five members Rap group of GTPases: Rap1A, Rap1B, Rap2A, Rap2B, and Rap2C. Rap1 and Rap2 are significantly different (~60% protein identity similarity), while the isoforms share 95% identity for Rap1, and 90% for Rap2. Rap1 and Rap2 have overlapping but distinct actions. For instance, in hippocampal spiny neurons, constitutively active (CA) Rap2 caused decreased length and complexity of axonal and dendritic branches, while CA Rap1 had no effect (Fu et al., 2007). Similarly, Rap1 promotes the formation of thin spines (Xie et al., 2005), and Rap2 leads to spine loss (Ryu et al., 2008). However, these mechanisms are via different signaling pathways, p38 MAPK for Rap1 (Morozov et al., 2003; Huang et al., 2004) and JNK for Rap2 (Zhu et al., 2005). Rap1 was also reported to regulate LTP and spatial memory (Morozov et al., 2003). Rap1 and Rap2 have antagonistic effects in some cases, such as in endothelial barrier resistance (Pannekoek et al., 2013). It would be interesting to examine the activation of various Raps after Prosapip1 knockout and subsequent loss

of SPAR synaptic localization. Overactive Rap may be the key to understanding the disruption of PSD scaffolding and NMDAR internalization in the Prosapip1 knockout mice.

Finally, the behavioral effects of Prosapip1 knockout can be further examined. As Prosapip1 is most prevalent in the PSD of glutamatergic synapses (Wendholt et al., 2006), it would be compelling to specifically knockout Prosapip1 in glutamatergic neurons and examine behavior. For example, this could be accomplished by infection of the dorsal hippocampus with an AAV expressing Cre driven by a CaMKII promoter. Furthermore, as the related protein PSD-Zip70 has shown to act in the PFC (Mayanagi et al., 2015), it would be intriguing to examine the behavioral effects of specific Prosapip1 knockout in other brain regions. While our specific knockout in the dorsal hippocampus replicated the loss of spatial learning and memory observed in the full-brain knockout, Prosapip1 in other regions, such as the PFC, may contribute to behaviors primarily controlled by those regions.

2.6 Materials and Methods

Animals

Prosapip1(flx/flx) mice were developed at the University of Pittsburgh as described below. Syn1-Cre(+) mice were purchased from Jackson Laboratory (Stock #003966, Jackson Labs, Bar Harbor, Maine). Electrophysiology experiments were performed at Texas A&M University. Prosapip1(flx/flx) and Prosapip1(flx/flx);Syn1-Cre mice were bred in the UCSF facility where they were group housed in a 12-hour light-dark cycle room. Unrestricted amounts of food and water were provided. Animal procedures were approved by the UCSF Institutional Animal Care and Use Committee (IACUC).

Prosapip1 Floxed Mouse Making

Guide RNA binding sites in intron 2 and in the 3'UTR located in Exon 5 of Prosapip1 (a.k.a, *Lzts3*) (see **Figure 2.1A**) were identified using the CRISPRator tool (Labuhn et al., 2018) within the CCTop (Stemmer et al., 2015) online platform (<http://crispr.cos.uni-heidelberg.de/>). The gRNA binding sites are located ~3.3kb from each other. These gRNA target sites were used to produce two Alt-R CRISPR-Cas9 crRNAs (IDT DNA, Coralville, IA) which were individually hybridized to a universal 67-mer Alt-R CRISPR-Cas9 tracrRNA (IDT DNA) to produce two gRNAs. Two 140 nt long PAGE purified Ultramer single stranded DNA Oligos (IDT DNA) with three phosphorotioate modifications on each end (Renaud et al., 2016) that were homologous to the target loci in intron 2 and Exon 5 (see **Figure 2.1B**) were used as a repair templates.

We initially attempted to sequentially introduce each loxP site into 1-cell and 2-cell stages of embryonic development (Horii et al., 2017). Single cell C57BL/6J embryos were electroporated with gRNA#6 (200ng/μl), IDT Alt-R® HiFi Cas9 Nuclease V3 protein

(75ng/μl), and Exon 5 repair template (200ng/μl) using a BioRad Gene-Pulser Xcell electroporator in a 1 mm-gap slide electrode (Protech International, #501P1-10) using square-wave pulses (five repeats of 3 msec 25V pulses with 100 msec interpulse intervals). Following this first electroporation, embryos were cultured overnight. Surviving two-cell embryos were electroporated with gRNA#7 (200ng/μl), IDT Alt-R® HiFi Cas9 Nuclease V3 protein (75ng/μl), and intron 2 repair template (200ng/μl) under conditions described above. Surviving embryos were transferred to the oviducts of CD1 (Charles River) pseudopregnant recipient females. Offspring were genotyped for the intron 2 lox insertion using PCR (forward primer 5' AGAGAAGTCTACGCTGTAGTCAG 3' and reverse primer 5' AAGCGGGAAGGTAGAGAGGT 3'; wild type product = 449bp, floxed product = 489bp) followed by Sanger sequencing. Offspring were genotyped for the Exon 5 lox insertion using PCR (forward primer 5' TGCACAACCTTCTGACACGT 3' and reverse primer 5' AGGGCACAGACAGTAGCACT 3'; wild type product = 408bp, floxed product = 448bp) followed by Sanger sequencing. Two founder animals were found that harbored loxP insertions at both the intron 2 and Exon 5 sites. Unfortunately, when mated to C57BL/6J females, the loxP sites segregated indicating that they were on different chromosomes. Therefore, F1 offspring that harbored only the loxP insertion at the intron 2 site were used as 1-cell embryo donors for insertion of the Exon 5 loxP site using electroporation conditions described above. One male offspring was produced that harbored both the intron 2 and Exon 5 loxP insertions on the same chromosome. This male was mated to C57BL/6J females to establish the floxed mouse line used here.

Guide RNA off target sites were predicted and ranked using CRISPOR (Concordet and Haeussler, 2018). The top 11 and 10 sites for gRNA#6 and gRNA#7, respectively

based on CFD score were amplified from this founder mouse DNA and Sanger sequenced. All predicted off target sites analyzed were wild type (data not shown).

Antibodies

Rabbit anti-SPAR (SIPA1L1) (1:500) (25086-1-AP) was ordered from ProteinTech. Mouse anti-Shank3 antibodies (1:500) (#ab93607) were purchased from Abcam. Rabbit anti-GluN2B (1:1000) (#4212), Rabbit anti-GluA1 (1:1000) (#13185S), and Rabbit anti-Creb (1:500) (#9197) antibodies were purchased from Cell Signaling. Goat anti-GluN2A antibodies (1:500) (#SC-1468) were purchased from Santa Cruz. Mouse anti-GAPDH antibodies (1:10,000) (#G8795) were purchased from Sigma. Mouse anti-PSD-95 antibodies (1:100K) (#05-494) were purchased from Millipore (Upstate).

Crude synaptosomal fractionation

Tissue is first homogenized in 500 μ L of 4°C Krebs buffer (125 mM NaCl, 1.2 mM KCl, 1.2 mM MgSO₄, 1.2 mM CaCl₂, 22 mM Na₂CO₃, 1 mM NaH₂PO₄, 10 mM Glucose) with 0.32 M sucrose + protease/phosphatase inhibitors. A portion of the homogenate (100 μ L) is saved as total homogenate (H), while the remaining homogenate is diluted by adding 500 μ L of Krebs buffer-sucrose to the remaining 400 μ L. The total homogenate is transferred to a 1.5mL Eppendorf tube. The glass homogenizer is washed with 500 μ L of Krebs buffer-sucrose, and the wash solution is added to the remaining homogenate. The sample is then centrifuged at 1,000g at 4°C for 10 minutes. The supernatant (S1) is carefully collected without disturbing the pellet. This process is repeated, and then the S1 supernatant is centrifuged at 16,000g 4°C for 20 min. The supernatant (S2) is saved and

the pellet is kept on ice. The resulting pellet contains the synaptosomal fraction. The pellet is then resuspended in 500 μ L of Krebs buffer-sucrose and again centrifuged at 16,000g 4°C for 20 min and resuspended in RIPA buffer for analysis.

Western blot analysis

Tissue collected from mice was homogenized in ice-cold radio immunoprecipitation assay (RIPA) buffer (containing 50 mM Tris-HCL, 5 mM EDTA, 120 mM NaCl, 1%NP-40, 0.1% deoxycholate, 0.5% SDS, and protease and phosphatase inhibitors). Homogenization was carried out using a sonic dismembrator. Protein concentration was determined using the BCA™ protein assay kit. Thirty μ g of each tissue lysate was loaded onto SDS-PAGE for separation, followed by transfer onto a nitrocellulose membrane at 300mA for 2 hours. The membranes were then blocked with 5% milk-PBS containing 0.1% Tween 20 at room temperature for 30 minutes before being probed with the appropriate primary antibodies overnight at 4°C. Following washing, the membranes were incubated with HRP-conjugated secondary antibodies for one hour at room temperature. Membrane development was performed using enhanced chemiluminescent reagent (ECL), and band intensities were quantified using ImageJ software (NIH).

Electrophysiology

Preparation of slices is outlined in (Gangal et al., 2023). In brief, we sectioned the hippocampus coronally to produce slices with a thickness of 250 μ m. These slices were initially cut in an ice-cold solution, which had a specific composition: 40 mM NaCl, 148.5 mM sucrose, 4.5 mM KCl, 1.25 mM NaH₂PO₄, 25 mM NaHCO₃, 0.5 mM CaCl₂, 7

mM MgSO₄, 10 mM dextrose, 1 mM sodium ascorbate, 3 mM myo-inositol, and 3 mM sodium pyruvate. This cutting solution was thoroughly saturated with a gas mixture comprising 95% O₂ and 5% CO₂. After cutting, the slices were incubated for 45 minutes. This incubation occurred in a mixture of equal parts cutting solution and an external solution. The external solution contained the following: 125 mM NaCl, 4.5 mM KCl, 2.5 mM CaCl₂, 1.3 mM MgSO₄, 1.25 mM NaH₂PO₄, 25 mM NaHCO₃, 15 mM sucrose, and 15 mM glucose. Like the cutting solution, this mixture was saturated with 95% O₂ and 5% CO₂.

Field potential recordings were conducted as detailed in previous studies (Palop et al., 2007; Wang et al., 2012). Specifically, the procedure involved the use of stimulation electrodes, which were filled with artificial cerebrospinal fluid (aCSF) and placed in the CA1 region of the dorsal hippocampus. The recording electrode, filled with 1M NaCl, was positioned in the CA1 region, approximately 100-150 μm away from the stimulating electrodes. The optimal location for the recording electrode was determined based on the site where a stable fiber volley and field potential response could be consistently observed following the delivery of a single electrical stimulation pulse (2 ms). The stimulation intensity was carefully adjusted to elicit 50% of the maximum possible response. Baseline field potentials were meticulously recorded over 10 mins at 10-second intervals. The HFS protocol for LTP included a regimen of 100 Hz, with 100 pulses every 20 seconds, repeated four times. Following the HFS protocol, field potential recordings were extended for 30 min. LTP was quantified based on the averaged fEPSP as a percentage of the baseline (% BL), comparing the measurements at 20-30 minutes post-HFS between the Prosapip1(flx/flx);Syn1-Cre(-) and Prosapip1(flx/flx);Syn1-Cre(+) groups. To inhibit

GABAergic transmission, picrotoxin (100 μ M) was applied to the bath. The measurement of fEPSP was performed using a MultiClamp 700B amplifier integrated with Clampex 10.4 software provided by Molecular Devices.

Whole-cell recordings were executed following the protocols previously established (Wang et al., 2012; Ma et al., 2018). For all these recordings, a cesium-based intracellular solution was employed. This solution comprised the following components (in mM): 119 CsMeSO₄, 8 TEA.Cl, 15 HEPES, 0.6 ethylene glycol tetraacetic acid (EGTA), 0.3 Na₃GTP, 4 MgATP, 5 QX-314.Cl, and 7 phosphocreatine. The pH of this solution was adjusted to 7.3 using CsOH. The temperature of the recording bath was maintained at a constant 32°C, and the perfusion speed was set between 2-3 ml/min. For the recordings, CA1 neurons were voltage-clamped at a holding potential of -70 mV. In order to measure N-methyl-D-aspartate (NMDA) receptor-mediated transmission, a low external concentration of Mg²⁺ (0.05 mM) was used. This was coupled with NBQX (10 μ M) and picrotoxin (100 μ M) to block α -amino-3-hydroxy-5-methyl-4-isoxazolepropionic acid (AMPA) receptor-mediated synaptic transmission and inhibitory synaptic currents. NMDA-induced currents were measured by bath-applying NMDA (20 μ M) for 30 seconds, with holding currents recorded every 5 seconds.

Input-output curves for NMDAR-mediated EPSC were created by electrical stimulation of varying intensities was delivered through electrodes strategically placed within the CA1 region. The paired-pulse ratio (PPR) was calculated by dividing the amplitude of the second electrically-evoked EPSC by that of the first, with an interval of 100 ms between the two pulses. Additionally, gap-free recordings of spontaneous excitatory postsynaptic currents were conducted over a duration of 2 minutes.

Behavior

All behavioral paradigms were completed between the hours of 9:00 and 18:00. Mice were tested between 8 and 20 weeks of age and were age-matched based on experiment. The mice were moved from their housing room, currently in the “light cycle,” to the dimly lit behavior room (10-15 lux) 30 minutes before the experiment and allowed to acclimate. The light/dark box, elevated plus maze, and Barnes maze experiments were done in full room light. During experiments, white noise was played through a speaker in the room at 50dB to reduce influence from noise outside of the room. The researcher remained in the room during the trial, but a wall was placed between the arena and the experimenter to prohibit mice from seeing the researcher. Mice were handled for 3 days for 1-2 minutes per day before experimentation began to reduce handling anxiety.

Locomotion

Mice were placed in a 43cm x 43cm open field and allowed to explore for 30 minutes. The center point of the mouse was tracked, and the primarily dependent variable was total locomotion during the trial. Other tracked variables were average and maximum velocity, center entrances, time spent in center, and binned locomotion into 1-minute periods to examine evolution of exploration of the space.

Novel Object Recognition

Mice were placed in a 43cm x 43cm chamber with two similar objects and allowed 20s of total familiarization time (nose point within 2cm radius of object), or 5 total minutes in the chamber, whichever came first, before being returned to home cage. After 24 hours,

mice were allowed to explore the test space containing one of the objects from before (familiar) and one novel object until total object interaction time of 20s was reached. If 20s of total interaction time was not reached before a 5-minute time limit, the trial was excluded. Mice that were climbing on objects were gently but quickly moved back to the starting position.

Novelty T-Maze

Protocol adapted from (Sanderson et al., 2009). Mice were placed in the “start” arm of a T-shaped maze. The dimensions of each transparent arm were 30cm×10cm×20cm (L×W×H). During training, the entrance to one arm (“novel arm”, assignment counterbalanced across groups) was blocked with clear plastic. Training consisted of five, 2-minute trials separated by an ITI in which each subject was allowed to explore the “start” and “familiar” arms. After the training sessions, the plastic blocking the “novel” arm was removed and mice were allowed to explore all arms of the maze. The test session began when the center point of the mouse left the start arm and ended when 2 minutes of total time was spent in the novel or familiar arm. Mice that showed anxiety behavior and an aversion to either arm during the test (no entrances, <250cm total movement) were excluded (2 mice).

Repeating Rotarod

Mice were placed facing forward on a rotarod device (Ugo Basile, Gemonio, Italy). The device was programmed to linearly ramp in speed from 5RPM to 80RPM over 5 minutes. Latency to fall was recorded. A complete revolution while holding on to the

treadmill was considered a failure, with the mouse being removed from the rod and trial suspended. After the trial, mice were placed back on the rod, but it remained static. There was a 5-minute inter-trial interval on same-day trials. 3 trials were performed each day for 3 consecutive days, 24 hours apart.

3-Chamber Social Interaction

Mice were placed in the center chamber of a transparent 3-chamber arena and allowed 3 minutes to habituate to the space. The mouse was blocked into the center chamber and then the trial was started by removing the doors and allowing 15 minutes to explore the “Social” or “Empty” chamber (Part I). The social chamber had a sex-matched, naïve mouse (4-5 weeks of age) in a cylindrical interaction cage, while the empty chamber had only the interaction cage. The chamber time and interaction time was recorded, with interaction time being defined as experimental mouse nose point being within interaction zone (5cm from interaction cage). Immediately after Part I, a novel mouse was introduced, also sex-matched and naïve, and mice were allowed 15 minutes to explore “Novel” or “Familiar” chamber (Part II). The familiar mouse is the social mouse from Part I, and the novel mouse was placed in the familiar mouse chamber during the first part of the trial to reduce side preference for this interaction partner.

Barnes Maze

Protocol adapted from (Pitts, 2018). The Barnes maze apparatus is a 122cm-diameter, white-acrylic circle with 40 evenly spaced, 5cm holes approximately 2.5cm from the edge of the circle. This experiment was done in light room conditions to increase the

motivation to escape. The volume of the white noise was also increased (90dB). There were four visual cues on each side of the platform, which consisted of brightly colored shapes (purple diamond, yellow star, green cube, red triangle).

The mouse was first habituated to the escape tunnel, a small box filled with Alphadry bedding, for 1 minute. It was then habituated to the experimental conditions. The mouse was placed in the center of the apparatus and allowed to explore until it entered the escape tunnel or 5 minutes elapsed. If the mouse did not organically reach the escape tunnel within the time limit, it was led to the hole to escape. There was at least 1 hour between habituation and the onset of acquisition training. The escape tunnel was moved between habituation and training trials.

There were 4 training trials per day for 4 consecutive days. There was an inter-trial interval of 30 minutes. During training trials, the position of the escape tunnel remained at a fixed location relative to the spatial cues. The mouse was placed in the center of the platform and tracked until it fully entered the escape tunnel or 5 minutes elapsed. If the mouse failed to reach the escape tunnel in the allotted time, it was led to the escape by the researcher. Following each trial, the platform is cleaned with 70% alcohol and the bedding inside the escape chamber is replaced.

For each trial, several variables are tracked to assess performance. These include distance traveled, latency to exit, incorrect hole visits (primary errors), and incorrect hole revisits (secondary errors). Errors are defined as nose point entering a hole that does not contain the exit. Finally, based on these errors, the search strategy was characterized. Mice searched the maze serially, spatially, or randomly. Serial searching mice spent most of the time on the periphery performing a systematic search of the holes in a clockwise

or counterclockwise manner, with 2 or less direction changes. Spatial search strategy was defined as <10 primary errors and a significantly reduced path and latency to exit. These mice use the surroundings to determine the shortest path to the exit and often are within 1-2 holes of the destination. All other results were defined as random search strategy. Random search strategy was usually characterized by multiple direction changes and skipping between holes, with many primary and secondary errors.

24 hours after the last training trial, the mice were tested with a probe trial. The escape tunnel was removed before the mouse was placed on the platform for 5 minutes. Total time spent in each quartile was recorded, along with visits to former correct and incorrect escapes.

Light/Dark Box

Mice were placed in the light side of a Light/Dark box apparatus and movement within the apparatus was recorded from above for 10 minutes. The “light” side of the box had translucent walls and no ceiling, allowing the light of the room to illuminate it. The “dark” side had opaque walls and a visible-light-filtering ceiling, allowing the mouse to experience a dark environment but the infrared camera to continue recording. We recorded the latency to enter the dark, transitions between zones, and time spent in zones.

Elevated Plus Maze

The elevated plus maze apparatus is a white “+”-shaped platform elevated 50cm above the floor with oppositely positioned “open” arms and “closed” arms. The closed

arms are enclosed by 30cm high opaque walls, while the open arms have no railing. The amount of exploration into the open arm is calculated to measure anxiety-like behavior.

Stereotaxic Surgery

Vaporized isoflurane was used to anesthetize mice. The mice were then headfixed in a stereotaxic frame (David Kopf Instruments). The experimental virus, or relevant control, was infused into the dorsal hippocampus (anteroposterior (AP) -2.3, mediolateral (ML) \pm 1.7, dorsoventral (DV) -1.7 mm measured from bregma) using stainless steel injectors (33 gauge; Small Parts Incorporated) connected to Hamilton syringes (10 μ l, 1701). Animals received 1 μ l of virus bilaterally at a rate of 0.1 μ l/min controlled by an automatic pump (Harvard Apparatus). After the infusion was complete, the injectors remained at the site for 10 minutes to allow diffusion of the virus.

Confirmation of Viral Expression

At the end of the experimental timeline, animals were euthanized via cervical dislocation and the brains were removed. The brains were placed on ice and dissected into 1-mm coronal sections. The fluorescent protein expressed by the virus (either green fluorescent protein or mCherry) was visualized using an EVOS FL tabletop fluorescent microscope (ThermoFisher Scientific). Images were taken for future reference. Animals that failed to exhibit fluorescence associated with viral overexpression were excluded from the study.

Statistical Analysis

Biochemical analysis Parametric tests were performed on normally distributed data. Data were analyzed using a two-tailed t-test with Welch's correction for normal populations. Mann-Whitney tests were performed on data derived from non-normal populations. The results were determined to be statistically significant if the resulting p-value was less than 0.05.

Electrophysiology analysis Parametric tests were performed on data deemed to be derived from a normally distributed population. Unpaired t-tests were performed on the average measurement over the experimental period. When multiple intensities were used, a two-way repeated measures ANOVA was performed. *Post hoc* pairwise comparisons (Tukey's) were performed after a significant result in the ANOVA.

Behavioral analysis Parametric tests were performed on data deemed by the D'Agostino-Pearson omnibus (K2) test to be derived from a normally distributed population. Behavioral experiments were first assessed using a three-way ANOVA with primary variables being genotype, sex, and experimental variable where appropriate. Where there was no significant difference between sexes, the data was consolidated by genotype. A two-way ANOVA was then performed on the consolidated data (genotype x experimental variable). *Post hoc* Šidák's multiple comparison's test was performed to measure experimental differences directly. When there was only one experimental variable, an unpaired t-test was performed. If the variance was unequal, Welch's correction was applied.

References

- Abel T, Nguyen PV, Barad M, Deuel TA, Kandel ER, Bourtchouladze R (1997) Genetic demonstration of a role for PKA in the late phase of LTP and in hippocampus-based long-term memory. *Cell* 88:615-626.
- Abraham WC, Logan B, Greenwood JM, Dragunow M (2002) Induction and experience-dependent consolidation of stable long-term potentiation lasting months in the hippocampus. *J Neurosci* 22:9626-9634.
- Adam G, Matus A (1996) Role of actin in the organisation of brain postsynaptic densities. *Brain Res Mol Brain Res* 43:246-250.
- Al Abed AS, Sellami A, Potier M, Ducourneau EG, Gerbeaud-Lassau P, Brayda-Bruno L, Lamothe V, Sans N, Desmedt A, Vanhoutte P, Bennetau-Pelissero C, Trifilieff P, Marighetto A (2020) Age-related impairment of declarative memory: linking memorization of temporal associations to GluN2B redistribution in dorsal CA1. *Aging Cell* 19:e13243.
- Alhadeff AL, Goldstein N, Park O, Klima ML, Vargas A, Betley JN (2019) Natural and Drug Rewards Engage Distinct Pathways that Converge on Coordinated Hypothalamic and Reward Circuits. *Neuron* 103:891-908 e896.
- Anand KS, Dhikav V (2012) Hippocampus in health and disease: An overview. *Ann Indian Acad Neurol* 15:239-246.
- Andrianantoandro E, Pollard TD (2006) Mechanism of actin filament turnover by severing and nucleation at different concentrations of ADF/cofilin. *Mol Cell* 24:13-23.
- Anker JJ, Kushner MG (2019) Co-Occurring Alcohol Use Disorder and Anxiety: Bridging Psychiatric, Psychological, and Neurobiological Perspectives. *Alcohol Res* 40.

- Arons MH, Thynne CJ, Grabrucker AM, Li D, Schoen M, Cheyne JE, Boeckers TM, Montgomery JM, Garner CC (2012) Autism-associated mutations in ProSAP2/Shank3 impair synaptic transmission and neurexin-neurologin-mediated transsynaptic signaling. *J Neurosci* 32:14966-14978.
- Bach ME, Hawkins RD, Osman M, Kandel ER, Mayford M (1995) Impairment of spatial but not contextual memory in CaMKII mutant mice with a selective loss of hippocampal LTP in the range of the theta frequency. *Cell* 81:905-915.
- Balleine BW, O'Doherty JP (2010) Human and rodent homologies in action control: corticostriatal determinants of goal-directed and habitual action. *Neuropsychopharmacology* 35:48-69.
- Bamburg JR (1999) Proteins of the ADF/cofilin family: essential regulators of actin dynamics. *Annu Rev Cell Dev Biol* 15:185-230.
- Barnes CA (1979) Memory deficits associated with senescence: a neurophysiological and behavioral study in the rat. *J Comp Physiol Psychol* 93:74-104.
- Bast T, da Silva BM, Morris RG (2005) Distinct contributions of hippocampal NMDA and AMPA receptors to encoding and retrieval of one-trial place memory. *J Neurosci* 25:5845-5856.
- Basu S, Lamprecht R (2018) The Role of Actin Cytoskeleton in Dendritic Spines in the Maintenance of Long-Term Memory. *Front Mol Neurosci* 11:143.
- Becker HC, Lopez MF (2004) Increased ethanol drinking after repeated chronic ethanol exposure and withdrawal experience in C57BL/6 mice. *Alcohol Clin Exp Res* 28:1829-1838.

- Becker HC, Mulholland PJ (2014) Neurochemical mechanisms of alcohol withdrawal. *Handb Clin Neurol* 125:133-156.
- Bernard O (2007) Lim kinases, regulators of actin dynamics. *Int J Biochem Cell Biol* 39:1071-1076.
- Blednov YA, Black M, Chernis J, Da Costa A, Mayfield J, Harris RA (2017a) Ethanol Consumption in Mice Lacking CD14, TLR2, TLR4, or MyD88. *Alcohol Clin Exp Res* 41:516-530.
- Blednov YA, Black M, Benavidez JM, Da Costa A, Mayfield J, Harris RA (2017b) Sedative and Motor Incoordination Effects of Ethanol in Mice Lacking CD14, TLR2, TLR4, or MyD88. *Alcohol Clin Exp Res* 41:531-540.
- Bliss TV, Collingridge GL (1993) A synaptic model of memory: long-term potentiation in the hippocampus. *Nature* 361:31-39.
- Boeckers TM (2006) The postsynaptic density. *Cell Tissue Res* 326:409-422.
- Boeckers TM, Bockmann J, Kreutz MR, Gundelfinger ED (2002) ProSAP/Shank proteins - a family of higher order organizing molecules of the postsynaptic density with an emerging role in human neurological disease. *J Neurochem* 81:903-910.
- Bokoch GM (2003) Biology of the p21-activated kinases. *Annu Rev Biochem* 72:743-781.
- Bosco EE, Mulloy JC, Zheng Y (2009) Rac1 GTPase: a "Rac" of all trades. *Cell Mol Life Sci* 66:370-374.
- Brim BL, Haskell R, Awedikian R, Ellinwood NM, Jin L, Kumar A, Foster TC, Magnusson KR (2013) Memory in aged mice is rescued by enhanced expression of the GluN2B subunit of the NMDA receptor. *Behav Brain Res* 238:211-226.

- Broadbent NJ, Squire LR, Clark RE (2004) Spatial memory, recognition memory, and the hippocampus. *Proc Natl Acad Sci U S A* 101:14515-14520.
- Bye CM, McDonald RJ (2019) A Specific Role of Hippocampal NMDA Receptors and Arc Protein in Rapid Encoding of Novel Environmental Representations and a More General Long-Term Consolidation Function. *Front Behav Neurosci* 13:8.
- Calabresi P, Picconi B, Tozzi A, Ghiglieri V, Di Filippo M (2014) Direct and indirect pathways of basal ganglia: a critical reappraisal. *Nat Neurosci* 17:1022-1030.
- Cannady R, Nguyen T, Padula AE, Rinker JA, Lopez MF, Becker HC, Woodward JJ, Mulholland PJ (2021) Interaction of chronic intermittent ethanol and repeated stress on structural and functional plasticity in the mouse medial prefrontal cortex. *Neuropharmacology* 182:108396.
- Castillo-Carniglia A, Keyes KM, Hasin DS, Cerda M (2019) Psychiatric comorbidities in alcohol use disorder. *Lancet Psychiatry* 6:1068-1080.
- Chandler LJ, Carpenter-Hyland E, Hendricson AW, Maldve RE, Morrisett RA, Zhou FC, Sari Y, Bell R, Szumlinski KK (2006) Structural and functional modifications in glutamateric synapses following prolonged ethanol exposure. *Alcohol Clin Exp Res* 30:368-376.
- Chang D, Nalls MA, Hallgrimsdottir IB, Hunkapiller J, van der Brug M, Cai F, International Parkinson's Disease Genomics C, and Me Research T, Kerchner GA, Ayalon G, Bingol B, Sheng M, Hinds D, Behrens TW, Singleton AB, Bhangale TR, Graham RR (2017) A meta-analysis of genome-wide association studies identifies 17 new Parkinson's disease risk loci. *Nat Genet* 49:1511-1516.

Chazeau A, Giannone G (2016) Organization and dynamics of the actin cytoskeleton during dendritic spine morphological remodeling. *Cell Mol Life Sci* 73:3053-3073.

Chen X, Levy JM, Hou A, Winters C, Azzam R, Sousa AA, Leapman RD, Nicoll RA, Reese TS (2015) PSD-95 family MAGUKs are essential for anchoring AMPA and NMDA receptor complexes at the postsynaptic density. *Proc Natl Acad Sci U S A* 112:E6983-6992.

Cheng Y, Huang CCY, Ma T, Wei X, Wang X, Lu J, Wang J (2017) Distinct Synaptic Strengthening of the Striatal Direct and Indirect Pathways Drives Alcohol Consumption. *Biol Psychiatry* 81:918-929.

Chin SM, Jansen S, Goode BL (2016) TIRF microscopy analysis of human Cof1, Cof2, and ADF effects on actin filament severing and turnover. *J Mol Biol* 428:1604-1616.

Coley AA, Gao WJ (2019) PSD-95 deficiency disrupts PFC-associated function and behavior during neurodevelopment. *Sci Rep* 9:9486.

Collingridge GL, Isaac JT, Wang YT (2004) Receptor trafficking and synaptic plasticity. *Nat Rev Neurosci* 5:952-962.

Concordet JP, Haeussler M (2018) CRISPOR: intuitive guide selection for CRISPR/Cas9 genome editing experiments and screens. *Nucleic Acids Res* 46:W242-W245.

Cooke SF, Bliss TV (2006) Plasticity in the human central nervous system. *Brain* 129:1659-1673.

Corbetta S, Gualdoni S, Ciceri G, Monari M, Zuccaro E, Tybulewicz VL, de Curtis I (2009) Essential role of Rac1 and Rac3 GTPases in neuronal development. *FASEB J* 23:1347-1357.

- Costa JF, Dines M, Lamprecht R (2020) The Role of Rac GTPase in Dendritic Spine Morphogenesis and Memory. *Front Synaptic Neurosci* 12:12.
- Daumas S, Halley H, Frances B, Lassalle JM (2005) Encoding, consolidation, and retrieval of contextual memory: differential involvement of dorsal CA3 and CA1 hippocampal subregions. *Learn Mem* 12:375-382.
- Davis S, Butcher SP, Morris RG (1992) The NMDA receptor antagonist D-2-amino-5-phosphonopentanoate (D-AP5) impairs spatial learning and LTP in vivo at intracerebral concentrations comparable to those that block LTP in vitro. *J Neurosci* 12:21-34.
- Dharavath RN, Pina-Leblanc C, Tang VM, Sloan ME, Nikolova YS, Pangarov P, Ruocco AC, Shield K, Voineskos D, Blumberger DM, Boileau I, Bozinoff N, Gerretsen P, Vieira E, Melamed OC, Sibille E, Quilty LC, Prevot TD (2023) GABAergic signaling in alcohol use disorder and withdrawal: pathological involvement and therapeutic potential. *Front Neural Circuits* 17:1218737.
- Dietz DM et al. (2012) Rac1 is essential in cocaine-induced structural plasticity of nucleus accumbens neurons. *Nat Neurosci* 15:891-896.
- Dolan RJ, Dayan P (2013) Goals and habits in the brain. *Neuron* 80:312-325.
- Dolnik A, Kanwal N, Mackert S, Halbedl S, Proepper C, Bockmann J, Schoen M, Boeckers TM, Kuhl SJ, Schmeisser MJ (2016) Sipa113/SPAR3 is targeted to postsynaptic specializations and interacts with the Fezzin ProSAPiP1/Lzts3. *J Neurochem* 136:28-35.
- Duvarci S, Pare D (2014) Amygdala microcircuits controlling learned fear. *Neuron* 82:966-980.

- Edwards DC, Sanders LC, Bokoch GM, Gill GN (1999) Activation of LIM-kinase by Pak1 couples Rac/Cdc42 GTPase signalling to actin cytoskeletal dynamics. *Nat Cell Biol* 1:253-259.
- Eichenbaum H (1997) Declarative memory: insights from cognitive neurobiology. *Annu Rev Psychol* 48:547-572.
- Elias GM, Funke L, Stein V, Grant SG, Brecht DS, Nicoll RA (2006) Synapse-specific and developmentally regulated targeting of AMPA receptors by a family of MAGUK scaffolding proteins. *Neuron* 52:307-320.
- Everitt BJ, Robbins TW (2013) From the ventral to the dorsal striatum: devolving views of their roles in drug addiction. *Neurosci Biobehav Rev* 37:1946-1954.
- Fleming IN, Elliott CM, Buchanan FG, Downes CP, Exton JH (1999) Ca²⁺/calmodulin-dependent protein kinase II regulates Tiam1 by reversible protein phosphorylation. *J Biol Chem* 274:12753-12758.
- Francis TC, Gaynor A, Chandra R, Fox ME, Lobo MK (2019) The Selective RhoA Inhibitor Rhosin Promotes Stress Resiliency Through Enhancing D1-Medium Spiny Neuron Plasticity and Reducing Hyperexcitability. *Biol Psychiatry* 85:1001-1010.
- Frey U, Morris RG (1998) Synaptic tagging: implications for late maintenance of hippocampal long-term potentiation. *Trends Neurosci* 21:181-188.
- Fu Z, Lee SH, Simonetta A, Hansen J, Sheng M, Pak DT (2007) Differential roles of Rap1 and Rap2 small GTPases in neurite retraction and synapse elimination in hippocampal spiny neurons. *J Neurochem* 100:118-131.

- Gangal H, Xie X, Huang Z, Cheng Y, Wang X, Lu J, Zhuang X, Essoh A, Huang Y, Chen R, Smith LN, Smith RJ, Wang J (2023) Drug reinforcement impairs cognitive flexibility by inhibiting striatal cholinergic neurons. *Nat Commun* 14:3886.
- Gao Q, Yao W, Wang J, Yang T, Liu C, Tao Y, Chen Y, Liu X, Ma L (2015) Post-training activation of Rac1 in the basolateral amygdala is required for the formation of both short-term and long-term auditory fear memory. *Front Mol Neurosci* 8:65.
- Gao Y, Dickerson JB, Guo F, Zheng J, Zheng Y (2004) Rational design and characterization of a Rac GTPase-specific small molecule inhibitor. *Proc Natl Acad Sci U S A* 101:7618-7623.
- Garcia-Mata R, Wennerberg K, Arthur WT, Noren NK, Ellerbroek SM, Burridge K (2006) Analysis of activated GAPs and GEFs in cell lysates. *Methods Enzymol* 406:425-437.
- Gerfen CR, Surmeier DJ (2011) Modulation of striatal projection systems by dopamine. *Annu Rev Neurosci* 34:441-466.
- Golden SA, Christoffel DJ, Heshmati M, Hodes GE, Magida J, Davis K, Cahill ME, Dias C, Ribeiro E, Ables JL, Kennedy PJ, Robison AJ, Gonzalez-Maeso J, Neve RL, Turecki G, Ghose S, Tamminga CA, Russo SJ (2013) Epigenetic regulation of RAC1 induces synaptic remodeling in stress disorders and depression. *Nat Med* 19:337-344.
- Grabrucker AM, Schmeisser MJ, Schoen M, Boeckers TM (2011) Postsynaptic ProSAP/Shank scaffolds in the cross-hair of synaptopathies. *Trends Cell Biol* 21:594-603.

- Gremel CM, Costa RM (2013) Orbitofrontal and striatal circuits dynamically encode the shift between goal-directed and habitual actions. *Nat Commun* 4:2264.
- Haditsch U, Anderson MP, Freewoman J, Cord B, Babu H, Brakebusch C, Palmer TD (2013) Neuronal Rac1 is required for learning-evoked neurogenesis. *J Neurosci* 33:12229-12241.
- Haditsch U, Leone DP, Farinelli M, Chrostek-Grashoff A, Brakebusch C, Mansuy IM, McConnell SK, Palmer TD (2009) A central role for the small GTPase Rac1 in hippocampal plasticity and spatial learning and memory. *Mol Cell Neurosci* 41:409-419.
- Hart G, Bradfield LA, Balleine BW (2018) Prefrontal Corticostriatal Disconnection Blocks the Acquisition of Goal-Directed Action. *J Neurosci* 38:1311-1322.
- Hermann D, Weber-Fahr W, Sartorius A, Hoerst M, Frischknecht U, Tunc-Skarka N, Perreau-Lenz S, Hansson AC, Krumm B, Kiefer F, Spanagel R, Mann K, Ende G, Sommer WH (2012) Translational magnetic resonance spectroscopy reveals excessive central glutamate levels during alcohol withdrawal in humans and rats. *Biol Psychiatry* 71:1015-1021.
- Herrick S, Evers DM, Lee JY, Udagawa N, Pak DT (2010) Postsynaptic PDLIM5/Enigma Homolog binds SPAR and causes dendritic spine shrinkage. *Mol Cell Neurosci* 43:188-200.
- Herring BE, Nicoll RA (2016) Long-Term Potentiation: From CaMKII to AMPA Receptor Trafficking. *Annu Rev Physiol* 78:351-365.

- Hill SY, De Bellis MD, Keshavan MS, Lowers L, Shen S, Hall J, Pitts T (2001) Right amygdala volume in adolescent and young adult offspring from families at high risk for developing alcoholism. *Biol Psychiatry* 49:894-905.
- Hoe HS, Lee JY, Pak DT (2009) Combinatorial morphogenesis of dendritic spines and filopodia by SPAR and alpha-actinin2. *Biochem Biophys Res Commun* 384:55-60.
- Hogarth L (2020) Addiction is driven by excessive goal-directed drug choice under negative affect: translational critique of habit and compulsion theory. *Neuropsychopharmacology* 45:720-735.
- Honkura N, Matsuzaki M, Noguchi J, Ellis-Davies GC, Kasai H (2008) The subspine organization of actin fibers regulates the structure and plasticity of dendritic spines. *Neuron* 57:719-729.
- Horii T, Morita S, Kimura M, Terawaki N, Shibutani M, Hatada I (2017) Efficient generation of conditional knockout mice via sequential introduction of lox sites. *Sci Rep* 7:7891.
- Hotulainen P, Hoogenraad CC (2010) Actin in dendritic spines: connecting dynamics to function. *J Cell Biol* 189:619-629.
- Huang CC, You JL, Wu MY, Hsu KS (2004) Rap1-induced p38 mitogen-activated protein kinase activation facilitates AMPA receptor trafficking via the GDI.Rab5 complex. Potential role in (S)-3,5-dihydroxyphenylglycine-induced long term depression. *J Biol Chem* 279:12286-12292.
- Huganir RL, Nicoll RA (2013) AMPARs and synaptic plasticity: the last 25 years. *Neuron* 80:704-717.

- Hwa L, Besheer J, Kash T (2017) Glutamate plasticity woven through the progression to alcohol use disorder: a multi-circuit perspective. *F1000Res* 6:298.
- Janak PH, Tye KM (2015) From circuits to behaviour in the amygdala. *Nature* 517:284-292.
- Jeyifous O, Lin EI, Chen X, Antinone SE, Mastro R, Drisdell R, Reese TS, Green WN (2016) Palmitoylation regulates glutamate receptor distributions in postsynaptic densities through control of PSD95 conformation and orientation. *Proc Natl Acad Sci U S A* 113:E8482-E8491.
- Kaizuka T, Takumi T (2018) Postsynaptic density proteins and their involvement in neurodevelopmental disorders. *J Biochem* 163:447-455.
- Kanellos G, Frame MC (2016) Cellular functions of the ADF/cofilin family at a glance. *J Cell Sci* 129:3211-3218.
- Kasai H, Matsuzaki M, Noguchi J, Yasumatsu N, Nakahara H (2003) Structure-stability-function relationships of dendritic spines. *Trends Neurosci* 26:360-368.
- Kennedy MB (2018) The Protein Biochemistry of the Postsynaptic Density in Glutamatergic Synapses Mediates Learning in Neural Networks. *Biochemistry* 57:4005-4009.
- Khantzian EJ (1985) The self-medication hypothesis of addictive disorders: focus on heroin and cocaine dependence. *Am J Psychiatry* 142:1259-1264.
- Kim JJ, Rison RA, Fanselow MS (1993) Effects of amygdala, hippocampus, and periaqueductal gray lesions on short- and long-term contextual fear. *Behav Neurosci* 107:1093-1098.

Kim JJ, Fanselow MS, DeCola JP, Landeira-Fernandez J (1992) Selective impairment of long-term but not short-term conditional fear by the N-methyl-D-aspartate antagonist APV. *Behav Neurosci* 106:591-596.

Kim JJ, Vitale D, Otani DV, Lian MM, Heilbron K, and Me Research T, Iwaki H, Lake J, Solsberg CW, Leonard H, Makarious MB, Tan EK, Singleton AB, Bandres-Ciga S, Noyce AJ, Global Parkinson's Genetics P, Blauwendraat C, Nalls MA, Foo JN, Mata I (2024) Multi-ancestry genome-wide association meta-analysis of Parkinson's disease. *Nat Genet* 56:27-36.

Koob G, Kreek MJ (2007) Stress, dysregulation of drug reward pathways, and the transition to drug dependence. *Am J Psychiatry* 164:1149-1159.

Koob GF, Volkow ND (2010) Neurocircuitry of addiction. *Neuropsychopharmacology* 35:217-238.

Kravitz AV, Kreitzer AC (2012) Striatal mechanisms underlying movement, reinforcement, and punishment. *Physiology (Bethesda)* 27:167-177.

Kumari M, Ticku MK (2000) Regulation of NMDA receptors by ethanol. *Prog Drug Res* 54:152-189.

Kuriu T, Inoue A, Bito H, Sobue K, Okabe S (2006) Differential control of postsynaptic density scaffolds via actin-dependent and -independent mechanisms. *J Neurosci* 26:7693-7706.

Labuhn M, Adams FF, Ng M, Knoess S, Schambach A, Charpentier EM, Schwarzer A, Mateo JL, Klusmann JH, Heckl D (2018) Refined sgRNA efficacy prediction improves large- and small-scale CRISPR-Cas9 applications. *Nucleic Acids Res* 46:1375-1385.

- Laguesse S, Morisot N, Phamluong K, Sakhai SA, Ron D (2018) mTORC2 in the dorsomedial striatum of mice contributes to alcohol-dependent F-Actin polymerization, structural modifications, and consumption. *Neuropsychopharmacology* 43:1539-1547.
- Laguesse S, Morisot N, Shin JH, Liu F, Adrover MF, Sakhai SA, Lopez MF, Phamluong K, Griffin WC, 3rd, Becker HC, Bender KJ, Alvarez VA, Ron D (2017) Prosapip1-Dependent Synaptic Adaptations in the Nucleus Accumbens Drive Alcohol Intake, Seeking, and Reward. *Neuron* 96:145-159 e148.
- Lee I, Kesner RP (2004) Differential contributions of dorsal hippocampal subregions to memory acquisition and retrieval in contextual fear-conditioning. *Hippocampus* 14:301-310.
- Leger M, Quiedeville A, Bouet V, Haelewyn B, Boulouard M, Schumann-Bard P, Freret T (2013) Object recognition test in mice. *Nat Protoc* 8:2531-2537.
- Li F, Tsien JZ (2009) Memory and the NMDA receptors. *N Engl J Med* 361:302-303.
- Li J, Zhang L, Chen Z, Xie M, Huang L, Xue J, Liu Y, Liu N, Guo F, Zheng Y, Kong J, Zhang L, Zhang L (2015) Cocaine activates Rac1 to control structural and behavioral plasticity in caudate putamen. *Neurobiol Dis* 75:159-176.
- Lisman J, Schulman H, Cline H (2002) The molecular basis of CaMKII function in synaptic and behavioural memory. *Nat Rev Neurosci* 3:175-190.
- Lovinger DM, Roberto M (2013) Synaptic effects induced by alcohol. *Curr Top Behav Neurosci* 13:31-86.
- Lovinger DM, Abrahao KP (2018) Synaptic plasticity mechanisms common to learning and alcohol use disorder. *Learn Mem* 25:425-434.

- Lueptow LM (2017) Novel Object Recognition Test for the Investigation of Learning and Memory in Mice. *J Vis Exp*.
- Lv L, Liu Y, Xie J, Wu Y, Zhao J, Li Q, Zhong Y (2019) Interplay between alpha2-chimaerin and Rac1 activity determines dynamic maintenance of long-term memory. *Nat Commun* 10:5313.
- Ma T, Barbee B, Wang X, Wang J (2017) Alcohol induces input-specific aberrant synaptic plasticity in the rat dorsomedial striatum. *Neuropharmacology* 123:46-54.
- Ma T, Cheng Y, Roltsch Hellard E, Wang X, Lu J, Gao X, Huang CCY, Wei XY, Ji JY, Wang J (2018) Bidirectional and long-lasting control of alcohol-seeking behavior by corticostriatal LTP and LTD. *Nat Neurosci* 21:373-383.
- Ma T, Huang Z, Xie X, Cheng Y, Zhuang X, Childs MJ, Gangal H, Wang X, Smith LN, Smith RJ, Zhou Y, Wang J (2022) Chronic alcohol drinking persistently suppresses thalamostriatal excitation of cholinergic neurons to impair cognitive flexibility. *J Clin Invest* 132.
- Maciver SK, Hussey PJ (2002) The ADF/cofilin family: actin-remodeling proteins. *Genome Biol* 3:reviews3007.
- Mackes JL, Willner J (2006) NMDA antagonist MK-801 impairs acquisition of place strategies, but not their use. *Behav Brain Res* 175:112-118.
- Malenka RC, Nicoll RA (1999) Long-term potentiation--a decade of progress? *Science* 285:1870-1874.
- Mark TL, Kassed CA, Vandivort-Warren R, Levit KR, Kranzler HR (2009) Alcohol and opioid dependence medications: prescription trends, overall and by physician specialty. *Drug Alcohol Depend* 99:345-349.

- Martinez LA, Klann E, Tejada-Simon MV (2007) Translocation and activation of Rac in the hippocampus during associative contextual fear learning. *Neurobiol Learn Mem* 88:104-113.
- Martins JS, Joyner KJ, McCarthy DM, Morris DH, Patrick CJ, Bartholow BD (2022) Differential brain responses to alcohol-related and natural rewards are associated with alcohol use and problems: Evidence for reward dysregulation. *Addict Biol* 27:e13118.
- Maruoka H, Konno D, Hori K, Sobue K (2005) Collaboration of PSD-Zip70 with its binding partner, SPAR, in dendritic spine maturity. *J Neurosci* 25:1421-1430.
- Matamales M, McGovern AE, Mi JD, Mazzone SB, Balleine BW, Bertran-Gonzalez J (2020) Local D2- to D1-neuron transmodulation updates goal-directed learning in the striatum. *Science* 367:549-555.
- Matsuura K, Kobayashi S, Konno K, Yamasaki M, Horiuchi T, Senda T, Hayashi T, Satoh K, Arima-Yoshida F, Iwasaki K, Negishi L, Yasui-Shimizu N, Kohu K, Kawahara S, Kirino Y, Nakamura T, Watanabe M, Yamamoto T, Manabe T, Akiyama T (2022) SIPA1L1/SPAR1 Interacts with the Neurabin Family of Proteins and is Involved in GPCR Signaling. *J Neurosci* 42:2448-2473.
- Mayanagi T, Yasuda H, Sobue K (2015) PSD-Zip70 Deficiency Causes Prefrontal Hypofunction Associated with Glutamatergic Synapse Maturation Defects by Dysregulation of Rap2 Activity. *J Neurosci* 35:14327-14340.
- McGuier NS, Padula AE, Lopez MF, Woodward JJ, Mulholland PJ (2015) Withdrawal from chronic intermittent alcohol exposure increases dendritic spine density in the lateral orbitofrontal cortex of mice. *Alcohol* 49:21-27.

Mira JP, Benard V, Groffen J, Sanders LC, Knaus UG (2000) Endogenous, hyperactive Rac3 controls proliferation of breast cancer cells by a p21-activated kinase-dependent pathway. *Proc Natl Acad Sci U S A* 97:185-189.

Morisot N, Berger AL, Phamluong K, Cross A, Ron D (2019a) The Fyn kinase inhibitor, AZD0530, suppresses mouse alcohol self-administration and seeking. *Addict Biol* 24:1227-1234.

Morisot N, Phamluong K, Ehinger Y, Berger AL, Moffat JJ, Ron D (2019b) mTORC1 in the orbitofrontal cortex promotes habitual alcohol seeking. *Elife* 8.

Morozov A, Muzzio IA, Bourtchouladze R, Van-Strien N, Lapidus K, Yin D, Winder DG, Adams JP, Sweatt JD, Kandel ER (2003) Rap1 couples cAMP signaling to a distinct pool of p42/44MAPK regulating excitability, synaptic plasticity, learning, and memory. *Neuron* 39:309-325.

Nachtigall EG, de CMJ, Izquierdo I, Furini CRG (2024) Cellular mechanisms of contextual fear memory reconsolidation: Role of hippocampal SFKs, TrkB receptors and GluN2B-containing NMDA receptors. *Psychopharmacology (Berl)* 241:61-73.

Naisbitt S, Kim E, Tu JC, Xiao B, Sala C, Valtschanoff J, Weinberg RJ, Worley PF, Sheng M (1999) Shank, a novel family of postsynaptic density proteins that binds to the NMDA receptor/PSD-95/GKAP complex and cortactin. *Neuron* 23:569-582.

Nakamura F (2013) FilGAP and its close relatives: a mediator of Rho-Rac antagonism that regulates cell morphology and migration. *Biochem J* 453:17-25.

Nakayama AY, Harms MB, Luo L (2000) Small GTPases Rac and Rho in the maintenance of dendritic spines and branches in hippocampal pyramidal neurons. *J Neurosci* 20:5329-5338.

Nall RW, Heinsbroek JA, Nentwig TB, Kalivas PW, Bobadilla AC (2021) Circuit selectivity in drug versus natural reward seeking behaviors. *J Neurochem* 157:1450-1472.

Nalls MA et al. (2019) Identification of novel risk loci, causal insights, and heritable risk for Parkinson's disease: a meta-analysis of genome-wide association studies. *Lancet Neurol* 18:1091-1102.

Nalls MA et al. (2014) Large-scale meta-analysis of genome-wide association data identifies six new risk loci for Parkinson's disease. *Nat Genet* 46:989-993.

Newcomer JW, Farber NB, Olney JW (2000) NMDA receptor function, memory, and brain aging. *Dialogues Clin Neurosci* 2:219-232.

Nguyen LK, Kholodenko BN, von Kriegsheim A (2018) Rac1 and RhoA: Networks, loops and bistability. *Small GTPases* 9:316-321.

Pak DT, Sheng M (2003) Targeted protein degradation and synapse remodeling by an inducible protein kinase. *Science* 302:1368-1373.

Pak DT, Yang S, Rudolph-Correia S, Kim E, Sheng M (2001) Regulation of dendritic spine morphology by SPAR, a PSD-95-associated RapGAP. *Neuron* 31:289-303.

Palop JJ, Chin J, Roberson ED, Wang J, Thwin MT, Bien-Ly N, Yoo J, Ho KO, Yu GQ, Kreitzer A, Finkbeiner S, Noebels JL, Mucke L (2007) Aberrant excitatory neuronal activity and compensatory remodeling of inhibitory hippocampal circuits in mouse models of Alzheimer's disease. *Neuron* 55:697-711.

Pannekoek WJ, Linnemann JR, Brouwer PM, Bos JL, Rehmann H (2013) Rap1 and Rap2 antagonistically control endothelial barrier resistance. *PLoS One* 8:e57903.

- Pastalkova E, Serrano P, Pinkhasova D, Wallace E, Fenton AA, Sacktor TC (2006) Storage of spatial information by the maintenance mechanism of LTP. *Science* 313:1141-1144.
- Pavlov D, Muhlrad A, Cooper J, Wear M, Reisler E (2007) Actin filament severing by cofilin. *J Mol Biol* 365:1350-1358.
- Peak J, Chieng B, Hart G, Balleine BW (2020) Striatal direct and indirect pathway neurons differentially control the encoding and updating of goal-directed learning. *Elife* 9.
- Peca J, Feliciano C, Ting JT, Wang W, Wells MF, Venkatraman TN, Lascola CD, Fu Z, Feng G (2011) Shank3 mutant mice display autistic-like behaviours and striatal dysfunction. *Nature* 472:437-442.
- Pennucci R, Gucciardi I, de Curtis I (2019) Rac1 and Rac3 GTPases differently influence the morphological maturation of dendritic spines in hippocampal neurons. *PLoS One* 14:e0220496.
- Peru YCdPRL, Acevedo SF, Rodan AR, Chang LY, Eaton BA, Rothenfluh A (2012) Adult neuronal Arf6 controls ethanol-induced behavior with Arfaptin downstream of Rac1 and RhoGAP18B. *J Neurosci* 32:17706-17713.
- Pilly PK, Grossberg S (2012) How do spatial learning and memory occur in the brain? Coordinated learning of entorhinal grid cells and hippocampal place cells. *J Cogn Neurosci* 24:1031-1054.
- Pitts MW (2018) Barnes Maze Procedure for Spatial Learning and Memory in Mice. *Bio Protoc* 8.

Qualmann B, Boeckers TM, Jeromin M, Gundelfinger ED, Kessels MM (2004) Linkage of the actin cytoskeleton to the postsynaptic density via direct interactions of Abp1 with the ProSAP/Shank family. *J Neurosci* 24:2481-2495.

Rao YL, Ganaraja B, Murlimanju BV, Joy T, Krishnamurthy A, Agrawal A (2022) Hippocampus and its involvement in Alzheimer's disease: a review. *3 Biotech* 12:55.

Ratner N, Mahler HR (1983) Structural organization of filamentous proteins in postsynaptic density. *Biochemistry* 22:2446-2453.

Razar R, Qu Y, Gunaseelan S, Chua JJE (2022) The importance of fasciculation and elongation protein zeta-1 in neural circuit establishment and neurological disorders. *Neural Regen Res* 17:1165-1171.

Reijnders MRF et al. (2017) RAC1 Missense Mutations in Developmental Disorders with Diverse Phenotypes. *Am J Hum Genet* 101:466-477.

Reim D, Weis TM, Halbedl S, Delling JP, Grabrucker AM, Boeckers TM, Schmeisser MJ (2016) The Shank3 Interaction Partner ProSAPiP1 Regulates Postsynaptic SPAR Levels and the Maturation of Dendritic Spines in Hippocampal Neurons. *Front Synaptic Neurosci* 8:13.

Renaud JB, Boix C, Charpentier M, De Cian A, Cochenec J, Duvernois-Berthet E, Perrouault L, Tesson L, Edouard J, Thinard R, Cherifi Y, Menoret S, Fontaniere S, de Croze N, Fraichard A, Sohm F, Anegon I, Concordet JP, Giovannangeli C (2016) Improved Genome Editing Efficiency and Flexibility Using Modified Oligonucleotides with TALEN and CRISPR-Cas9 Nucleases. *Cell Rep* 14:2263-2272.

- Richter M, Murai KK, Bourgin C, Pak DT, Pasquale EB (2007) The EphA4 receptor regulates neuronal morphology through SPAR-mediated inactivation of Rap GTPases. *J Neurosci* 27:14205-14215.
- Ridley AJ (2006) Rho GTPases and actin dynamics in membrane protrusions and vesicle trafficking. *Trends Cell Biol* 16:522-529.
- Ridley AJ, Paterson HF, Johnston CL, Diekmann D, Hall A (1992) The small GTP-binding protein rac regulates growth factor-induced membrane ruffling. *Cell* 70:401-410.
- Romero-Barragan MT, Gruart A, Delgado-Garcia JM (2021) Transsynaptic Long-Term Potentiation in the Hippocampus of Behaving Mice. *Front Synaptic Neurosci* 13:811806.
- Ron D (2004) Signaling cascades regulating NMDA receptor sensitivity to ethanol. *Neuroscientist* 10:325-336.
- Ron D, Berger A (2018) Targeting the intracellular signaling "STOP" and "GO" pathways for the treatment of alcohol use disorders. *Psychopharmacology (Berl)* 235:1727-1743.
- Ross MM, Aizenman E (2023) GluA1-Shank3 interaction decreases in response to chronic neuronal depolarization. *Neurosci Lett* 809:137305.
- Rossato JI, Radiske A, Gonzalez MC, Apolinario G, de Araujo RLS, Bevilaqua LRM, Cammarota M (2023) NMDARs control object recognition memory destabilization and reconsolidation. *Brain Res Bull* 197:42-48.
- Ryu J, Futai K, Feliu M, Weinberg R, Sheng M (2008) Constitutively active Rap2 transgenic mice display fewer dendritic spines, reduced extracellular signal-

- regulated kinase signaling, enhanced long-term depression, and impaired spatial learning and fear extinction. *J Neurosci* 28:8178-8188.
- Sacktor TC (2008) PKMzeta, LTP maintenance, and the dynamic molecular biology of memory storage. *Prog Brain Res* 169:27-40.
- Sala C, Vicidomini C, Bigi I, Mossa A, Verpelli C (2015) Shank synaptic scaffold proteins: keys to understanding the pathogenesis of autism and other synaptic disorders. *J Neurochem* 135:849-858.
- SAMHSA CfBHSaQ (2022) Table 5.4A – Drug Use Disorder in Past Year: Among People Aged 12 or Older; by Age Group and Demographic Characteristics, Numbers in Thousands, 2021 and 2022. In: 2019 National Survey on Drug Use and Health.
- Sanderson DJ, Good MA, Skelton K, Sprengel R, Seeburg PH, Rawlins JN, Bannerman DM (2009) Enhanced long-term and impaired short-term spatial memory in GluA1 AMPA receptor subunit knockout mice: evidence for a dual-process memory model. *Learn Mem* 16:379-386.
- Schmeisser MJ, Grabrucker AM, Bockmann J, Boeckers TM (2009) Synaptic cross-talk between N-methyl-D-aspartate receptors and LAPSER1-beta-catenin at excitatory synapses. *J Biol Chem* 284:29146-29157.
- Schubert V, Dotti CG (2007) Transmitting on actin: synaptic control of dendritic architecture. *J Cell Sci* 120:205-212.
- Scott RW, Olson MF (2007) LIM kinases: function, regulation and association with human disease. *J Mol Med (Berl)* 85:555-568.

- Seeburg DP, Feliu-Mojer M, Gaiottino J, Pak DT, Sheng M (2008) Critical role of CDK5 and Polo-like kinase 2 in homeostatic synaptic plasticity during elevated activity. *Neuron* 58:571-583.
- Shan Q, Ge M, Christie MJ, Balleine BW (2014) The acquisition of goal-directed actions generates opposing plasticity in direct and indirect pathways in dorsomedial striatum. *J Neurosci* 34:9196-9201.
- Sheng M, Kim E (2000) The Shank family of scaffold proteins. *J Cell Sci* 113 (Pt 11):1851-1856.
- Sholl DA (1953) Dendritic organization in the neurons of the visual and motor cortices of the cat. *J Anat* 87:387-406.
- Singer BF, Fadanelli M, Kawa AB, Robinson TE (2018) Are Cocaine-Seeking "Habits" Necessary for the Development of Addiction-Like Behavior in Rats? *J Neurosci* 38:60-73.
- Spangler EL, Bresnahan EL, Garofalo P, Muth NJ, Heller B, Ingram DK (1991) NMDA receptor channel antagonism by dizocilpine (MK-801) impairs performance of rats in aversively motivated complex maze tasks. *Pharmacol Biochem Behav* 40:949-958.
- Spilker C, Acuna Sanhueza GA, Bockers TM, Kreutz MR, Gundelfinger ED (2008) SPAR2, a novel SPAR-related protein with GAP activity for Rap1 and Rap2. *J Neurochem* 104:187-201.
- Squire LR, Stark CE, Clark RE (2004) The medial temporal lobe. *Annu Rev Neurosci* 27:279-306.

- Stemmer M, Thumberger T, Del Sol Keyer M, Wittbrodt J, Mateo JL (2015) CCTop: An Intuitive, Flexible and Reliable CRISPR/Cas9 Target Prediction Tool. *PLoS One* 10:e0124633.
- Straube B (2012) An overview of the neuro-cognitive processes involved in the encoding, consolidation, and retrieval of true and false memories. *Behav Brain Funct* 8:35.
- Swanson AM, DePoy LM, Gourley SL (2017) Inhibiting Rho kinase promotes goal-directed decision making and blocks habitual responding for cocaine. *Nat Commun* 8:1861.
- Tashiro A, Minden A, Yuste R (2000) Regulation of dendritic spine morphology by the rho family of small GTPases: antagonistic roles of Rac and Rho. *Cereb Cortex* 10:927-938.
- Tejada-Simon MV (2015) Modulation of actin dynamics by Rac1 to target cognitive function. *J Neurochem* 133:767-779.
- Toda S, Shen HW, Peters J, Cagle S, Kalivas PW (2006) Cocaine increases actin cycling: effects in the reinstatement model of drug seeking. *J Neurosci* 26:1579-1587.
- Tolias KF, Bikoff JB, Burette A, Paradis S, Harrar D, Tavazoie S, Weinberg RJ, Greenberg ME (2005) The Rac1-GEF Tiam1 couples the NMDA receptor to the activity-dependent development of dendritic arbors and spines. *Neuron* 45:525-538.
- Toure A, Dorseuil O, Morin L, Timmons P, Jegou B, Reibel L, Gacon G (1998) MgcRacGAP, a new human GTPase-activating protein for Rac and Cdc42 similar to *Drosophila rotundRacGAP* gene product, is expressed in male germ cells. *J Biol Chem* 273:6019-6023.

- Tu G, Ying L, Ye L, Zhao J, Liu N, Li J, Liu Y, Zhu M, Wu Y, Xiao B, Guo H, Guo F, Wang H, Zhang L, Zhang L (2019) Dopamine D(1) and D(2) Receptors Differentially Regulate Rac1 and Cdc42 Signaling in the Nucleus Accumbens to Modulate Behavioral and Structural Plasticity After Repeated Methamphetamine Treatment. *Biol Psychiatry* 86:820-835.
- Tu JC, Xiao B, Naisbitt S, Yuan JP, Petralia RS, Brakeman P, Doan A, Aakalu VK, Lanahan AA, Sheng M, Worley PF (1999) Coupling of mGluR/Homer and PSD-95 complexes by the Shank family of postsynaptic density proteins. *Neuron* 23:583-592.
- Turner KM, Balleine BW (2024) Stimulus control of habits: Evidence for both stimulus specificity and devaluation insensitivity in a dual-response task. *J Exp Anal Behav* 121:52-61.
- Tye KM, Prakash R, Kim SY, Fenno LE, Grosenick L, Zarabi H, Thompson KR, Gradinaru V, Ramakrishnan C, Deisseroth K (2011) Amygdala circuitry mediating reversible and bidirectional control of anxiety. *Nature* 471:358-362.
- Urban NN, Henze DA, Lewis DA, Barrionuevo G (1996) Properties of LTP induction in the CA3 region of the primate hippocampus. *Learn Mem* 3:86-95.
- Van Aelst L, D'Souza-Schorey C (1997) Rho GTPases and signaling networks. *Genes Dev* 11:2295-2322.
- Vandaele Y, Ahmed SH (2021) Habit, choice, and addiction. *Neuropsychopharmacology* 46:689-698.
- Vetter IR, Wittinghofer A (2001) The guanine nucleotide-binding switch in three dimensions. *Science* 294:1299-1304.

- Vinson C, Myakishev M, Acharya A, Mir AA, Moll JR, Bonovich M (2002) Classification of human B-ZIP proteins based on dimerization properties. *Mol Cell Biol* 22:6321-6335.
- Vyas Y, Montgomery JM (2016) The role of postsynaptic density proteins in neural degeneration and regeneration. *Neural Regen Res* 11:906-907.
- Wackernah RC, Minnick MJ, Clapp P (2014) Alcohol use disorder: pathophysiology, effects, and pharmacologic options for treatment. *Subst Abuse Rehabil* 5:1-12.
- Walker DL, Gold PE (1991) Effects of the novel NMDA antagonist, NPC 12626, on long-term potentiation, learning and memory. *Brain Res* 549:213-221.
- Wang J, Lanfranco MF, Gibb SL, Yowell QV, Carnicella S, Ron D (2010) Long-lasting adaptations of the NR2B-containing NMDA receptors in the dorsomedial striatum play a crucial role in alcohol consumption and relapse. *J Neurosci* 30:10187-10198.
- Wang J, Ben Hamida S, Darcq E, Zhu W, Gibb SL, Lanfranco MF, Carnicella S, Ron D (2012) Ethanol-mediated facilitation of AMPA receptor function in the dorsomedial striatum: implications for alcohol drinking behavior. *J Neurosci* 32:15124-15132.
- Wang J, Cheng Y, Wang X, Roltsch Hellard E, Ma T, Gil H, Ben Hamida S, Ron D (2015) Alcohol Elicits Functional and Structural Plasticity Selectively in Dopamine D1 Receptor-Expressing Neurons of the Dorsomedial Striatum. *J Neurosci* 35:11634-11643.
- Wang J, Carnicella S, Phamluong K, Jeanblanc J, Ronesi JA, Chaudhri N, Janak PH, Lovinger DM, Ron D (2007) Ethanol induces long-term facilitation of NR2B-NMDA

- receptor activity in the dorsal striatum: implications for alcohol drinking behavior. *J Neurosci* 27:3593-3602.
- Wang W, Ju YY, Zhou QX, Tang JX, Li M, Zhang L, Kang S, Chen ZG, Wang YJ, Ji H, Ding YQ, Xu L, Liu JG (2017) The Small GTPase Rac1 Contributes to Extinction of Aversive Memories of Drug Withdrawal by Facilitating GABA(A) Receptor Endocytosis in the vmPFC. *J Neurosci* 37:7096-7110.
- Wang X, Liu D, Wei F, Li Y, Wang X, Li L, Wang G, Zhang S, Zhang L (2020) Stress-Sensitive Protein Rac1 and Its Involvement in Neurodevelopmental Disorders. *Neural Plast* 2020:8894372.
- Warnault V, Darcq E, Morisot N, Phamluong K, Wilbrecht L, Massa SM, Longo FM, Ron D (2016) The BDNF Valine 68 to Methionine Polymorphism Increases Compulsive Alcohol Drinking in Mice That Is Reversed by Tropomyosin Receptor Kinase B Activation. *Biol Psychiatry* 79:463-473.
- Wendholt D, Spilker C, Schmitt A, Dolnik A, Smalla KH, Proepper C, Bockmann J, Sobue K, Gundelfinger ED, Kreutz MR, Boeckers TM (2006) ProSAP-interacting protein 1 (ProSAPiP1), a novel protein of the postsynaptic density that links the spine-associated Rap-Gap (SPAR) to the scaffolding protein ProSAP2/Shank3. *J Biol Chem* 281:13805-13816.
- Won S, Incontro S, Nicoll RA, Roche KW (2016) PSD-95 stabilizes NMDA receptors by inducing the degradation of STEP61. *Proc Natl Acad Sci U S A* 113:E4736-4744.
- Wong KW, Mohammadi S, Isberg RR (2006) Disruption of RhoGDI and RhoA regulation by a Rac1 specificity switch mutant. *J Biol Chem* 281:40379-40388.

- Worthylake DK, Rossman KL, Sondek J (2000) Crystal structure of Rac1 in complex with the guanine nucleotide exchange region of Tiam1. *Nature* 408:682-688.
- Wrase J, Makris N, Braus DF, Mann K, Smolka MN, Kennedy DN, Caviness VS, Hodge SM, Tang L, Albaugh M, Ziegler DA, Davis OC, Kissling C, Schumann G, Breiter HC, Heinz A (2008) Amygdala volume associated with alcohol abuse relapse and craving. *Am J Psychiatry* 165:1179-1184.
- Wu P, Ding ZB, Meng SQ, Shen HW, Sun SC, Luo YX, Liu JF, Lu L, Zhu WL, Shi J (2014) Differential role of Rac in the basolateral amygdala and cornu ammonis 1 in the reconsolidation of auditory and contextual Pavlovian fear memory in rats. *Psychopharmacology (Berl)* 231:2909-2919.
- Xiao L, Hu C, Yang W, Guo D, Li C, Shen W, Liu X, Aijun H, Dan W, He C (2013) NMDA receptor couples Rac1-GEF Tiam1 to direct oligodendrocyte precursor cell migration. *Glia* 61:2078-2099.
- Xie Z, Huganir RL, Penzes P (2005) Activity-dependent dendritic spine structural plasticity is regulated by small GTPase Rap1 and its target AF-6. *Neuron* 48:605-618.
- Xie Z, Srivastava DP, Photowala H, Kai L, Cahill ME, Woolfrey KM, Shum CY, Surmeier DJ, Penzes P (2007) Kalirin-7 controls activity-dependent structural and functional plasticity of dendritic spines. *Neuron* 56:640-656.
- Yang N, Higuchi O, Ohashi K, Nagata K, Wada A, Kangawa K, Nishida E, Mizuno K (1998) Cofilin phosphorylation by LIM-kinase 1 and its role in Rac-mediated actin reorganization. *Nature* 393:809-812.

- Yang X, Gong R, Qin L, Bao Y, Fu Y, Gao S, Yang H, Ni J, Yuan TF, Lu W (2022) Trafficking of NMDA receptors is essential for hippocampal synaptic plasticity and memory consolidation. *Cell Rep* 40:111217.
- Yin HH, Ostlund SB, Knowlton BJ, Balleine BW (2005) The role of the dorsomedial striatum in instrumental conditioning. *Eur J Neurosci* 22:513-523.
- Zhang C, Liu J, Zhao Y, Yue X, Zhu Y, Wang X, Wu H, Blanco F, Li S, Bhanot G, Haffty BG, Hu W, Feng Z (2016) Glutaminase 2 is a novel negative regulator of small GTPase Rac1 and mediates p53 function in suppressing metastasis. *Elife* 5:e10727.
- Zhang H, Ben Zablah Y, Zhang H, Jia Z (2021) Rho Signaling in Synaptic Plasticity, Memory, and Brain Disorders. *Front Cell Dev Biol* 9:729076.
- Zhang H, Etherington LA, Hafner AS, Belelli D, Coussen F, Delagrangé P, Chaouloff F, Spedding M, Lambert JJ, Choquet D, Groc L (2013) Regulation of AMPA receptor surface trafficking and synaptic plasticity by a cognitive enhancer and antidepressant molecule. *Mol Psychiatry* 18:471-484.
- Zhu JJ, Qin Y, Zhao M, Van Aelst L, Malinow R (2002) Ras and Rap control AMPA receptor trafficking during synaptic plasticity. *Cell* 110:443-455.
- Zhu Y, Pak D, Qin Y, McCormack SG, Kim MJ, Baumgart JP, Velamoor V, Auberson YP, Osten P, van Aelst L, Sheng M, Zhu JJ (2005) Rap2-JNK removes synaptic AMPA receptors during depotentiation. *Neuron* 46:905-916.
- Zorumski CF, Mennerick S, Izumi Y (2014) Acute and chronic effects of ethanol on learning-related synaptic plasticity. *Alcohol* 48:1-17.

Zucker RS, Regehr WG (2002) Short-term synaptic plasticity. *Annu Rev Physiol* 64:355-405.

Publishing Agreement

It is the policy of the University to encourage open access and broad distribution of all theses, dissertations, and manuscripts. The Graduate Division will facilitate the distribution of UCSF theses, dissertations, and manuscripts to the UCSF Library for open access and distribution. UCSF will make such theses, dissertations, and manuscripts accessible to the public and will take reasonable steps to preserve these works in perpetuity.

I hereby grant the non-exclusive, perpetual right to The Regents of the University of California to reproduce, publicly display, distribute, preserve, and publish copies of my thesis, dissertation, or manuscript in any form or media, now existing or later derived, including access online for teaching, research, and public service purposes.

DocuSigned by:

Zachary William Hoisington

8EFFBB3BB2B5448...

Author Signature

3/1/2024

Date